THE UNIVERSITY OF CHICAGO

PKC δ GERMLINE VARIANTS AND GENETIC DELETION IN MICE AUGMENT ANTI-TUMOR IMMUNITY THROUGH REGULATION OF MYELOID CELLS

A DISSERTATION SUBMITTED TO
THE FACULTY OF THE DIVISION OF THE BIOLOGICAL SCIENCES
AND PRITZKER SCHOOL OF MEDICINE
IN CANDIDACY FOR THE DEGREE OF
DOCTOR OF PHILOSOPHY

COMMITTEE ON IMMUNOLOGY

BY
KYLE RYAN CRON

CHICAGO, ILLINOIS
AUGUST 2022

‘He said he hoped a lot of us would have careers in science,’ she said. She didn't see anything funny in that. She was remembering a lesson that had impressed her. She was repeating it, gropingly, dutifully. ‘He said, the trouble with the world was...’

‘The trouble with the world was,’ she continued hesitatingly, ‘that people were still superstitious instead of scientific. He said if everybody would study science more, there wouldn't be all the trouble there was.’

‘He said science was going to discover the basic secret of life someday,’ the bartender put in. He scratched his head and frowned. ‘Didn't I read in the paper the other day where they'd finally found out what it was?’

‘I missed that,’ I murmured.

‘I saw that’, said Sandra. ‘About two days ago.’

‘That's right,’ said the bartender.

‘What is the secret of life?’ I asked.

‘I forget,’ said Sandra.

‘Protein.’ The bartender declared. ‘They found out something about protein.’

‘Yeah.’ said Sandra, ‘that's it.’
— Kurt Vonnegut, *Cat's Cradle*

TABLE OF CONTENTS

Supplementary tables may be found online

LIST OF FIGURES

Chapter 3

Chapter 4

LIST OF TABLES

Supplementary Files

Supplementary tables may be found online.

Table S1: Genes uniquely expressed for each cluster
Table S2: All differentially expressed genes identified within the C1qa cluster
Table S3: All GSEA results for the C1qa cluster
Table S4: M1 and M2 gene lists
Table S5: PKCd-like human ortholog gene list

ACKNOWLEDGEMENTS

I cannot overstate how much of a collaborative effort this thesis was. It is a product of a lifetime of encouragement and support from friends, family, and all those in-between. To my love, my rock, Miriam Ofstein, this Ph.D. is as much yours as it is mine and I could not have completed it without you.

I have been interested in science from the earliest possible age and I will be forever grateful for how my family did everything they could to encourage my interests. Without their constant love and support, I would never have taken the first steps towards becoming a scientist. My high school teachers Dr. Robert Langdon, Ronee Krashes, and Peter Erbland encouraged my passion and gave me direction in life when I needed it the most. I also want to thank Dr. Edith Lord at the University of Rochester, who provided me my very first opportunity to experience a lab hands-on. In Dr. Lord's lab I was surrounded by incredibly talented and hardworking post-doctoral and graduate students, including my mentor Dr. Scott Gerber. In collaboration with Dr. Gerber, I discovered the power of the immune system and found my lifelong passion for tumor immunology. My next opportunity was given to me in the lab of Dr. Alan D'Andrea, under the tutelage of Dr. David Kozono and technician Kaya Zhu. Over the course of two years, I learned many additional scientific skills, but also how to overcome roadblocks and properly pilot ideas before expanding to larger scale experiments. I also made several lifelong friends here, in particular Helena Mistry, who was always happy to sing along to Rihanna or Drake whenever I was feeling overwhelmed.

I then joined the University of Chicago under the advisement of Dr. Yang-Xin Fu, who taught me to always learn from the work of others no matter the source. Shortly after, I was

offered a place in the lab of Dr. Thomas Gajewski. Dr Gajewski is the biggest contributor to the success of this project, and I am so thankful for his support and guidance throughout the process. The enthusiasm Dr. Gajewski has for science and his creative approaches to scientific problems is incredible and I remain eternally grateful for the path you have put me on. Dr. Gajewski's belief in this project never wavered, even when mine did, and his relentless drive always pushed me to improve my work. His ability to look beyond the data to craft a compelling story that allows us to reach a deeper understanding of the science is absolutely unparalleled.

To the rest of the Gajewski lab, there is no amount of gratitude that can match the support you've provided me over the years. You've all made our lab in GCIS W423J into a one that is exciting to work in, thanks to your intelligence and willingness to support each other. In particular, I must thank Ayelet Sivan and Keston Aquino-Michaels. Their work on the genome-wide association study formed the foundation of this entire project and they always made themselves available to answer any questions or discuss concerns. Without them, none of the data shown in this study would have been possible.

I must also acknowledge my fellow graduate students and collaborators. In particular, Jess Fessler for her help with the analysis of the single cell RNAseq dataset, Emily Higgs for her assistance with the biobank data, and Alexandra Cabanov, who always made herself available to lend a hand during a long experiment day. I also want to thank Seoho Lee, who assisted with many of these experiments. I could not have asked for a better trainee and friend. I want to thank our post-docs Andrea Ziblat, Shuyin Li, Sherin Rouhani, Jon Trujilo, and Vyara Matson for their insightful scientific discussions. Finally, I want to thank previous lab members Stefani Spranger, Jay Williams, Brendan Horton, Athalia Pyzer, and Blake Flood, who were all a constant source of support and guidance even after their tenure in Dr. Gajewski's lab.

While reflecting and writing these acknowledgements, I realized just how much the success of a scientist's career is dictated by the opportunities provided to them by others. One opportunity leads to another, and a small act of kindness can result in a lifelong passion and career. It is our responsibility as scientists not only to pursue knowledge, but to open doors for any and all who would not otherwise have the opportunities.

ABSTRACT

Antibodies blocking the PD-1/PD-L1 axis and other immune checkpoints have revolutionized cancer care. Clinical response is favored in tumors showing a T cell-inflamed tumor microenvironment at baseline [1,2], which is tremendously variable between patients and also across tumor types [3]. Despite the importance of this immunobiological phenotype, the mechanisms explaining such inter-patient heterogeneity are just beginning to be understood. Based on the notion that hypomorphic germline variants in immunoregulatory genes are linked to autoimmune diseases [4], one hypothesis is that germline variants might favor spontaneous immune priming and T cell infiltration into tumors. To investigate this possibility, we utilized TCGA data and identified germline variants in the PKCδ gene associated with decreased expression of *PRKCD* and an increased immune gene signature in the tumor microenvironment. Genetic deletion of PKCδ in mice resulted in improved endogenous anti-tumor immunity and increased efficacy of PD-1/PD-L1 blockade. Single cell RNAseq of immune cells in the tumor revealed expression of *Prkcd* in myeloid cells, and PKCδ deletion caused a macrophage shift from an M2-like to an M1-like phenotype. Conditional deletion of PKCδ in macrophages recapitulated the improved tumor control phenotype and response to anti-PD-L1 treatment. Analysis of clinical samples from melanoma patients confirmed an association between *PRKCD* variants and M1/M2 phenotype, and between a PKCδ KO-like gene signature and clinical benefit from anti-PD-1. Our results suggest that reduced PKCδ in host cells leads to improved anti-tumor immunity and PD-1 blockade efficacy through a myeloid shift to an M1-like phenotype, and further identify PKCδ as a candidate therapeutic target.

Chapter 1: Introduction

1.1 Basics of anti-tumor immunity

Cancer is characterized by variability

Cancer is commonly misunderstood by the public to be a single disease that will ultimately have a single cure. In reality, the term "cancer" actually encompasses an incredibly complex set of diseases all revolving around the formation of malignant tumors from dysregulated cell growth. The complexity of cancer stems from the extreme variation observed in all aspects of tumor biology, perhaps best demonstrated when comparing tumors arising in different tissues. For example, while lung squamous cell carcinoma (LUSC) tumors typically have 8.15 mutations per megabase (Mb) or nearly 25,000 total mutations across the genome, acute myeloid leukemia (AML) tumors have only 0.28 mutations/Mb or around 800 total mutations [5]. Even within a single tissue there can be tremendous differences in biological characteristics of tumors, as observed with the uveal and cutaneous melanoma subtypes. Despite both arising from the exact same cell type, melanocytes, the biology of these diseases is quite distinct based on the tissue from which the melanocytes originated [6]. To complicate matters further, a tumor from a single patient will have individual cells with distinct genetic and molecular features and this heterogeneity is often the source of tumor cell-intrinsic resistance to therapy [7]. Beyond the tumor cells themselves, another aspect contributing to variability is the endogenous response mounted by the patient's own immune system, which even within a tumor subtype can vary from quite strong to nearly non-existent [8,9]. Therapies that stimulate and enhance this endogenous anti-tumor immune response have seen enormous clinical benefit in a subset of patients over a range of cancer types [10]. However, the strength of a patient's individual

anti-tumor immune response is widely variable, ultimately dictated by a complex set of inter-related mechanisms not fully understood [11].

An overview of the CD8$^+$ T cell-mediated anti-tumor response

The most important effector cell in anti-tumor immunity is the CD8$^+$ thymocyte cell (T cell), able to target and kill tumor cells in a precise and antigen-specific fashion. Most currently successful immunotherapies revolve around expanding or enhancing the function of these cells. As such, understanding the mechanisms controlling CD8$^+$ T cell-mediated anti-tumor immunity, both positively and negatively, is critical for developing new interventions that may expand the population of patients with the potential to derive clinical benefit. The induction of an endogenous CD8$^+$ T cell anti-tumor immune response begins with the involvement of innate immune cells, that sense tumor-derived damage-associated molecular patterns (DAMPs) in the tumor microenvironment (TME) [12]. These early innate cells can include NK cells, innate lymphoid cells, macrophages, and dendritic cells (DCs). In particular, the Batf3-lineage of dendritic cells (cDC1 cells) are critically important in multiple preclinical models and in human cancer settings, as cDC1 cells are the major antigen presenting cell (APC) type involved in the cross-presentation of antigens to CD8$^+$ T cells. Batf3 knockout (KO) mice fail to control immunogenic tumors and have markedly diminished induction of tumor antigen-specific CD8+ T cells [13,14]. The initial recruitment of Batf3-DCs into tumors is driven by the chemokines XCL1 and CCL4. XCL1 can be produced by NK cells and a subset of T cells, while CCL4 is produced by myeloid cells and tumor cells [15,16]. Once within the tumors, activation and maturation of cDC1 cells involve type I IFNs, either produced by other APCs or in some instances by the tumor cells themselves [17,18]. Mice deficient in the type I IFN receptor (IFNAR KO mice) also fail to control immunogenic tumors, show diminished T cell priming, and have markedly reduced

Batf3-DCs in the TME [14,19]. Meanwhile boosting local IFN production leads to improved $CD8^+$ T cell-mediated anti-tumor immunity [20]. The induction of type I IFNs in the host APC compartment is mediated by innate immune pathway engagement. The most important of these pathways appears to be the cGAS/STING pathway, which is activated by tumor-derived DNA that finds its way into the cytosol of DCs [21]. STING KO mice show poor rejection of immunogenic tumors, markedly diminished type I IFN production by DCs, and poor endogenous T cell priming [22,23]. Overall the T cell-inflamed tumor microenvironment can be collectively defined by the presence of transcripts induced by type I IFNs and IFN-γ, transcripts specific to activated $CD8^+$ T cells and cDC1s, and the transcripts for the chemokines that recruit those cell types [24].

The initial priming of $CD8^+$ T cells against tumor-derived antigens is thought to occur in the tumor-draining lymph nodes (TdLNs) [25]. Evidence for this notion includes the fact that activated $CD8^+$ T cells against a defined antigen are detected first in the lymph node, followed by in the circulation, and then subsequently within the tumor microenvironment. In addition, cDC1s must express the lymph node-homing chemokine receptor CCR7 for efficient priming to occur [26,27]. In an elegant set of experiments involving pH sensitive and pH resistant fluorescent tumor antigens, Broz et al. and Roberts et al. revealed that while many myeloid cell populations within the tumor microenvironment uptake tumor antigen via phagocytosis, only cDC1s can traffic to the TdLN with intact antigen by sequestering it within pH neutral intracellular compartments [27–29]. cDC1s are also unique among APCs in their ability to process and present antigen via “cross-priming”, which results in presentation of exogenously acquired antigen on MHC-I and is essential to their ability to effectively prime and stimulate $CD8^+$ T cells [30,31]. Once antigen-loaded cDC1s enter the TdLN, they engage and prime naïve $CD8^+$ T cells expressing

TCRs that correspond to the peptide:MHC-I complexes presented on the cDC1 surface [32]. This interaction induces a large proliferative expansion of antigen specific $CD8^+$ T cells and causes them to acquire the ability to produce effector molecules, including IFN-γ, perforin, and granzyme B [33]. These fully primed $CD8^+$ T cells, commonly referred to as cytotoxic T lymphocytes (CTLs), exit the TdLN where they become detectable systemically in the blood and spleen. $CD8^+$ T cells are then recruited into the TME via CXCL9 and CXCL10 chemokine gradients typically produced by tumor-infiltrating cDC1s [34,35]. Once CTLs infiltrate the tumor, these tumor-infiltrating lymphocytes (TILs) recognize cancer cells via antigen specific peptide:MHC-TCR interactions resulting in the destruction of tumor cells. Meanwhile the presence of cDC1s within the TME continues to be important in the continued recruitment and function of $CD8^+$ T cells [36,37]. This entire path marks the successful $CD8^+$ T cell-mediated anti-tumor immune response and is required for durable anti-tumor immunity.

1.2 Immunosuppressive mechanisms inhibiting CTL responses in the tumor microenvironment

If left completely unchecked even minor immune responses will run rampant, causing destruction of normal and target tissues alike in a process known as autoimmunity. Thus, a large portion of the immune system is dedicated to negative feedback pathways and inhibitory factors that suppress activated immune cells and inflammation. The most well-known of these immune suppressive cells is the T regulatory cell (Treg), which are essential for immune homeostasis as acute loss of these cells leads to widespread tissue destruction and autoimmunity [38]. In the context of cancer, Tregs are generally associated with poor prognosis as the presence of these cells can directly suppress the activation of effector cells [39–42].

In addition to pathways that normally maintain immune homeostasis, there are many other mechanisms preventing endogenous immunity from eradicating a tumor. While patients can experience immune exclusion, a phenomenon characterized by a complete lack of immune cells within the TME, even patients with tumor-infiltrating $CD8^+$ T cells often experience CTL dysfunction. Both exclusion and dysfunction are forms of immunosuppression that lead to uncontrollable tumor growth, yet the underlying mechanisms determining the degree and type of immunosuppression in a patient are not fully understood. At the most basic level, there are often structural factors built into the tumor architecture that inhibit T cell immunity. Frequently tumors are surrounded by a tough shell of stromal cells, physically blocking infiltration of immune cells into the TME [43]. Tumors can also be very poorly vascularized, and many immune cells are particularly sensitive to the resulting hypoxic environments [44,45]. Another effect of poor vasculature is that without the steady flow of fresh blood from properly developed blood vessels, the intense energy consumption by tumor cells often causes localized nutrient deprivation leading to CTL dysfunction [46]. Tumor cells can also produce immune inhibitory factors such as TGF-β and IDO that directly suppress T cell function while simultaneously increasing the suppressive abilities of other immune cells [47,48]. Additionally, certain oncogenic signaling pathways, traditionally viewed as only causing aberrant growth signaling, can directly impact immunosuppression [49,50]. For example, active β-catenin signaling in tumor cells not only increases cellular proliferation but also silences CCL4 transcription, causing a recruitment failure of cDC1s and a complete collapse of $CD8^+$ T cell priming and anti-tumor immunity [16]. Thus, tumor cells themselves can be an important source immunosuppressive mechanisms leading to immune exclusion or dysfunction.

The functional characteristics of myeloid cells are dictated by environmental signals

A defining characteristic of myeloid cell populations is their plasticity, and the ability of these cells to respond to environmental factors is unrivaled when compared to other cell types [51]. As such, exposure of myeloid cell compartments to the TME results in huge shifts in the function and behavior of these cells, typically towards an immunosuppressive phenotype. These newly developed immunosuppressive populations are often referred to as myeloid derived suppressive cells (MDSCs), which develop from infiltrating neutrophil and monocyte populations [52]. MDSCs are named due to their functional ability to suppress cells *ex vivo*, rather than based upon uniquely identifying surface markers, making it impossible as of now to reliably distinguish bonafide MDSCs from newly arrived neutrophils and monocytes that may initially lack suppressive characteristics [53]. Regardless, it is well documented that neutrophils/MDSCs in the TME produce large amounts of immunosuppressive factors including reactive oxygen species (ROS), iNOS, and Arg1 [54–56]. These factors shape the TME, often inducing other immunosuppressive cells, albeit direct cellular contact is required for neutrophils to mediate these effects.

Another important immunosuppressive myeloid cell population comes from the macrophage compartment. Macrophages that are "alternatively activated" by treatment with IL-4 are known as "M2" macrophages and exhibit a tissue repair phenotype generally associated with anti-inflammation, tissue remodeling, and wound healing [57]. Within the context of cancer, tumor-associated macrophages (TAMs) develop from both tissue resident macrophages and monocyte-derived macrophages, often assuming an M2-like immunosuppressive phenotype associated with increased tumor burden and poor patient outcome [58,59]. Development of M2-like TAMs occurs from exposure to cytokines found in the TME like TGF-β, IL-10, and IL-4, which can be produced by tumor cells and other immune populations [60]. Similar to MDSCs, M2-like TAMs

can also produce and act through Arg1, however unlike MDSCs they do not require cell-cell contact to mediate effects as they also produce many immunosuppressive cytokines which act at a distance, including TGF-β, IL-10, and IL-4 [61]. One can appreciate the intense positive feedback loop potential here, with M2-like TAMs reinforcing their own immunosuppressive phenotype while also causing any newly arrived macrophages to develop the M2-like phenotype. M2 TAMs can also have functional effects on T cells by recruiting Tregs through CCL20 and CCL22 expression [62], as well as directly inhibiting CTL activity through expression of ligands for inhibitory receptors like PD-L1 [63].

Macrophages, like all myeloid cells, can drastically shift their phenotype based on environmental factors and while TAMs default towards an immunosuppressive phenotype, in the right circumstances they can also become proinflammatory while in the tumor [64]. Similar to the classical inflammatory "M1" macrophage phenotype observed outside of tumors, TAMs are induced and become M1-like after exposure to inflammatory cytokines like IFN-γ and TNFα [62,65]. Once induced, production of TNFα, IL-1β, and IL-12 by M1-like TAMs contributes to a pro-inflammatory environment within the tumor and is thought to directly impact $CD8^+$ T cell functionality [61,66]. Indeed, recent clinical data has shown that increased M1/M2 ratios within tumors are correlated with survival, and it is theorized that a repolarization event shifting TAMs from M2-like to M1-like could have significant therapeutic benefit [65,67]. It is important to note that rather than existing as easily defined binary states, there is strong evidence that macrophage activation lies along a spectrum, with "M1" inflammatory cells at one end and "M2" anti-inflammatory cells at the other [68]. Thus, when phenotyping a macrophage population, one must state the markers used before identifying where these cells may lie along the activation spectrum. The concept of a spectrum of activation is further reinforced by the observable plasticity of these

cells, as their marker expression and location on the spectrum is entirely defined by the combined effects of all external stimulatory factors [69]. Experiments involving IFN-β treatment of B16 cells provide a proof of concept that TAMs indeed can transition from M2-like towards a M1-like inflammatory phenotype in vivo [70], however to date there are no clinically available drugs capable of converting TAMs from an M2-like to M1-like phenotype and it remains an area rich for development.

Checkpoint signaling, therapeutic successes and failures

There are intrinsic negative feedback mechanisms within $CD8^+$ T cells that cause inhibition, dysfunction, and anergy [24]. These surface markers are collectively referred to as "inhibitory checkpoint signaling" and when bound to their ligand trigger inhibitory cascade signaling within CTLs, reducing their ability to produce cytokines and lyse tumor cells [71]. The most well characterized of the immune checkpoint molecules is the PD-1/PD-L1 interaction, where PD-1 expressed on activated $CD8^+$ T cells triggers cellular inhibition after cell-cell contact with tumor cells and TAMs expressing the corresponding ligand PD-L1 [72]. This signaling is quite powerful, as disruption of the PD-1/PD-L1 axis is sufficient to improve $CD8^+$ T cell responses leading to clinical success and durable responses, even as a monotherapy [73,74]. While anti-PD-1-based monotherapy therapy is FDA approved and used across several tumor types, superior clinical results have already been observed when paired with another checkpoint marker such as CTLA-4. This promise of enhanced synergy through inhibition of multiple checkpoint markers has led to a vast number of checkpoint inhibitors currently working through clinical trials, pairing with current PD-1 therapeutics [75].

Despite checkpoint therapy leading to durable complete responses in some patients, treatment in a majority of patients ultimately fails. For example, in a study of melanoma patients

who received combination therapy, only 22% experienced complete response to Nivolumab + Ipilimumab after 5 years [76]. More interesting however was that the objective response rate over those 5 years was 58%, implying many patients initially responded, then became resistant to treatment and relapsed. Clinical success clearly shows that checkpoint signaling is the dominant suppressive mechanism in a substantial fraction of melanoma patients, but the high relapse rate begs the question: what is different between patients with a complete response compared to those with a partial response, and why do many patients ultimately relapse? It is likely that in these relapsing partial responders, one or more alternative immunosuppressive mechanisms emerge as the dominant force in restraining CTLs, allowing for escape. In order to overcome these clinical hurdles, careful examinations of immunosuppressive mechanisms are crucial for development of novel therapeutic interventions capable of synergizing with anti-PD-1-based therapies.

While addition of other checkpoint inhibitors will likely improve the overall number of responding patients, perhaps the most promising area of study is the combination of these drugs with treatments outside of checkpoint inhibition, such as with other immunotherapies, radiotherapy, and chemotherapy [77]. For example, complete elimination of TAMs using a CSF-1R inhibitor significantly improved response to anti-PD-1 treatment in mice [78]. Even if elimination of a single immunosuppressive mechanism is not sufficient for complete response, it could then be paired with checkpoint-based immunotherapy to target multiple pathways of immune inhibition simultaneously. While substantial progress has been made, the question remains: can we identify novel mechanisms controlling tumor inflammation and develop therapies to overcome immunosuppression?

1.3 Characteristics of the inflamed and non-inflamed tumor microenvironment

Generally, one can classify patients by either having a T cell-inflamed TME, or a non-T cell-inflamed TME [36]. Traditionally T cell inflammation was determined by immunohistochemistry (IHC) staining of tumor biopsies, however as the expression of T cell associated genes strongly correlates with the presence of T cells, current methods utilize RNA sequencing (RNAseq) [35,79]. While the specific immunosuppressive mechanism(s) preventing tumor shrinkage by CTLs is often not known in these cases, determining the inflammatory status of a patient is still important as it correlates with improved overall survival in melanoma patients [3]. Furthermore, across many tumor types a T cell-inflamed gene expression pattern is necessary for response to checkpoint therapy [1]. Indeed, identifying the inflammation status of a patient not only assists with identifying likely responders to checkpoint therapy, but the effects of certain radiotherapy and chemotherapy treatments contain significant contributions from the endogenous immune response making tumor inflammation a potentially critical factor even in therapies traditionally not associated with immunity [18,80].

Potential mechanisms controlling inter-patient heterogeneity in the T cell-inflamed tumor microenvironment

With the ability to define an T cell-inflamed and non-T cell-inflamed TME, it is possible to uncover the mechanisms underlying the tremendous variability observed across patients by leveraging and comparing these two states. Across all tumor types represented in the cancer genome atlas (TCGA) there is substantial variation in the relative expression of T cell associated genes, as well as in the range within each patient population. With tumors such as melanoma and non-small cell lung cancer, around 30-40% of samples can be scored as T cell-inflamed, where other tumors such as primary brain cancers and uveal melanoma, fewer than 1% of tumors can

be scored as such [9]. Skin cutaneous melanoma (SKCM) samples are particularly useful, as approximately one-third are T cell-inflamed, one third are non-T cell-inflamed, and one-third are intermediate [9]. This range generates an ideal scenario for investigating the underlying mechanisms of inter-patient heterogeneity. Our laboratory has pursued three major hypotheses for inter-patient heterogeneity that mechanistically may contribute to the magnitude of the T cell-inflamed TME [81]. These are tumor cell-intrinsic oncogenic events, environmental factors such as the composition of the gut microbiota, and germline variants in immune regulatory genes. Oncogenic pathways impact on the process of carcinogenesis, but also may regulate expression of immunologically relevant genes by cancer cells [49]. In a mouse melanoma model, constitutive β-catenin signaling directly inhibited CCL4 cytokine production, leading to a lack of cDC1 infiltration and a failed $CD8^+$ T cell response [16,82]. The commensal gut microbiota has been shown to be extraordinarily powerful in shaping overall system-wide immunity [83]. In a mouse melanoma model, the presence of specific Bifidobacterium strains was sufficient to improve T cell infiltration and overall anti-tumor immunity [84]. In addition, distinct commensal bacteria associated with clinical response versus resistance to anti-PD-1 therapy were identified in patients with metastatic melanoma [85]. This has led to fecal microbial transplantation as a potential therapeutic strategy for expanding immunotherapy efficacy [86]. Finally, it is well established that germline variants in immune regulatory genes can have causal effects on the development of autoimmune diseases [42,87]. This phenomenon forms the basis of our third hypothesis, in which germline polymorphisms in immune regulatory genes may affect the host endogenous T cell immune response to solid tumors.

1.4 Genome-wide association studies allow for identification of novel gene targets

Since the advent of high throughput DNA sequencing and the human genome project, a major goal of researchers has been to determine the impact of inherited germline polymorphisms on human health and disease. These studies have been extremely fruitful, producing clinically actionable findings leading to novel therapeutic approaches as well as determining overall disease risk for patient groups. One method, known as the genome-wide association (GWA) study, has been an incredibly useful tool for identifying novel connections between regions of the genome and specific phenotypes [88]. A particularly successful area has been identifying polymorphisms linked with immune-mediated disease states such as autoimmunity, inflammation, and allergy. In fact, a review in 2013 cataloged 199 independently associated genetic loci linked across 12 different autoimmune disorders including Crohn's disease, multiple sclerosis, and rheumatoid arthritis, showcasing the power of such studies [89].

The fine line between SNPs and eQTLs

The typical GWA scan examines the connection between a phenotype of interest and single nucleotide polymorphisms (SNPs), testing any potential relationship via statistical methods. A SNP is simply a location on the genome where a single base is different in one group of individuals compared to other members within a population, and in 2015 the 1000 genomes project estimated there are nearly 85 million SNPs across all of humanity [90]. SNPs can be "silent" and have no detectable effect on gene expression, or they can directly influence gene expression and are classified as expression quantitative trait loci (eQTLs). SNP eQTLs can occur either in cis, when the SNP is located within 1 Mb (megabase) of the gene it effects, or in trans, when the SNP is located 5 Mb or more from the gene it alters [91]. Trans-acting eQTLs can also exist silently in coding region of a gene while only influencing expression of a different, distant

gene, underscoring the idea that a SNP's location does not automatically dictate how it might affect gene expression. Thus, when a SNP of interest is identified, it must be interrogated with a gene tissue expression (GTEX) database to determine whether it acts as an eQTL on any particular gene regardless of where it is located.

The powerful advantage of GWA studies is that they are unbiased, allowing the examination of genomic regions normally ignored due to experimental constraints and bias. While many early GWA studies connected genes to qualitative binary phenotypes, such as whether a patient did or did not have a certain disease, modern day GWA studies often utilize quantitative traits. In fact, there is evidence that utilizing quantitative phenotypes in GWA scans boosts the power to detect genetic effects [92]. For example, rather than classifying patients as either inflamed or non-inflamed, developing a quantitative score describing the dynamic range of such a phenotype would theoretically yield greater statistical power and may uncover an association with a smaller sample size compared to a traditional binary phenotype.

1.5 Background information on Protein Kinase C Delta

PKCδ, encoded by the gene *PRKCD*, is part of a multigene superfamily of serine/threonine kinases implicated in a wide range of biological processes and which span 10 different isotypes split into 3 subtypes [93]. While all PKCs require a phospholipid activator like phosphatidylserine, the secondary messenger requirements determine how each isoform is classified. Classical PKCs include α, β, and γ, which require both Ca^{+2} and diglyceride (DAG) for activation, while atypical PKCs (ι and ζ) do not require either. PKCδ along with ν, ε, and ο are considered novel isoforms, which require DAG but not Ca^{+2} [94]. In addition to these secondary activation molecules, PKCδ is regulated by phosphorylation sites, as well as through

proteolysis which yields a catalytically active fragment [95]. PKCδ has several unique features compared to the other PKC family members including tyrosine phosphorylation sites not found across the other isoforms in both the regulatory and catalytic domains [96]. This had led to speculation that PKCδ may be uniquely regulated among all PKCs [97].

PKC family members cover a broad array of functions and roles across cell types and PKCδ in particular has been connected to a wide range of functions and ligands making it difficult to generalize it's exact functional roles in health and disease [97]. A fundamental reason behind this confusion is that many cell types express multiple PKC family members, making it difficult to identify functional contributions of individual isoforms, especially with older experimental techniques. Complicating matters, studies investigating PKC isoform functions often utilize the pharmacologic agonist PMA, which is non-specific and strongly activates all PKCs. Many older studies also used pharmacologic inhibitors, which are not entirely specific and can exert off-target effects. With these considerations in mind, the ideal approach for studying PKCδ function is through genetic deletion leading to a loss of functional protein.

PKCδ effects on human health

While the *in vitro* data from the field suggests PKCδ may have functional roles in several different cell types, PKCδ loss *in vivo*, gives rise to a clear autoimmune phenotype in both humans and mice. Germline mutations leading to complete loss of PKCδ protein expression have been identified in human patients, all of whom present with cases of familial systemic lupus erythematosus (lupus) [98]. These patients are reported to have defective B cell apoptosis and hyperproliferation, as well as loss of B cell tolerance resulting in production of autoantibodies, but have no other major abnormalities [99]. The importance of PKCδ to the immune system was

further confirmed after investigation of PKCδ KO mice, which also showed signs of lupus but otherwise developed normally with no other gross abnormalities [100]. Similar to the observation in humans, B cells from these mice were found to be hyperproliferative and produce autoantibodies, and a transfer of PKCδ KO B cells into wildtype (WT) host animals suggested that these effects may be B cell-intrinsic [101]. Meanwhile T cell function did not seem to be altered in these contexts. While other studies utilizing PKCδ KO mice have linked PKCδ loss in mice to insulin sensitivity [102], increased hepatic insulin signaling [103], and increased arteriosclerosis after vein grafts [104], the main phenotypic effects appear to be entirely immune-based. However, no investigations of a potential role for host PKCδ in anti-tumor immunity and immunotherapy efficacy has been reported, thus supporting further investigation as our own preliminary data emerged.

Chapter 2: Materials and Methods

2.1 Melanoma T cell-inflamed gene signature score

A list of 13 genes was previously shown to be associated with a T cell-inflamed tumor microenvironment, consisting of *CCL2, CCL3, CCL4, CXCL9, CXCL10, CD8A, GZMK, HLA-DMA, HLA-DMB, HLA-DOA, HLA-DOB, ICOS, IRF1* [16]. Using the cancer genome atlas skin cutaneous melanoma dataset (TCGA-SKCM), we fit a sparse linear regression (Elastic Net) by modeling the independent response vector as the mean of the 13 empirically studied genes, and the dependent variables as a matrix of genome-wide gene expression values (around 18,000 transcripts). The model selected 69 genes associated with the 13 gene empirical signature which were as follows: *AIM2, ANKRD22, APOL4, B2M, C16orf54, C4orf7, CCL4L2, CCL5, CCL8, CD244, CD38, CD52, CD69, CD74, CD80, CD8B, CD96, CIITA, CRTAM, CST7, CTLA4, CXCL11, CXCR6, DOCK8, FAM26F, FASLG, GBP1, GBP2, GBP4, GBP5, GPR18, GZMA, GZMH, HAPLN3, HAVCR2, HLA-B, HLA-DPA1, HLA-DPB1, HLA-DPB2, HLA-DQA2, HLA-DQB1, HLA-DRA, HOXA5, IFNG, IGSF6, IL15RA, IL18BP, ITGAL, KLHL5, LAG3, LGALS2, LY9, PIM1, PLA2G7, PLEK, PSMB9, PTGER4, RASGEF1B, SH2D1A, SLA2, SPN, THBD, TNF, TNIP3, TRAT1, UBD, XCL1, XIRP1, ZBED2*. This combined list of 82 genes is hereafter referred to as the T cell-inflamed gene signature.

2.2 Genome-wide association study

A total of 258 samples were accessed from TCGA-SKCM. To form the phenotype for a GWA study, RNAseq values were log2 normalized, centered, and scaled. For each individual patient, the mean expression level for all 82 genes representing the averaged T cell-inflamed

gene signature score was computed. The following quality controls were utilized: SNPs were filtered based on having a minor allele frequency (MAF) of > 0.10, and a Hardy-Weinberg Equilibrium (HWE) > 0.005. Individuals were filtered based on European ancestry, relatedness < 0.05, and SNP missingness at < 0.05. Bonferroni's method was used to correct for multiple testing to determine genome-wide significance. We subsequently interrogated the genome-wide significant SNP rs1483185 , rs1483186 and rs750170 as expression quantitative trait loci (eQTLs) using MatrixEQTL in a lymphoblastoid cell line dataset [105,106].

2.3 Calculation of gene signature scores for expanded TCGA analysis

A quantitative scoring system was used to assign a value to each tumor sample in TCGA-SKCM dataset based on the expression profile 160 genes from a T cell-inflamed gene signature previously described [107]. For the M1/M2 ratio, externally validated M1 and M2 lists generated from the CIBERSORT regression model were utilized (Table S4) [108]. RNA sequencing gene expression data for melanoma and lung squamous was downloaded from TCGA data in the form of Z scores from the PanCancerAtlas [109,110]. Each signature score is the summation of all the Z scores for the genes in that list. The M1/M2 ratio was calculated by dividing the summed M1 score by the summed M2 score, yielding a single number. TCGA cases were labeled as homozygous minor, heterozygous, or homozygous major for each single nucleotide variant (SNV) at the alleles of interest for *PRKCD* (rs143185, rs143186, and rs1483185). The T cell-inflamed gene signature score and M1/M2 scores were then compared between each germline SNV group by ordinary one-way ANOVA and multiple comparisons (GraphPad, Prism 9).

2.4 Generation of mouse bone marrow chimeras

PKCδ-KO (also referred to *Prkcd*$^{-/-}$) mice were obtained as a generous gift from the lab of Dr. C. Ronald Kahn and bred at the University of Chicago [11]. *Prkcd*$^{+/+}$ (PKCδ-WT) and *Prkcd*$^{-/-}$ (PKCδ-KO) donor mice were sacrificed at 6-10 weeks. Femurs and tibias were collected and flushed with PBS using a 26G needle. Kneecaps were minced using scissors and the bone marrow was passed through a 70uM filter (Fisher, 352350). CD90.2 cells were then depleted via MACS column separation (Miltenyl, 130-121-278) before bone marrow cells were counted and resuspended in PBS for sterile intravenous injection. 24 hours before engraftment, B6.SJL-*Ptprc*^{a}/BoyAiTac mice (Taconic, 4007, CD45.1) sex-matched transplant recipient mice were irradiated with 5 Gy and 5.5 Gy (Cesium 137 source) with a 3-hour rest period in between. Bone marrow was injected intravenously via retro-orbital injection with a minimum of 4.0×10^6 cells injected per host mouse in a volume of 100ul PBS. Mice were allowed to rest of a minimum of 8 weeks before experimental use. All animal procedures were approved by the Institutional Animal Care and Use Committee of the University of Chicago.

2.5 PKCδ colony background check

The genetic backgrounds of mice were assessed at the DartMouse™ Speed Congenic Core Facility at the Geisel School of Medicine at Dartmouth. DartMouse uses the Illumina, Inc. (San Diego, CA) GoldenGate Genotyping Assay to interrogate 1449 SNPs spread throughout the genome. The raw SNP data were analyzed using DartMouse's SNaP-Map™ and Map-Synth™ software, allowing the determination for each mouse of the genetic background at each SNP location.

2.6 Tumor implantation

B16-F10-SIY-dsRed (referred to as B16-SIY subsequently) were thawed, grown in cDMEM media (DMEM, 10% FBS, 1% NEAA, 1% Penn-Strep, 1% MOPS buffer) and passaged 2-5 times before experimentation. Cells were washed 3x with PBS before being resuspended at $2x10^6$ cells per 100ul of PBS and 100ul of cells was injected subcutaneously into the right flank. The length, width, and height of a tumor was measured by calipers 3 times a week and the volume was calculated using the following formula. (4/3 * pi * L/2 * W/2 * H/2)

$$\frac{4}{3} \times \pi \times \frac{L}{2} \times \frac{W}{2} \times \frac{H}{2}$$

2.7 Cell isolation

Tumors were excised, mechanically dissociated, and incubated with a mixture of 10 mg/ml collagenase type IV (Sigma, C5138), 1 mg/ml hydrogenase type V (Sigma, H6254), and 2,000 units/ml DNAse type IV (Sigma, D5025-150ku) for 45 minutes at 37 °C before being washed with PBS through a 70uM filter (Corning, 352350). Digested tumor samples were then passed through a Ficoll-Paque gradient (Cytivia Life Sciences, 17144003), and the bilayer was collected. Spleens were mechanically dissociated and washed through a 70uM filter before RBC lysis by incubation with Gey's solution for 2 minutes at room temperature (RT). For splenic DC isolation, spleens were gently mechanically dissociated and incubated with the same collagenase mixture as above for 20 minutes at 37 °C before being washed with PBS through a 70uM filter.

2.8 Flow cytometry and cell sorting

Cells were incubated with appropriate antibodies (Table 1) in FACS buffer (PBS, 5% FBS, 10uM EDTA) for at least 30 minutes at 4 °C. When necessary, cells were fixed in 1% PFA

or fixed and permeabilized using a kit (Invitrogen, 00-5523-00). Any intracellular staining was performed overnight at 4 °C. Both traditional (BD Fortessa 4-15, BD LSR Fortessa X-20) and spectral flow cytometers (Cytek Aurora) were employed, and analysis performed using FlowJo software (Treestar). Fluorescence activated cell sorting (FACS) was performed entirely under sterile conditions. Sorting was performed on a AriaIIIu (BD) and samples were sorted into FACS buffer before further analysis. To ensure purity, post-sort samples were run immediately after initial sort set up, and a given population of interest was required to be >90% of all live cells. Percentages of T cells was calculated as follows ((Number of living cells in population/ Number of living $CD3^+$ T cells)X 100). Number per gram tumor was calculated as follows ((number of living cells/ tumor weight)X sample dilution factor).

Table 1: Table of flow cytometry antibodies

Antigen	Fluorophore	clone	dilution	verdor	cat-number
Caspase3	BV605	C92-605	1:50	BD Bioscience	564094
CD70	BV711	FR70	1:200	BD Bioscience	740741
Ki-67	BV711	B56	1:200	BD Bioscience	563755
Brilliant Stain Buffer	N/A	N/A	1:2.5	BD Bioscience	566349
Brilliant Stain Buffer Plus	N/A	N/A	1:5	BD Bioscience	566385
CD69	BUV563	H12F3	1:200	BD Bioscience	741234
CD72	BUV395	K10.6	1:200	BD Bioscience	745642
CD86	BUV496	PO3	1:200	BD Bioscience	750437
CD8a	BUV395	53-6.7	1:200	BD Bioscience	563786
Ly6G	BUV661	1A8	1:200	BD Bioscience	741587
CD11c	AF647	N418	1:200	BioLegend	117312
CD4	PerCP-Cy5.5	RM4-5	1:200	BioLegend	100540
FC BLOCK	N/A	93	1:100	BioLegend	101302
CD103	BV421	2E7	1:200	BioLegend	121422
CD11b	APC	M1/70	1:200	BioLegend	101212
CD11b	BV570	M1/70	1:200	BioLegend	101233
CD11c	BV650	N418	1:200	BioLegend	117339
CD14	FITC	Sa14-2	1:200	BioLegend	123308

Table 1: Continued

CD19	AmCyan BV510	6D5	1:200	BioLegend	115546
CD206	BV605	C068C2	1:200	BioLegend	141721
CD3	(PacBlue) BV421	17A2	1:200	BioLegend	100228
CD3	Alexa Fluor 700	17A2	1:200	BioLegend	100216
CD3	APC-Cy7	145-2C11	1:200	BioLegend	100330
CD3	BV711	17A2	1:200	BioLegend	100241
CD4	BV605	RM4-5	1:200	BioLegend	100547
CD4	BV711	RM4-5	1:200	BioLegend	100549
CD4	Spark NIR 685	GK1.5	1:200	BioLegend	100476
CD45.1	Pac Blue	A20	1:200	BioLegend	110722
CD45.2	APC-Cy7	104	1:200	BioLegend	109823
CD45.2	BV785	104	1:200	BioLegend	109839
CD80	PE/Dazzle 594	16-10A1	1:200	BioLegend	104738
CD84	PE	mCD84.7	1:200	BioLegend	122805
CD8a	BV510	53-6.7	1:200	BioLegend	100751
CD8a	BV605	53-6.7	1:200	BioLegend	100744
CD8a	BV711	53-6.7	1:200	BioLegend	100747
CXCR2 (CD182)	PE-Cy7	SA044G4	1:200	BioLegend	149315
F4/80	FITC	BM8	1:100	BioLegend	123107
I-A/I-E	Pacific Blue	M5/114.15.2	1:200	BioLegend	107620
I-A/I-E	PE-Cy7	M5/114.15.2	1:200	BioLegend	107630
Fixable Viability	Zombie NIR	N/A	1:800	BioLegend	423105
Ly6C	Alexa Fluor 700	HK1.4	1:200	BioLegend	128023
Ly6C	BV785	HK1.4	1:200	BioLegend	128041
NK1.1	APC-Cy7	PK136	1:200	BioLegend	108724
CD8a	PerCP-eFluor 710	53-6.7	1:200	eBioscience	46-0081-82
F4/80	PerCP-Cy5.5	BM8	1:100	eBioscience	45-4801-80
Foxp3	Alexa Fluor 488	FJK-16s	1:100	eBioscience	53-5773-82
Fixable Viability	eFluor506		1:500	ebioscience	65-0866-14
CD45	AF532	30-F11	1:200	Invitrogen	58-0451-82
SIY	PE	SIYRYYGL	1:25	ProImmune	1803

2.9 Stimulation of donor T cells

A round bottom tissue culture 96 well plate was coated overnight at 4 °C with anti-CD3 (0.3 ug/ml, biolegend, 100339) and anti-CD28 (0.5 ug/ml, biolegend, 102115) antibodies. Plates

were washed and blocked with cRPMI media (RPMI, 10% FBS, 1% NEAA, 1% Penn-Strep, 1% MOPS buffer, 1x 2-Beta ME) for minimum 30 minutes at RT. Spleens were isolated and mechanically dissociated before RBC lysis by incubation with Gey's solution for 2 minutes at RT. Splenic cells were then incubated with cell trace violet dye per manufacturer's instructions (Invitrogen, C34557). Cells were added at $1x10^6$ cells per well in cRPMI and incubated for either 48 or 72 hours at 37 °C and 6% CO2. Cells were stained with the following and assessed for proliferation and cytokine production (Live-Dead APC-Cy7, CD4 PerCP-Cy5.5, CD8 BV711, CD44 PE-Cy7, IFN-γ APC, TNFα FITC, B220 PE, MHCII PE).

2.10 Cross-priming and free peptide priming assays

Splenic DC and T cells were isolated as described above. Dendritic cells were isolated via negative selection of splenic cells post collagenase treatment using a MACS Pan DC Isolation kit and manufacturer's protocols were followed (130-100-875). 2CxRag2$^{-/-}$ mice were bred at the University of Chicago and previously described [111]. Splenic 2C CD8$^+$ T cells were isolated by using a CD8$^+$ T cell MACS negative isolation kit (Miltenyi, 130-104-075). For the free peptide assay, 2C CD8$^+$ T cells were incubated in 10uM CFSE (Invitrogen, C34553), diluted in serum free DMEM for 10 minutes at 37 °C, and cells were mixed every 2 minutes. For the cross-priming assay, 2C CD8$^+$ T cells were instead incubated with cell trace violet (Invitrogen, C34557) as per manufacturer's instructions. In a round bottom tissue culture plate, 50,000 DCs and 100,000 dye labeled 2C CD8$^+$ T cells were added per well in cDMEM. In the free peptide assay, each well received either 0.2, 0.4, 0.8, 1.6, 16, or 160 nM of SIY peptide. For the cross-priming assay, B16-SIY cells were utilized as the source of antigen and irradiated with 100 Gy, ensuring most cells could be actively processed by the DCs. Using the concentration of cells

assessed prior to irradiation, 5,000, 25,000, or 50,000 irradiated cells were added to wells. To provide comparison to the free peptide assay, a set of wells received 160 nM of SIY peptide instead of irradiated B16-SIY. As a control to assess the inherent stimulatory capabilities of irradiated B16-SIY cells, labeled 2C cells were cocultured with 25,000 irradiated B16-SIY cells with no DCs present. For the free peptide assay donor DCs came from an N of 4 mice, and the cross-priming assay came from an N of 2, and in both cases mice were treated as independent replicates. Additionally, all stimulation conditions utilized duplicate wells as technical replicates and results from each duplicate pair were averaged during analysis. In both assays, unlabeled 2C $CD8^+$ T cells were used as a negative staining control, wells coated with anti-CD3 (0.3 ug/ml, biolegend, 100339) and anti-CD28 (0.5 ug/ml, biolegend, 102115) antibodies were used as a positive control for proliferation, and wells receiving media with no antigen acted as the negative control for proliferation. Cells were incubated for 3 days at 37 °C and 6% CO2 and then stained with the following for analysis: Live-Dead APC-Cy7, CD3 BV711, CD11c BV605, CD8 PE, CD44 PE-Cy7, IFN-γ APC, IL-2 PerCP-Cy5.5, CFSE.

2.11 Enzyme-Linked Immunospot (ELISPOT) assay

Spleens from tumor-naïve WT-engrafted mice, tumor-bearing WT-engrafted mice, or tumor-bearing KO-engrafted mice were collected, with each individual mouse being considered an experimental replicate. Splenic cells were isolated as described above and plated at $1x10^6$ cells per well in T cell growth media (DMEM, 10% FBS, 1% NEAA, 1% Penn-Strep, 1% MOPS buffer, 0.1 mM beta-2ME). Negative control wells received T cell growth media only, while experimental wells received 160nM of H-$2K^b$ SIY peptide (SIYRYYGL), and positive control wells received PMA (50ng/ml) and Ionomycin (500ng/ml). Each experimental replicate had the

following technical replicates which were then averaged for each group: 2 negative control wells, 3 SIY peptide wells, and 1 positive control well. Cells were incubated overnight at 37 °C and 6% CO2 and the ELISPOT was performed according to the manufacture's protocol using the BD Mouse IFN-γ Elispot kit (BD Biosciences, 551083).

2.12 Rag KO T cell transfer

6-8 week old Male RAG2KO mice (B6.129S6-Rag2^{tm1Fwa} N12) were purchased from Taconic (RAGN12-M) and housed in our facilities. Spleens were isolated from donor *Prkcd*$^{+/+}$ or *Prkcd*$^{-/-}$ mice, mechanically dissociated, and treated with a mixture of 10mg/ml collagenase type IV (sigma, C5138), 1mg/ml hydrogenase type V (Sigma, H6254), and 200units/ml DNAse type IV (sigma, D5025) for 20 minutes at 37 °C before being washed with PBS through a 70uM filter (Corning, 352350). A MACS kit was used to positively select for Thy1.2 (CD90.2) cells. Purity verification was performed via flow cytometry and 5x10^6 donor cells per mouse were injected into hosts in 100ul of PBS via intravenous retro orbital injection. 24 hours later B16-SIY tumors were then established, and growth was tracked.

2.13 Anti-PD-L1 therapy

In bone marrow-engrafted animals, B16-SIY tumors were established until an average volume of 100 mm^3 was reached and then mice were split into control or treatment groups. The average volume of each group was matched at the time of separation. 3 times per week, 100ug of anti-PD-L1 (B7-H1, BioXcell, BE0101) was administered in 100ul of PBS via intraperitoneal (i.p.) injection, while control mice received 100ul of PBS via i.p. injection on the same days. In conditional KO animals, 100ug of anti-PD-L1 (B7-H1, BioXcell, BE0101) was administered in

100ul of PBS via i.p. injection 3 times per week starting 7 days after tumor implantation for 5 total doses, with control mice receiving 100ul of PBS via i.p. injection on the same days.

2.14 Single cell RNA sequencing

Engrafted mice were injected with B16-SIY and sacrificed after 26 days on 2 separate occasions and processed independently. On each collection day, immune cells from tumors were isolated as described above and stained with Live-Dead (APC-Cy7) and CD45.2 (FITC). Live $CD45.2^{+}$ cells were sorted into FACS buffer before being washed 3x in PBS. Single cell partitioning and library creation was performed by the University of Chicago Genomics core using a chromium controller from 10x genomics following the "Chromium Single Cell 3′ Reagent Kits v3" user guide and associated reagents. 10,000 cells were targeted and encapsulated per sample. Libraries were sequenced in PE100 format of an SP-100 flowcell of an Illumina Novaseq 6000 instrument.

2.15 Processing and analysis of scRNAseq data

Demultiplexing and alignment to the mm10 transcriptome (version 3.0.0) was performed, with count matrices created using the Cell Ranger pipeline (version 3.0.2). scRNA-seq count matrices were read by Seurat (version 3.2.3) (Stuart, Cell, 2019), and a single Seurat object was created from all samples from both collection days. Quality control filtering of cells was based on the following: less then 5% mitochondria genes expressed, with a minimum of 200 counts, and the number of unique molecular identifiers (UMIs) was set between 50 and 3,000. Overall, 41,187 cells passed the quality control metrics. Datasets were normalized using the "SCTransform" function and the top 3,000 features were identified using

"SelectIntegrationFeatures". These were used as anchor features while the Seurat object was prepared for integration using "PrepSCTIntegration", then all datasets were integrated using the "FindIntegrationAnchors" function. The scaled and integrated data was then processed using "RunPCA" with the first 100 principal components, followed by UMAP clustering analysis. Optimal UMAP resolution was determined by examining each resolution between 0.1 to 0.9 using 0.1 steps using the clustree r package [112]. A final resolution of 0.6 was chosen and markers for each cluster were determined using the "FindAllMarkers" function with a min.pct of 0.25 and a log fold-change threshold of 0.25. In total 24 unique clusters were identified, and each cluster was labeled by identifying a top uniquely expressed genes when compared to all other clusters (Table S1). For each unique cluster, "FindMarkers" was used to identify differentially expressed genes between WT and KO samples using the MAST test method. Genes that had a false discovery rate (fdr) >= 0.05 and a log fold-change (fc) magnitude >= 0.25 were considered significant. The fgsea package was used to perform gene set enrichment analysis for all DEGs in each cluster. The DoHeatmap package was used to illustrate differences in select genes by plotting the gene expression log-averaged across all cells in a given cluster, for each biological replicate.

2.16 Conditional KO mouse generation

A *Prkcd*$^{fl/fl}$ conditional KO (cKO) line was generated using Cyagen's TurboKnockout® gene targeting service. Exons 7-9 were targeted for conditional KO in C57BL/6J ES cells (Extended Data Fig. 4). Deletion of this region predicted a complete loss of function for the protein and was confirmed by genotyping (Table 2). Two independent strains were developed, labeled 2B4 and 2C1. The main strain featured throughout the paper is 2B4 although no

functional differences were observed at any point between the strains. Both were crossed with B6.Cg-*Commd10*$^{Tg(Vav1\text{-}icre)A2Kio}$/J (Jackson, 008610, referred to subsequently as "*Vav1*-iCre") as well as B6.129P2-*Lyz2*$^{tm1(cre)Ifo}$/J (Jackson, 004781, referred to subsequently as "LysM-Cre") at the University of Chicago. Female littermates between the ages of 7 and 12 weeks were used for all experiments.

Table 2: Table of primers for mouse genotyping

Target	Primer 1	Primer 2	Primer 3	WT Product	Mut Product
PKCδ	GCTCTATTGCCTCGGCTTCAT	AGGTGAGAAAGACAGCAAAGGG		563 bp	N/A
LacZ	TGATGCGGTGCTGATTACGAC	GTCAAAACAGGCGGCAGTAAG		N/A	225 bp
PKCδ cKO Target	TATGTTTTGAGAGCTTAGCAGGTG	GATGCTGTATAGGGGCAGGAAAG		199 bp	316 bp
PKCδ cKO Delete	TATGTTTTGAGAGCTTAGCAGGTG	GATGCTGTATAGGGGCAGGAAAG		N/A	259 bp
Vav1-iCre	AGATGCCAGGACATCAGGAACCTG	ATCAGCCACACCAGACACAGAGATC		N/A	236 bp
LysM-Cre	CCCAGAAATGCCAGATTACG	CTTGGGCTGCCAGAATTTCTC	TTACAGTC GGCCAGG CTGAC	350 bp	700 bp

2.17 Western blot

Spleens were isolated and mechanically dissociated before RBC lysis by incubation with Gey's solution for 2 minutes at room temperature. 1.2ml of Triton-X plus 1x protease inhibitor (Invitrogen, C34557) was added to the entire spleen and placed on ice for 30 mins. Samples were spun at max speed for 10 mins and supernatant was collected. A Bradford assay was performed to determine protein concentration. Laemelli buffer (Biorad 1610747) with 10% Beta-Mercaptoethanol was added to samples and boiled for 100 °C for 10 minutes. 10% Acrylamide gels were created in house and 30ug of protein was added to each well. 0.1% SDS in 1x Glycine/Tris running buffer was used and gels were run at 120V for at least 1 hour. Wet transfer onto nitrocellulose membrane was performed using transfer buffer consisting of 1x Glycine/Tris plus 1.5% Methanol for 1 hour at 100V. Membranes were then blocked for minimum of 1 hour

at RT using Odyssey® Blocking Buffer (LI-COR #927-50000) followed by incubation overnight at 4 °C with anti-PKCδ (Cell Signaling, 9616) or anti-Beta-Actin (Cell Signaling, 4970) antibody diluted in TBST. Secondary antibody and protein levels were measured by immunofluorescence using a Li-Cor Odyssey XF imaging system.

2.18 RNA isolation and qRT-PCR

Immune cells from tumors are isolated and sorted as described above. Tumor-associated macrophages (TAMs) marked as Live-Dead$^-$ CD45$^+$ CD90.2$^-$ B220$^-$ CD11b$^+$ Ly6G$^-$ F4/80$^+$ were isolated before being washed 3x in cold PBS. RNA was isolated using Qiagen RNeasy micro kit (Qiagen 74004) and cDNA was created using the High-Capacity cDNA Reverse Transcription Kit with RNase Inhibitor (Applied Biosystems™, 4374966). qPCR reactions were carried out using TaqMan master mix (Life Technologies) and defined primer/probe sets (Roche universal probe library) (Table 3). Reactions primers for *Trem2*, *Il1b*, and *TNF* genes were selected using the Roche primer design center website (discontinued) and the Roche universal probe library was used. Reactions were run on a StepOnePlus™ Real-Time PCR System (Applied Biosystems, 4376600) in MicroAmp™ Fast Optical 96-Well reaction plates (Applied Biosystems, 434907). Each sample was run in duplicate wells and the CT of those wells was averaged before expression levels were calculated DCT = $CT_{Gapdh} - CT_{Gene\ of\ interest}$; expression level = 2^{DCT}.

Table 3: Table of mouse qRT-PCR primers

Target	Primer 1	Primer 2	Probe (TaqMan)
IL-1β	agttgacggaccccaaaag	agctggatgctctcatcagg	38
CD72	ctgcactagcggacaaagc	ctgtaggacagcggggaat	1
TNFα	ctgtagcccacgtcgtagc	ttgagatccatgccgttg	25

2.19 Melanoma patient bulk RNAseq analysis

Patient data was collected according to the Biological Sciences Division Institutional Review Boards at the University of Chicago under the protocols 15-0837, 15-0788, and 17-0686. Samples were either formalin-fixed paraffin-embedded or fresh frozen before they were submitted for bulk RNA sequencing at the University of Chicago sequencing core. Patients were selected as follows. Metastatic melanoma patients that received immunotherapy after sample collection and had no history of prior immunotherapy treatments. Patients with Uveal, Acral, Mucosal types were removed, leaving cutaneous and unknown primary types. All tumor samples were collected before treatment anti-PD-1-based therapy. Patients were required to have clinical outcome data marked as either progressive disease (PD), stable disease (SD), partial response (PR), or complete response (CR). Kallisto and tximport were used to align to gencode primary assembly sequence (release 39) and export sequencing data while Limma and edgeR R packages were used to process the count matrices. Samples were filtered by a minimum of 5,100,000 reads and genes were filtered using the following cutoffs: a minimum of 30 samples were required to express a given gene and with a minimum counts per million (CPM) of 1. Normalization was done using the "calcNormFactors" function with the TMM method. Count data was transformed using "limmavoom" and data was centered using the scale function in R. The PKCδ-KO-related gene signature was created from genes in the C1qa cluster that were increased in PKCδ KO animals and had a positive log fold-change >0.25 and a fdr < 0.05. The biomaRt R package was used to convert the mouse gene list into their human orthologs. Any genes that did not have a match were dropped. 119 of 129 total genes were identified to have human counterparts and utilized for the signature (Table S5). The median expression of all signature genes was calculated for each patient and then plotted via violin plot. Patients were grouped by either "progression"

which consisted of the progressive disease (PD) group, or “disease control” which consisted of stable disease (SD), partial response (PR), and complete response (CR). A student’s t- test was performed on the data to assess significance.

2.20 Statistical analysis

All statistical analyses were performed using GraphPad Prism (Graphpad) with the exception of the GWA scan and scRNAseq analysis. Unless otherwise noted, all data are shown as mean ± s.e.m. and significance assumed with $p \leq 0.05$. Significance for growth curves was determined by two-way ANOVA and Sidak’s Multiple Comparisons test. Significance for bar graphs determined by unpaired t test. Significance for data presented in violin plots was determined by ordinary one-way ANOVA and Tukey’s multiple comparisons test. Survival curves were determined by Kaplan-Meier survival analysis and p values for Gehan-Brewslow-Wilcoxon test were reported.

Chapter 3: Using a genome-wide association study to identify a novel target for enhancing anti-tumor immunity

3.1 Introduction

The degree of endogenous immune cell infiltration in solid tumors can be predictive of response to PD-1/PD-L1 blockade yet is dramatically variable between individual patients [1,2]. As the underlying mechanisms determining the degree of a T cell-inflamed versus non-T cell-inflamed tumor microenvironment are not fully understood, uncovering novel molecular mechanisms that determine the inflammatory status of tumors is crucial for expanding the population of patients that clinically respond to checkpoint blockade therapy [11]. We hypothesized that one potential mechanism could involve germline polymorphisms in immune regulatory genes influencing a patient's baseline immune response to solid tumor-derived antigens. The Cancer Genome Atlas (TCGA), is a repository of over 20,000 primary cancer samples spanning 33 cancer types that includes tumor bulk RNA sequencing (RNAseq), tumor exome sequencing, and germline single nucleotide polymorphism (SNP) analysis. This resource enabled us to perform an unbiased genome wide association (GWA) study to detect novel associations between germline polymorphisms and the degree of immune cell infiltration into the tumor based on RNAseq. Any polymorphisms determined to be expression quantitaitive trait loci (eQTL)s after interrogation through a gene tissue expression (GTEX) database could then be followed up with mechanistic investigations in mouse models (Figure 3.1).

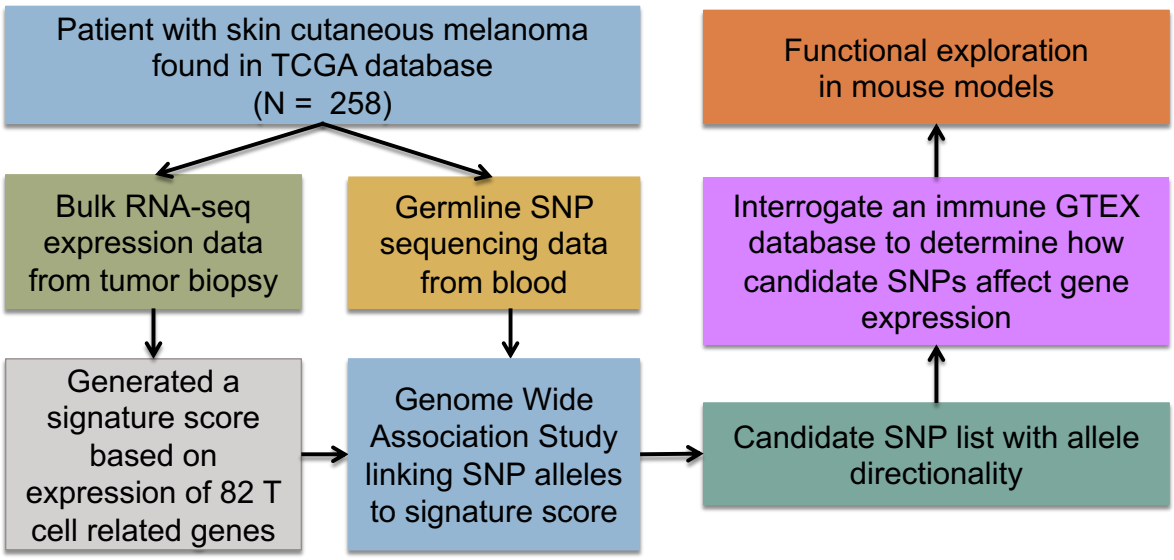

Figure 3.1: The workflow for identifying and confirming novel targets in anti-tumor immunity using a genome wide association study

3.2 GWA scan reveals multiple hits within the gene PRKCD

To investigate a potential association between germline variants and tumor immune gene signatures, skin cutaneous melanoma (SKCM) was chosen as a model as patients have a wide range of T cell-based inflammation, and because a substantial portion of the patients with T cell-inflamed tumors respond to anti-PD-1-based immunotherapy. Immune gene expression has previously been shown to reflect the degree of immune cell infiltration [35,79]. We first developed an immune gene signature score consisting of 82 total T cell-related genes that could be utilized as a quantitative phenotype reflective of the inflammatory status of each patient's tumor (Figure 3.2). We then integrated tumor RNAseq data with germline SNP data from 258 patients in the TCGA melanoma dataset and performed a GWA scan linking the magnitude of the T cell gene signature score with matched germline SNP data (Figure 3.3A). One SNP reached the threshold for genome-wide significance and was located within the 5' untranslated region (UTR) of the gene *PRKCD*, 3 Kb from the transcription start site (TSS).

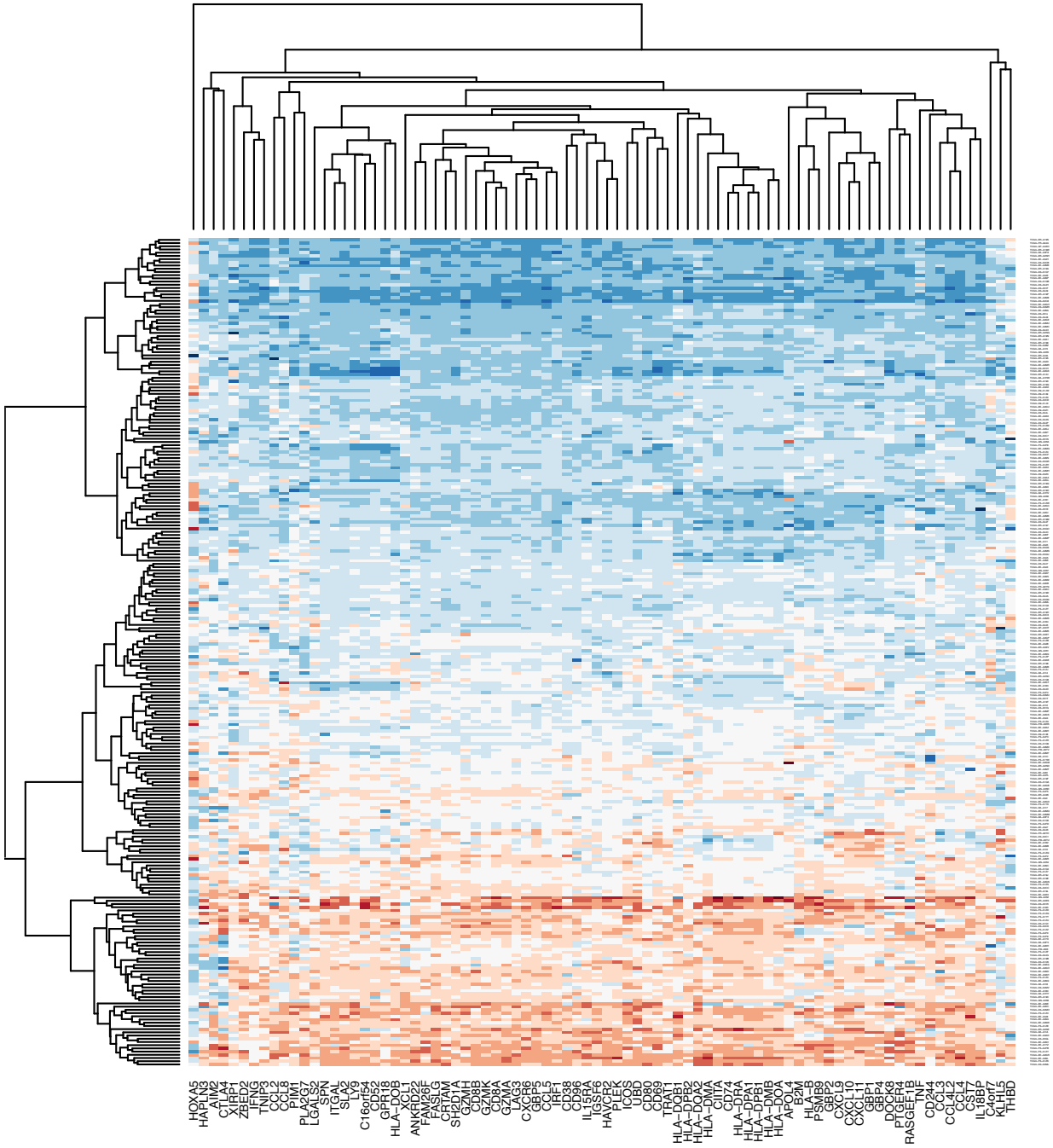

Figure 3.2: Heatmap of T cell signature genes across melanoma patients
Expression of 82 genes in the immune gene signature score featured as a heatmap with 258 patients utilized in the GWAS. Hierarchical clustering of samples was performed across the patient group.

Additionally, two other SNPs (rs1483186, rs750170) also located within *PRKCD* locus reached above the significance threshold, encouraging further examination. To determine directionality,

samples were plotted by genotype and gene score, revealing that the minor allele of the top GWA scan hit (SNP rs1483185) was positively associated with a higher magnitude T cell gene signature score ($p = 8.812e^{-08}$, Bonferroni corrected <0.05) (Figure 3.3B).

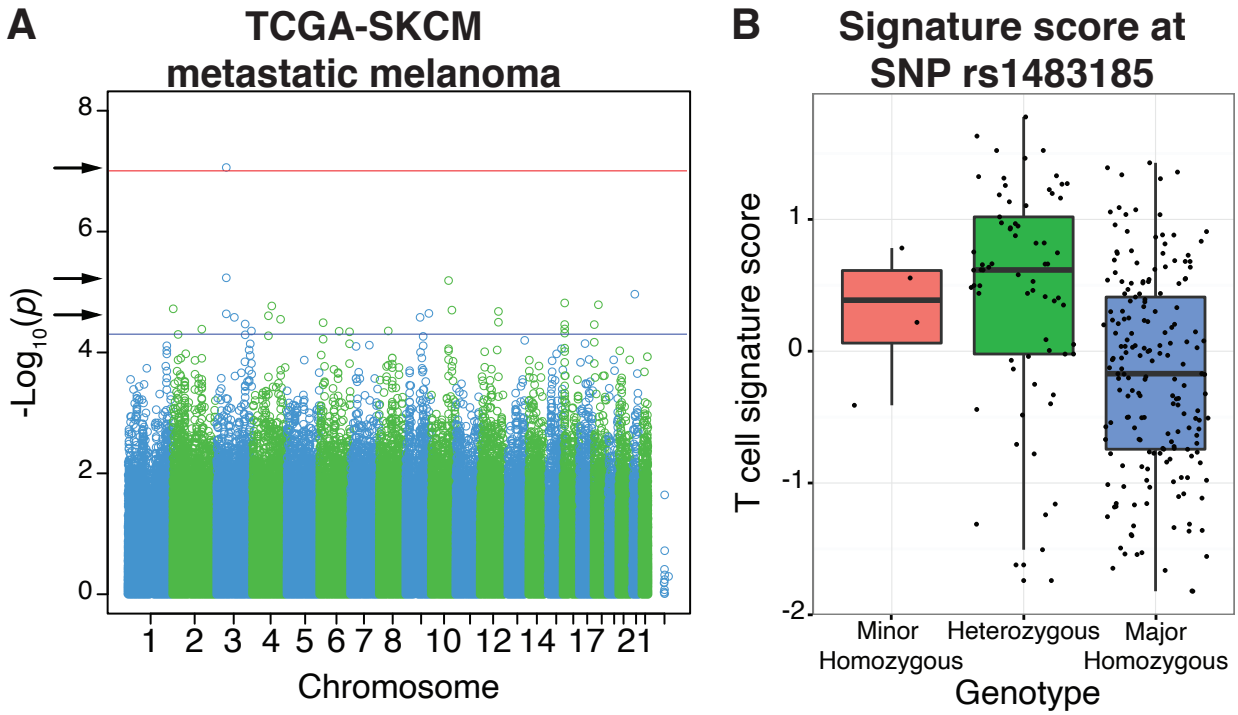

Figure 3.3: Genome wide association study reveals a SNP located in the *PRKCD* gene associated with increased T cell gene expression
(A) Manhattan plot of genome wide association results showing -log10(p-values) for all SNPs ordered by chromosomal position. Blue dashed line indicates suggestive significance threshold (p-value < 10^{-4}), red dashed line indicates threshold for genome wide significance (p-value < 10^{-7}). Arrows point to SNPs located within the gene *PRKCD*. **(B)** T cell gene expression score for each patient, plotted by genotype at SNP rs1483185 (p-value = $8.812e^{-08}$, Bonferroni corrected <0.05).

3.3 Validation of top SNP hits and confirmation of eQTL status

To extend these results, we also examined the relationship of the top SNPs with a more expansive T cell gene signature consisting of 160 genes [107]. In agreement with our GWA study results, the minor allele of SNP rs1483185, along with the minor alleles of SNP rs1483186 and SNP rs750170 correlated with an increase in the 160-gene signature score (Figure 3.4A-3.4C).

To go beyond melanoma, the lung squamous TCGA dataset was examined and the minor allele of SNP rs1483185 was again correlated with an increase in the 160-gene signature score (Figure 3.4D).

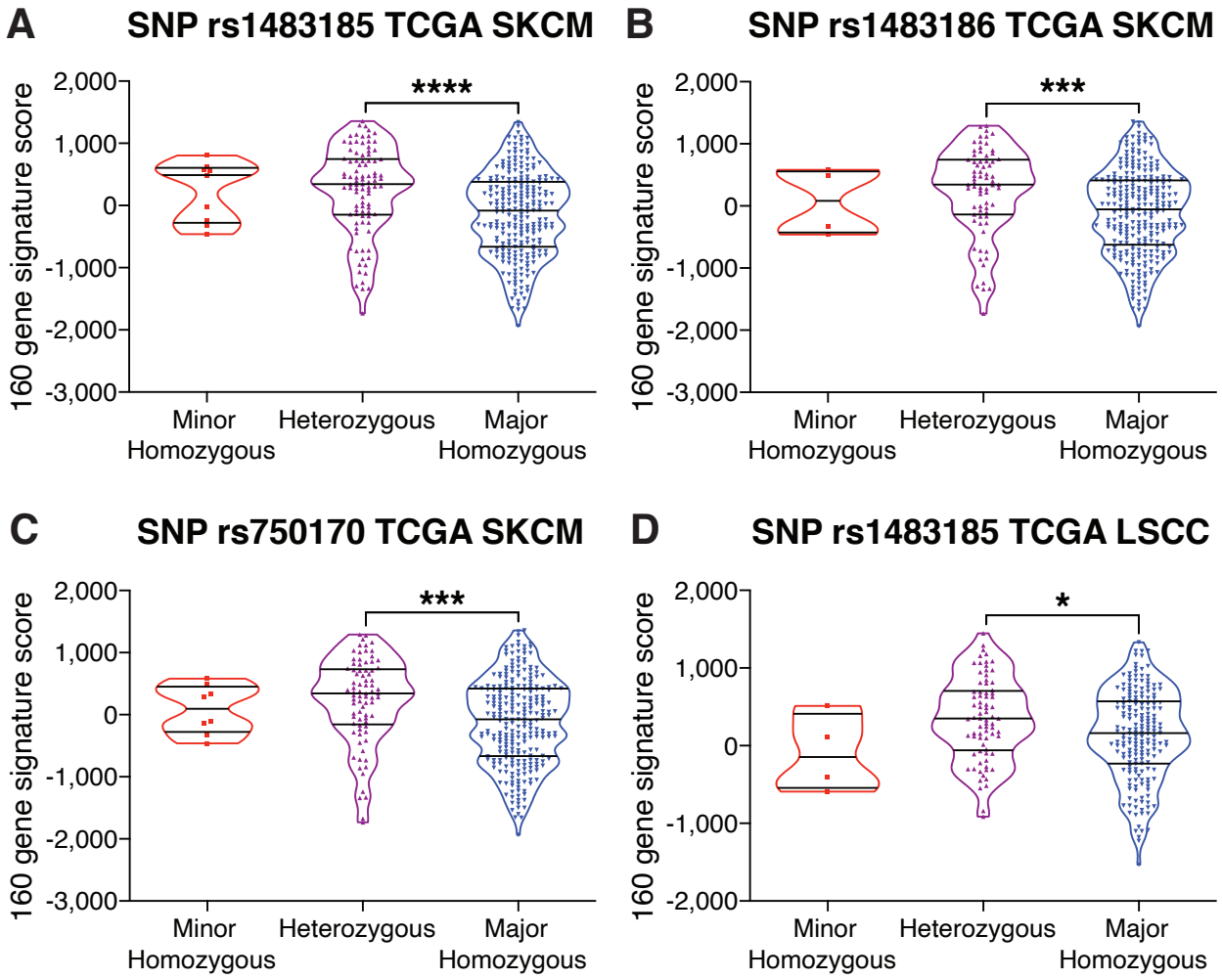

Figure 3.4: SNP alleles correlate with the 160 gene signature score in SKCM and LUAD
(A) Violin plot of patient 160 gene signature scores from a TCGA skin cutaneous melanoma (SKCM) dataset separated by homozygous minor, heterozygous, or homozygous major alleles at the SNP rs1483185. **(B)** Violin plot of patient 160 gene signature scores from a TCGA skin cutaneous melanoma (SKCM) dataset separated by homozygous minor, heterozygous, or homozygous major alleles at the SNP rs1483186. **(C)** Violin plot of patient 160 gene signature scores from a TCGA skin cutaneous melanoma (SKCM) dataset separated by homozygous minor, heterozygous, or homozygous major alleles at the SNP rs750170. **(D)** Violin plot of patient 160 gene signature scores from a TCGA lung squamous cell carcinoma (LUSC) dataset separated by homozygous minor, heterozygous, or homozygous major alleles at the SNP rs1483185.

Whether a given SNP is an eQTL for a gene, and how the alleles of that eQTL-SNP affect the directionality of gene expression, can be inferred using gene tissue expression (GTEX) databases. To address these questions, we utilized the MatrixEQTL algorithm in a lympoblastoid cell line dataset. We interrogated SNP rs1483185 and determined that the minor allele associated with decreased expression of the *PRKCD* gene and thus acting in a cis manner (Beta = 0.0551, p = 0.006) (Figure 3.5A, Figure 3.5B) [113]. Moreover, both rs1483186 and rs750170 also showed the same directionality as rs1483185 and were cis-acting with the minor allele associating with decreased expression of *PRKCD* (Figure 3.5B). Collectively, these data indicate that reduced host PKCδ gene expression is associated with increased T cell-based inflammation in the tumor microenvironment.

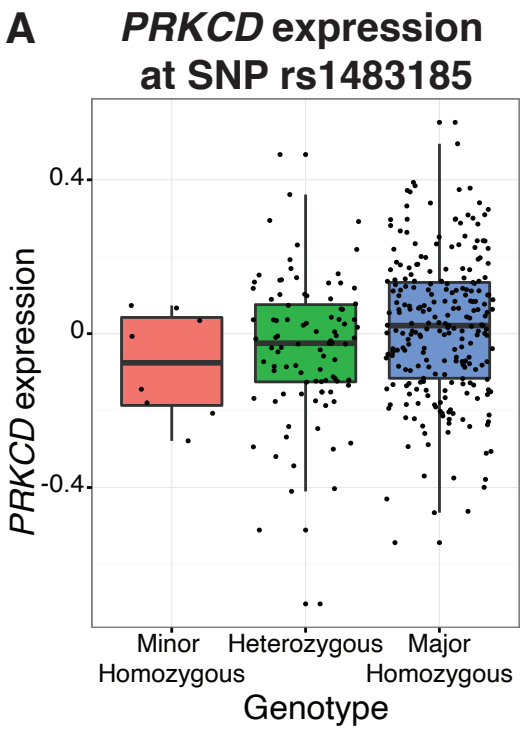

B

SNP	Gene	Beta	p-value
rs1483185	ENSG00000163932	0.05509	0.00646
rs1483186	ENSG00000163932	0.05054	0.01803
rs750170	ENSG00000163932	0.05471	0.00605

Figure 3.5: SNPs identified in the genome wide association study are eQTLs for *PRKCD*
(A) *PRKCD* expression in a lymphoblastoid cell line dataset, plotted by genotype at SNP rs1483185 (p-value = $6e^{-03}$). **(B)** Data table featuring the effect of SNPs rs1483185, rs1483186, rs750170 on the expression of gene *PRKCD* (ENSG00000163932) and the adjusted p-values.

3.4 Utilization of and phenotyping of PKCδ KO mice

To study a potential immune regulatory role of host PKCδ, gene-targeted mouse systems were pursued. Previous studies had linked genetic loss of PKCδ in humans with autoimmunity, including familial lupus [98,99], and an autoimmune phenotype had been reported in PKCδ gene-targeted mice [100,101]. We therefore aimed to test the hypothesis that deletion of the PKCδ gene in host immune cells might augment anti-tumor immunity. We obtained PKCδ KO mice through a generous collaboration with Dr. Ronald Kahn, which were originally developed on a 129 genetic background and backcrossed to C57/BL6 (B6) over 14 generations for studies in hepatic insulin signaling [103]. We obtained the B6 backcrossed strain and Western blot analysis of splenocytes collected from homozygous PKCδ KO mice revealed a complete loss of detectable PKCδ protein (Figure 3.6A). However, while establishing this colony two things became immediately apparent. First, fur color of these mice was not uniformly black, implying an incomplete backcross to the B6 strain. Second, *Prkcd*$^{+/-}$ x *Prkcd*$^{+/-}$ het by het breeding yielded approximately only 5% *Prkcd*$^{-/-}$ mice rather than 25% as predicted by normal mendelian birth ratios. To investigate the completeness of the backcross to B6, we performed a SNP analysis of 17 randomly chosen colony mice utilizing the DartMouse™ sequencing service and found that despite 14 generations of backcrossing, only 88-91% of the overall mouse genome was homozygous for B6 SNPs and a full 5-6% of the genome was homozygous for 129 SNPs (Figure 3.6B). From this we hypothesized that a component of the 129 genome was necessary to obtain viability in homozygous KO mice. Incomplete backcrossing is problematic, as it raises the potential of minor histocompatibility mismatch when using a tumor from the B6 background. As it was unclear whether the reduced number of *Prkcd*$^{-/-}$ live births was due to embryonic lethality or an issue with fertilization, we extracted embryos of pregnant mice day 11.5 and 12.5 post

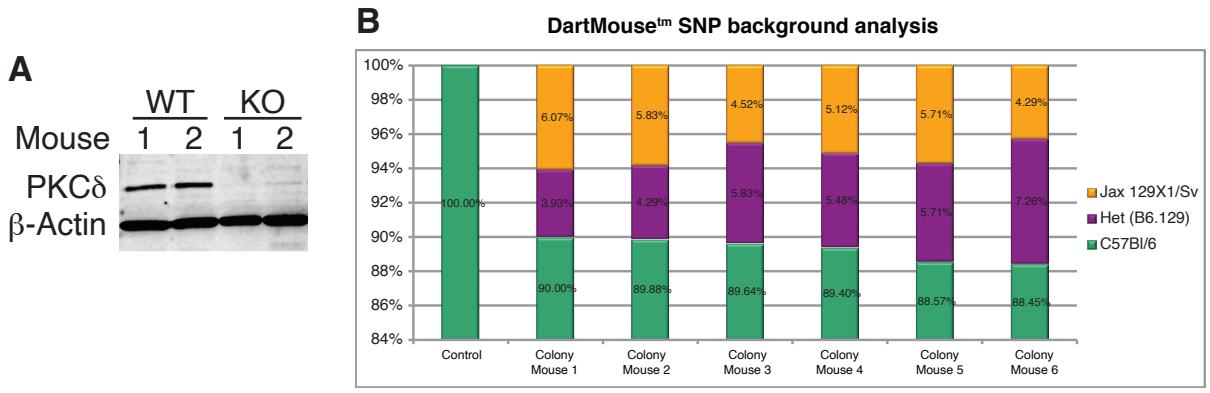

Figure 3.6: Western blot and SNP background analysis of *Prkcd*$^{-/-}$ colony mice
(A) Detectable PKCδ expression in spleenocytes as measured by western blot across 2 independent mice. **(B)** Dartmouse™ SNP analysis of 6 randomly chosen colony mice, with the percentage of total genomic DNA on the Y axis of each bar graph. Yellow indicates the percentage of genomic DNA that contains SNPS associated with the 129 background, green for SNPs associated with the C57/Bl6 background, and purple for areas of the genome heterozygous with one SNP copy each.

impregnation, removed the yolk sacks, and extracted fetal DNA for genotyping (Figure 3.7). Indeed, there was only a single KO embryo detected across 15 total samples, on par with ratios detected after live birth. The failure of *Prkcd*$^{-/-}$ mice to develop to this developmental stage precluded the possibility of utilizing fetal liver transplantation into WT hosts as a model system and indicated that the defect likely occurs at the level of fertilization. Subsequently, other investigators also experiencing breeding difficulties with *Prkcd*$^{-/-}$ mice on a partial B6 background identified defects at the level of PKCδ KO gametes, which apparently rendered those gametes less competitive during fertilization [114].

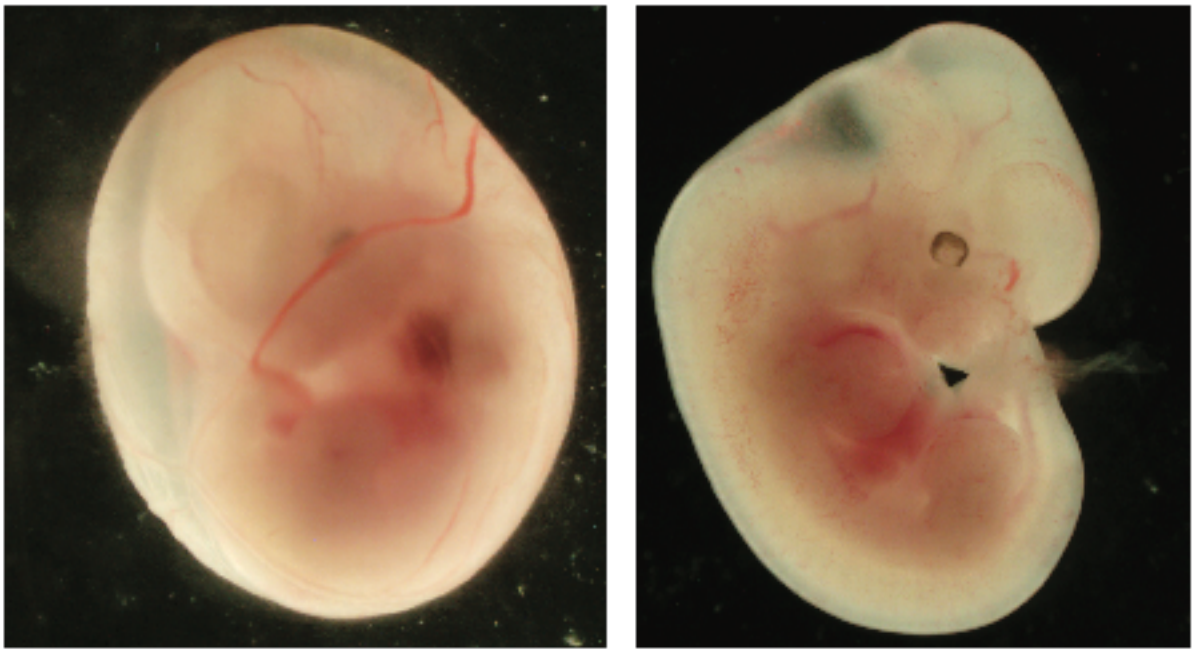

Figure 3.7: Pictures of mouse embryos after 12.5 days of development
Embryo still wrapped in the yolk sack on the left, and on the right after the yolk sack has been removed.

3.5 *Prkcd*$^{-/-}$ bone marrow engrafted mice have a T cell-dependent delay in tumor growth

To overcome the dual issues of minor histocompatibility mismatch and inadequate numbers of *Prkcd*$^{-/-}$ offspring, we created bone marrow (BM) chimeras using congenically marked CD45.1 B6 hosts engrafted with donor bone marrow from *Prkcd*$^{-/-}$ animals. This method allowed for a single *Prkcd*$^{-/-}$ donor animal to typically produce 10 *Prkcd*$^{-/-}$ BM-engrafted animals, greatly increasing our experimental numbers. Additionally, T cell development in a B6 host insured all immune cells would be fully tolerized to the B6 background. This strategy also enabled focus of PKCδ deficiency to be on the immune system, as PKCδ loss was isolated exclusively to the hematopoietic compartment.

To confirm the viability of this model system we examined the spleens of engrafted mice to determine the success of engraftment (generally considered to be around 90% donor cells),

and whether there were any homeostatic differences between WT- and KO-engrafted animals. Engraftments with both WT and KO donor BM routinely produced mice with CD45 compartments that consisted of 90-95% donor CD45-2^{+} cells, and only mice displaying similarly successful engraftments were used in subsequent experiments (Figure 3.8A, Figure 3.8B). Examining the splenic T cell compartments of *Prkcd*$^{-/-}$ BM-engrafted mice showed no differences in CD8^{+} T cell populations compared to WT counterparts, although there was an increase in the total number of FoxP3^{+} T regulatory (Treg) cells in the PKCδ KO setting consistent with counter-regulation of heightened endogenous immunity (Figure 3.9A, Figure 3.9B).

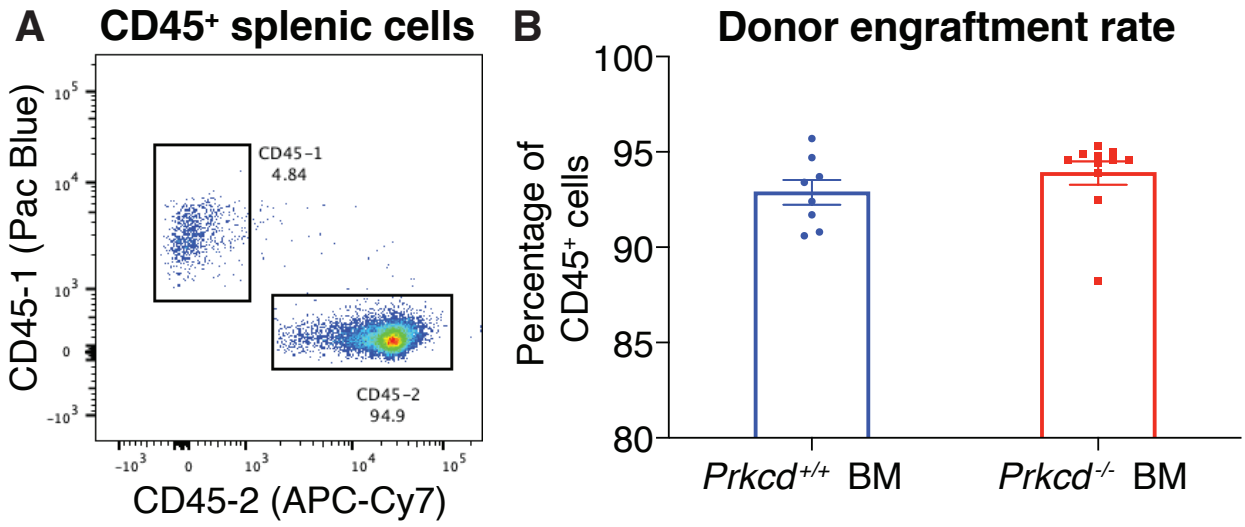

Figure 3.8: Reconstitution of bone marrow engrafted mice is successful
(A) Flow plot of live total CD45^{+} cells (add Colors) with gates identifying the CD45-1^{+} host cells and CD45-2^{+} donor cells. **(B)** Bar plots from a randomly selected experiment exhibiting the percentage of total CD45 cells that are CD45-2^{+} donor cells.

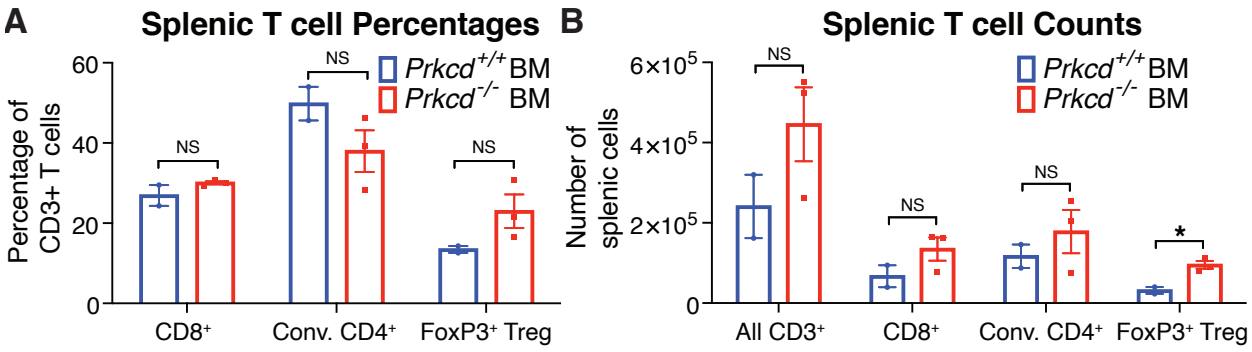

Figure 3.9: Reconstituted mice do not have major changes to their splenic T cell compartments at baseline
(A) Percentages of splenic T cells populations per total $CD3^+$ T cell population measured by flow cytometry in *Prkcd*$^{+/+}$ BM engrafted mice (blue), or *Prkcd*$^{-/-}$ BM engrafted mice (red) in naïve mice. **(B)** Total number of splenic T cells populations measured by flow cytometry in *Prkcd*$^{+/+}$ BM engrafted mice (blue), or *Prkcd*$^{-/-}$ BM engrafted mice (red) in naïve mice.

Moving forward with this model, mice were implanted with B16-SIY melanoma tumor cells which allowed measuring of $CD8^+$ T cell responses against a model antigen. We observed that tumors grew significantly slower in mice engrafted with *Prkcd*$^{-/-}$ BM compared to animals engrafted with *Prkcd*$^{+/+}$ BM (Figure 3.10A). We also observed that *Prkcd*$^{+/-}$ BM-engrafted mice

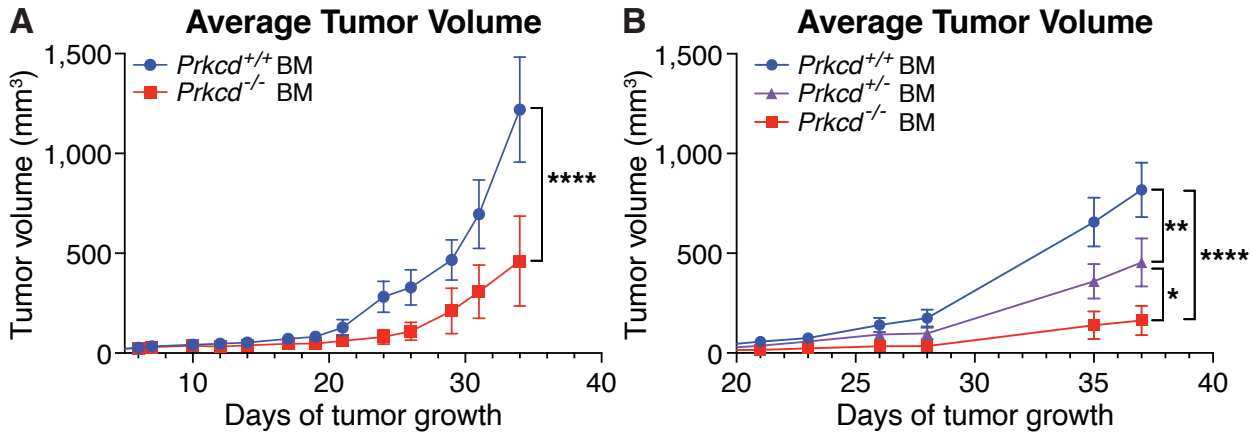

Figure 3.10: Hematopoietic loss of PKCδ leads to delay in tumor growth
(A) B16-SIY tumor volume growing in *Prkcd*$^{+/+}$ bone marrow (BM) engrafted (blue, N=5) or *Prkcd*$^{-/-}$ BM engrafted animals (red, N=5). **(B)** B16-SIY tumor volume growing in *Prkcd*$^{+/+}$ bone marrow (BM) engrafted (blue, N=10), *Prkc*$^{+/-}$ BM engrafted animals (purple, N=10), and *Prkcd*$^{-/-}$ BM engrafted animals (red, N=5).

displayed an intermediate growth phenotype between the WT- and KO- engrafted groups (Figure 3.10B). All subsequent experiments were done comparing *Prkcd*$^{+/+}$ and *Prkcd*$^{-/-}$ animals.

To assess whether the improved tumor control was due to altered host CD8^{+} T cell immunity, we treated mice with a CD8β depleting antibody immediately before tumor implantation. With depletion, tumors implanted in *Prkcd*$^{+/+}$ and *Prkcd*$^{-/-}$ BM-engrafted mice grew faster but also at the same rate, arguing that the growth delay caused by the absence of host PKCδ was due to improved CD8^{+} T cell-dependent immunity (Figure 3.11).

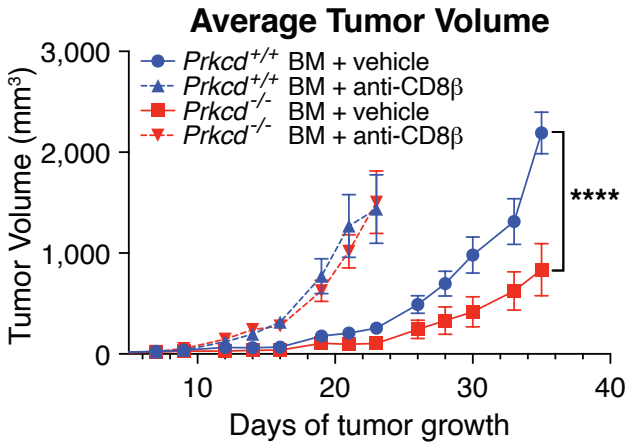

Figure 3.11: PKCδ mediated growth delay requires presence of CD8^{+} T cells
B16-SIY tumor volume of animals engrafted with *Prkcd*$^{+/+}$ BM (blue) and treated with PBS vehicle (circle, solid line, N=5), or anti-CD8β (triangle, dotted line, N=5) or engrafted with *Prkcd*$^{-/-}$ BM (red) and treated with PBS vehicle (square, solid line, N=9), or anti-CD8β (upside down triangle, dotted line, N=10). Treatments were administered 1 day before and 6 days after tumor injection.

3.6 T cell functionality is not intrinsically improved in PKCδ KO cells

We first investigated whether T cells were intrinsically functionally superior in the absence of PKCδ. T cells were isolated from the spleens of *Prkcd*$^{+/+}$ and *Prkcd*$^{-/-}$ donor mice, stimulated with anti-CD3 and anti-CD28, and proliferation and cytokine production were measured. There was no difference in the ability of CD8^{+} T cells to produce IFN-γ, TNFα, and

express CD44 (Figure 3.12A) after 48 hours, and these cells proliferated similarly (Figure 3.12B). $CD8^+$ cells were also examined 72 hours after stimulation and the $CD4^+$ compartment was similarly examined at both time points with no detectable differences (data not shown).

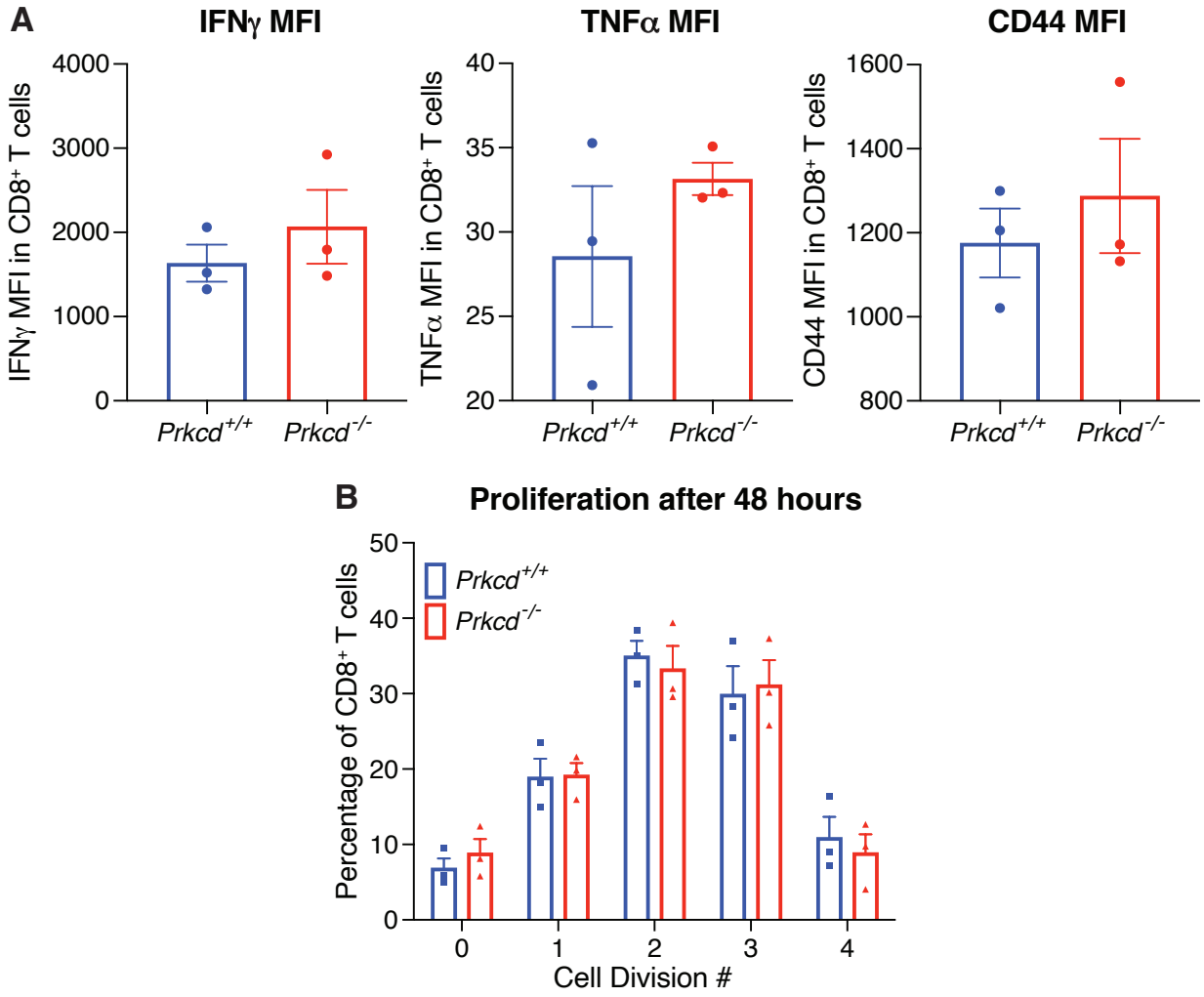

Figure 3.12: PKCδ KO T cells show no functional differences compared to PKCδ WT T cells
(A-B) $CD8^+$ T cells isolated from the spleens of WT or PKCδ KO mice and stimulated ex vivo with CD3 and CD28 antibodies for 48 hours.
(A) Mean fluorescent intensity of IFN-γ, TNFα, CD44 cytokines (from left to right) **(B)** Proliferation as measured by CFSE dilution, with the percentage of each division as a part of the whole.

To assess whether a functional property of PKCδ KO T cells was improved in the tumor context in vivo, we transferred T cells from either *Prkcd*$^{+/+}$ or *Prkcd*$^{-/-}$ donor mice into RAG2$^{-/-}$

hosts. As RAG2$^{-/-}$ mice lack all T and B cells, in this environment only the transferred T cells will be deficient for PKCδ while all other immune cells, including APCs and other myeloid cells, will have normal PKCδ expression. Bulk T cell adoptive transfer did delay tumor growth, indicating the transferred cells were functional and able to provide a degree of tumor control. However, there was no difference in tumor growth when comparing mice that received PKCδ WT T cells versus PKCδ KO T cells (Figure 3.13). Together, these data indicate that improved tumor control with PKCδ KO hematopoietic transfer is not due to intrinsically enhanced T cell functionality.

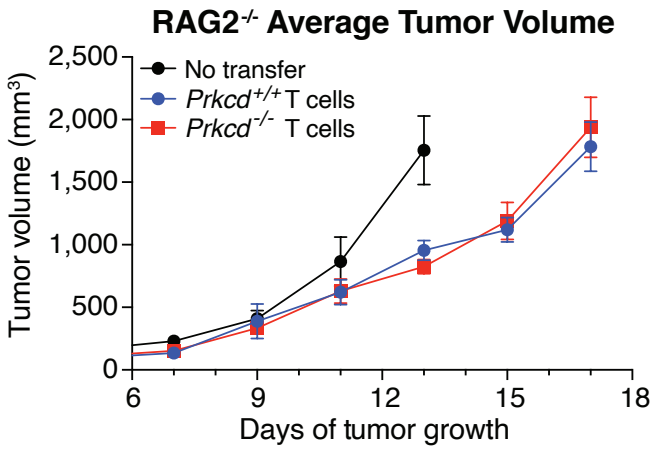

Figure 3.13: Transfer of T cells into RAG$^{-/-}$ hosts shows no intrinsic differences between PKCδ WT and PKCδ KO T cells
T cells were isolated from spleens and transferred via i.v. injection into RAG$^{-/-}$ hosts 1 day before injection with B16-SIY. Tumor growth is tracked in mice that received no transfer of T cells (black), PKCδ WT T cells (blue), or PKCδ KO T cells (red).

3.7 CD8^{+} T cell priming is unaltered with loss of hematopoietic PKCδ

If T cells were not intrinsically functionally improved in the absence of hematopoietic PKCδ, then a second potential mechanism for improved tumor growth control is an improvement in cross-priming leading to an expanded systemic population of tumor-antigen specific CD8^{+} T

cells. To investigate this possibility, we first examined DC functionality *in vitro* by comparing the ability of DCs to stimulate the proliferation of 2C TCR transgenic (tg) T cells in response to cognate SIY SIINFEKL peptide. We found that both PKCδ WT and PKCδ KO DCs were able to present SIY peptide and induce 2C proliferation to similar extents (Figure 3.14A, Figure 3.14B). DC functionality was further probed using a cross-priming assay with irradiated B16-SIY as the source of antigen, as free peptide can bypass the cross-presentation pathway [115]. In fact, DCs from *Prkcd*$^{+/+}$ and *Prkcd*$^{-/-}$ animals were able to process and present antigen from dying B16-SIY cells and stimulate 2C proliferation at similar levels, indicating that PKCδ KO DCs were not intrinsically more efficient at priming (Figure 3.14C, Figure 3.14D).

To evaluate the potential for augmented cross-priming *in vivo*, the number of tumor antigen-specific CD8$^+$ T cells in tumor-bearing mice was assessed using SIY-K^b pentamer staining. At day 10 following tumor implantation, the numbers of SIY-specific CD8$^+$ T cells was comparable in the spleens of *Prkcd*$^{+/+}$ and *Prkcd*$^{-/-}$ BM-engrafted mice (Figure 3.15A, Figure 3.15B). For a more functional assessment, we collected splenocytes from tumor-bearing engrafted mice and performed an IFN-γ ELISPOT assay which measures the extent of cytokine production after antigen-specific stimulation with the SIY peptide *in vitro*. In fact, a comparable number of IFN-γ spots was observed among splenocytes obtained from *Prkcd*$^{+/+}$ and *Prkcd*$^{-/-}$ BM-engrafted mice. In addition, there was no difference in the amount of IFN-γ produced per cell as measured by mean spot size (Figure 3.15C, Figure 3.15D). We conclude that endogenous CD8$^+$ T cell priming in response to antigen-expressing tumor is not augmented in PKCδ KO hosts.

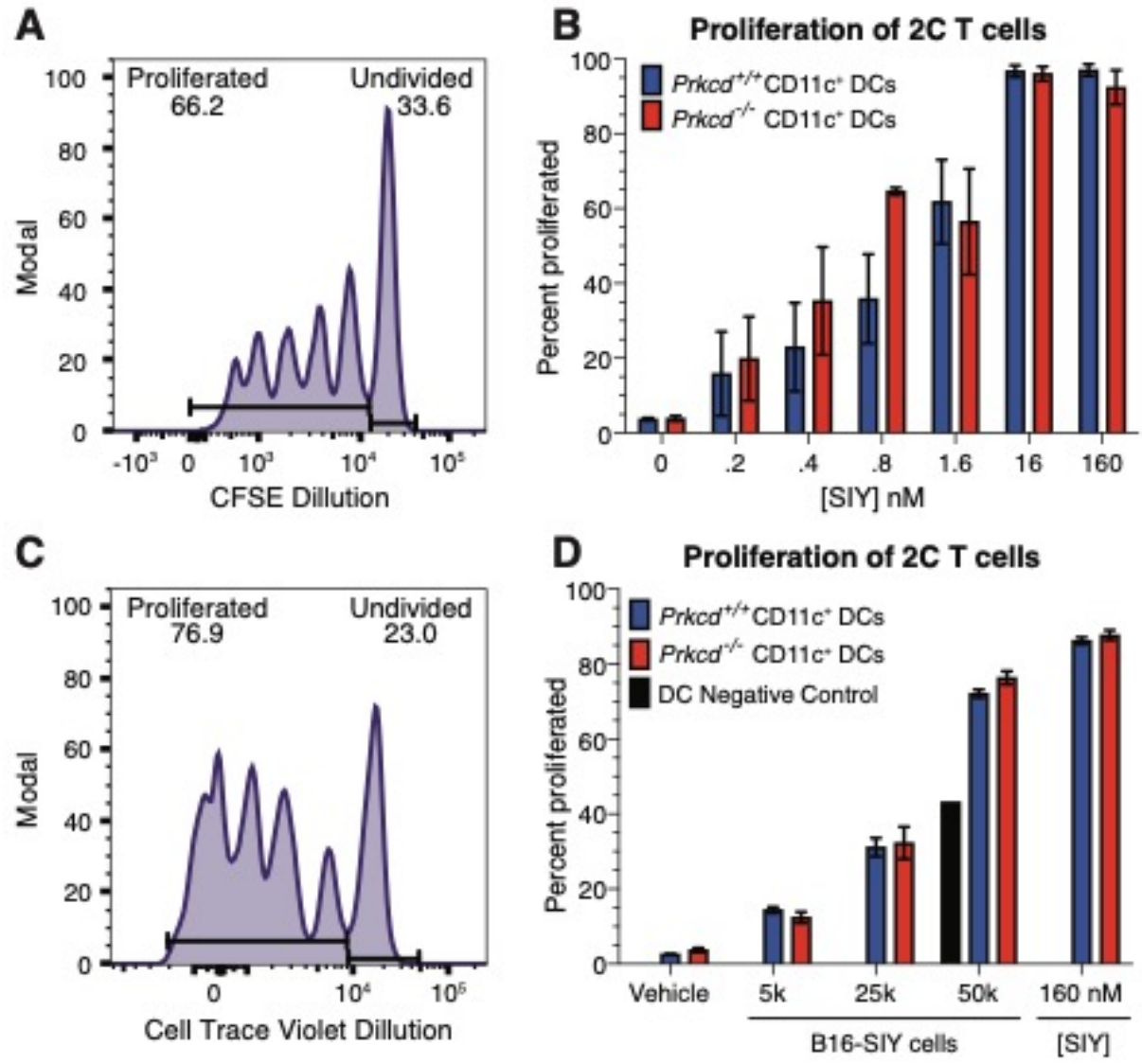

Figure 3.14: in vitro priming assays reveal no intrinsic differences between PKCδ WT and KO dendritic cells

(A) Representative histogram plot showing 2C cells identified by flow cytometry that have proliferated after stimulation with 0.8 nM SIY. Gating indicates what dilutions were considered proliferated. **(B)** Total proliferation of 2C CD8 T cells as measured by CFSE dilution WT (blue, N=4) KO (red, N=4). **(C)** Representative histogram plot showing 2C cells identified by flow cytometry that have proliferated after stimulation with 0.8 nM SIY. Gating indicates what dilutions were considered proliferated. **(D)** Total proliferation of CD8 T cells as measured by cell trace violet dilution (blue, N=2) KO (red, N=2).

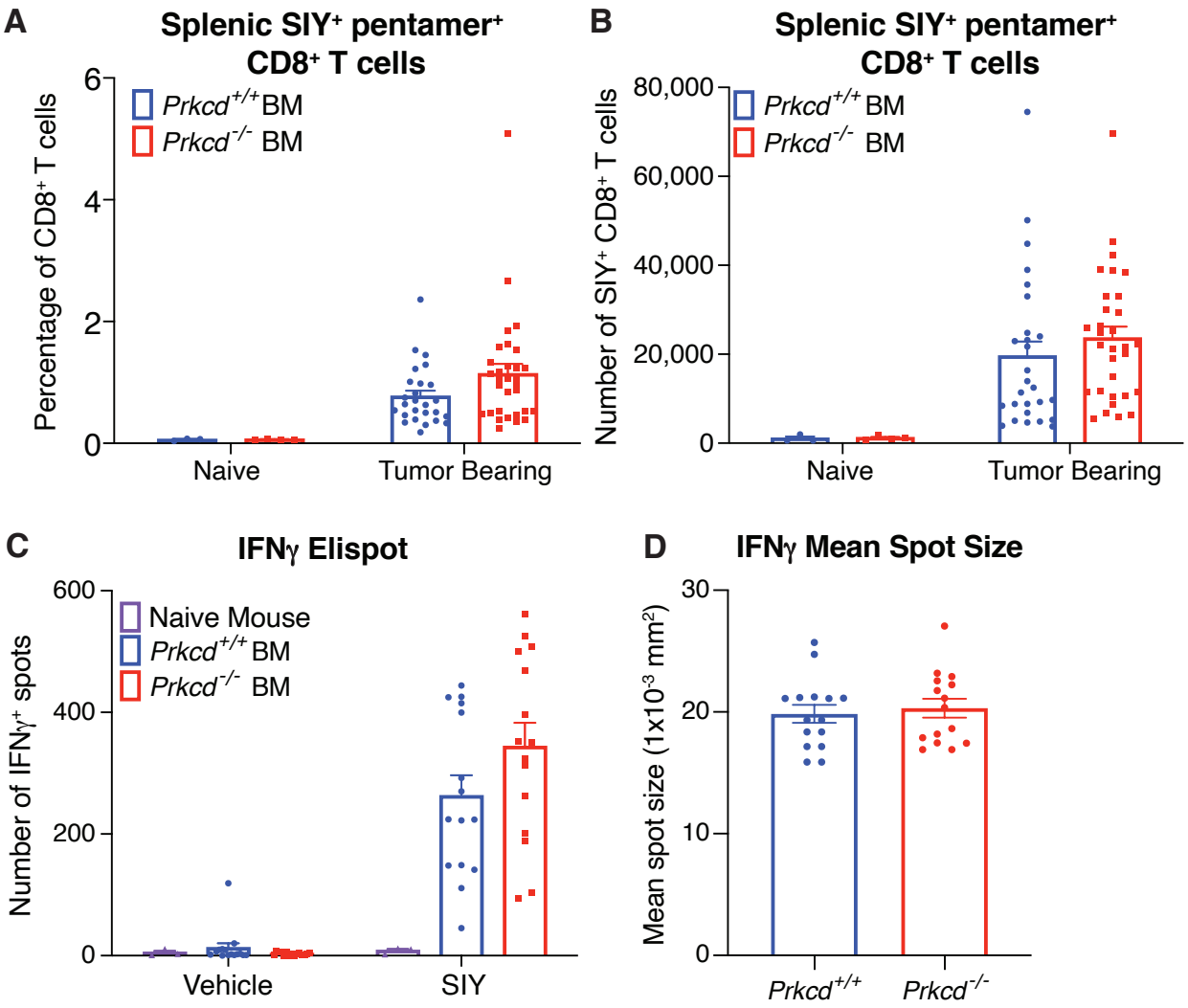

Figure 3.15: No increase in antigen-specific T cell populations *in vivo* after 10 days of tumor growth
(A) Percentage of splenic $CD8^+$ T cells that stain positively for SIY tetramer by flow cytometry in *Prkcd*$^{+/+}$ BM engrafted mice (blue), or *Prkcd*$^{-/-}$ BM engrafted mice (red) when mice are either tumor naïve (left) or after 10 days of tumor growth (right). **(B)** Total number of splenic $CD8^+$ T cells that stain positively for SIY tetramer by flow cytometry in *Prkcd*$^{+/+}$ BM engrafted mice (blue), or *Prkcd*$^{-/-}$ BM engrafted mice (red) when mice are either tumor naïve (left) or after 10 days of tumor growth (right). **(C)** The number of IFN-γ producing splenic cells after 10 days of tumor growth was determined by ELISPOT in *Prkcd*$^{+/+}$ BM engrafted (blue) and *Prkcd*$^{-/-}$ BM engrafted mice (red) mice, with tumor naïve *Prkcd*$^{+/+}$ BM engrafted (purple) serving as a negative control. All groups were stimulated with either PBS vehicle (left) or SIY peptide (right). **(D)** The mean size of spots (10^{-3} mm^2) of IFN-γ producing splenic cells after 10 days of tumor growth was determined by ELISPOT in *Prkcd*$^{+/+}$ BM engrafted (blue) and *Prkcd*$^{-/-}$ BM engrafted mice (red) mice with all groups stimulated by SIY.

3.8 PKCδ loss leads to increased CD8$^+$ T cell numbers within the tumor microenvironment over time

If T cell-intrinsic biology and endogenous cross-priming of tumor antigen-specific T cells were not augmented in the absence of PKCd, then the improved immune-mediated tumor control observed was likely occurring at the level of the TME. This stage could operationally be separated into early T cell trafficking into the tumor site and expanded numbers of functional T cells within the TME over time. Using SIY-K^b pentamer staining, we examined the tumor-infiltrating lymphocyte (TIL) compartment after 10 days of tumor growth and found that the numbers of SIY-specific CD8$^+$ T cells was comparable between *Prkcd*$^{+/+}$ and *Prkcd*$^{-/-}$ BM-engrafted mice (Figure 3.16A). In addition, bulk populations of CD8$^+$ T cells and FoxP3$^+$ Tregs were comparable as measured per gram of tumor mass (Figure 3.16B, Figure 3.16C). These data indicate that, after 10 days of tumor growth, there is not improved recruitment of T cells into the TME, nor are there reduced numbers of tumor-infiltrating FoxP3$^+$ Tregs which could create a less suppressive TME.

To evaluate whether improved anti-tumor immunity might be reflected over time at the level of the TME, we characterized the immune infiltrate at later time points as the tumors grew, focusing on day 35. Indeed, tumors from *Prkcd*$^{-/-}$ BM-engrafted animals analyzed at day 35 showed more CD3$^+$ and CD8$^+$ T cells per gram of tumor (Figure 3.17A, Figure 3.17B). This phenomenon was specific to the CD8$^+$ T cell compartment, as PKCδ KO samples did not have significantly increased numbers of FoxP3$^+$ T reg cells or conventional CD4$^+$ T cells per gram of tumor (Figure 3.17C, Figure 3.17D). Splenic CD8$^+$ and CD3$^+$ T cell populations remained unchanged at this time point indicating the increase in CD8$^+$ T cells was localized to the tumor microenvironment (Figure 3.17E, Figure 3.17F). Thus, like patients possessing a hypomorphic

allele of the PKCδ gene, tumors in PKCδ-deficient mice demonstrated greater T cell infiltration in the tumor microenvironment over time.

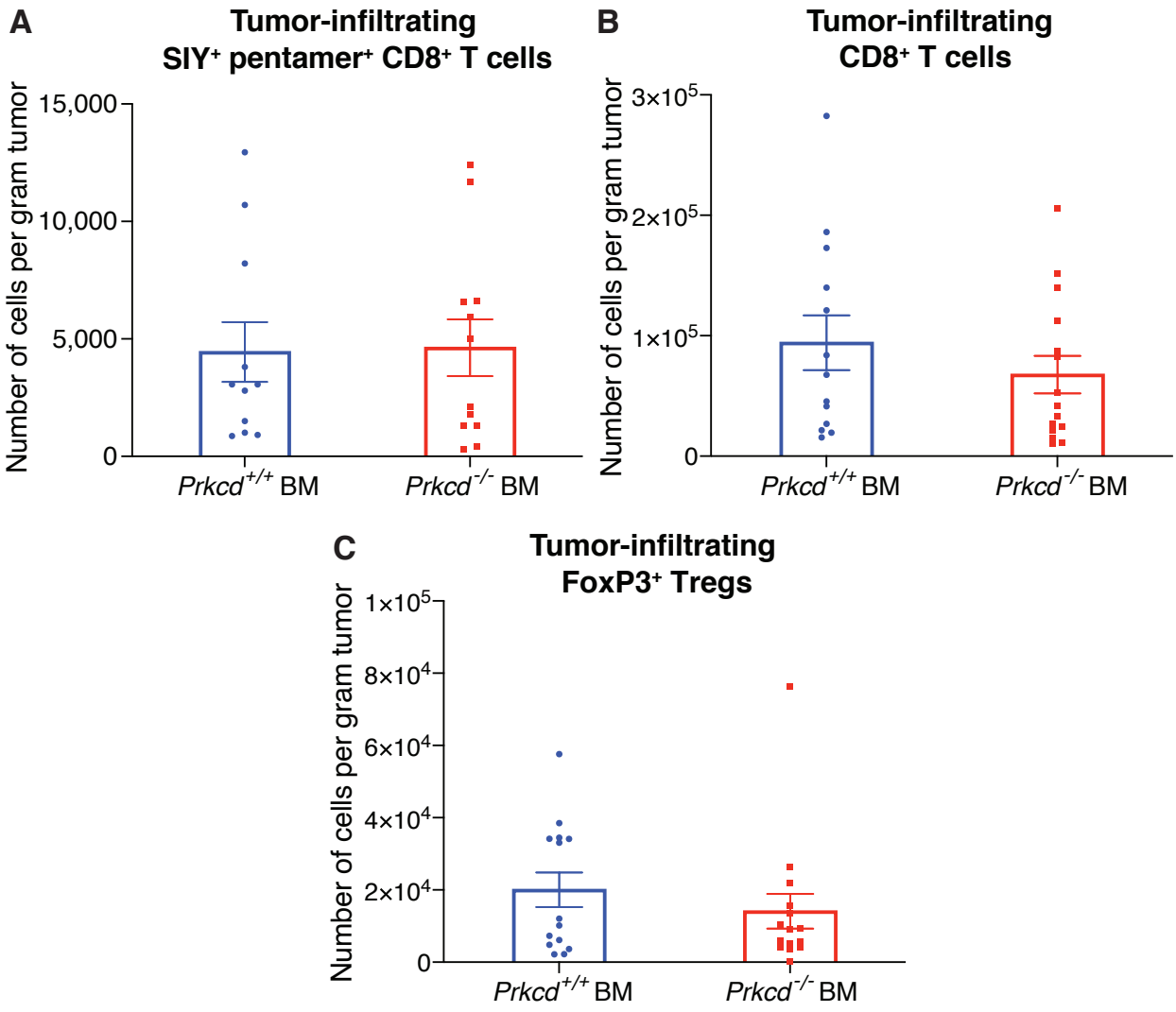

Figure 3.16: Recruitment of T cells into the tumor at day 10 is unaltered in PKCδ KO mice
(A) Total number per gram of tumor of $CD8^+$ T cells that stain positively for SIY tetramer by flow cytometry in *Prkcd*$^{+/+}$ BM engrafted mice (blue), or *Prkcd*$^{-/-}$ BM engrafted mice (red) after 10 days of tumor growth. **(B)** Total number per gram of tumor of $CD8^+$ T cells identified by flow cytometry in *Prkcd*$^{+/+}$ BM engrafted mice (blue), or *Prkcd*$^{-/-}$ BM engrafted mice (red) after 10 days of tumor growth. **(C)** Total number per gram of tumor of $FoxP3^+$ T regulatory cells identified by flow cytometry in *Prkcd*$^{+/+}$ BM engrafted mice (blue), or *Prkcd*$^{-/-}$ BM engrafted mice (red) after 10 days of tumor growth.

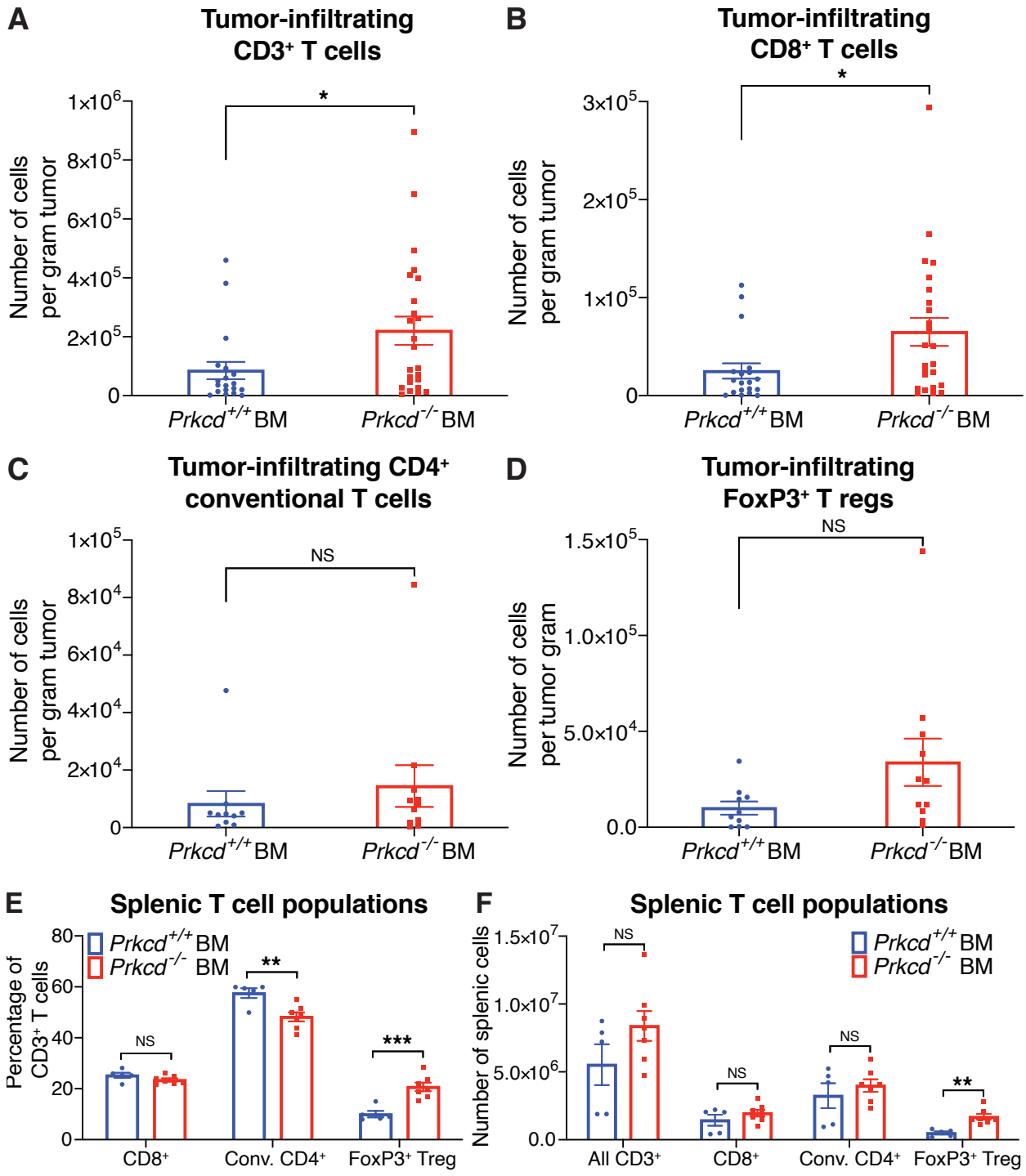

Figure 3.17: Increased numbers of tumor infiltrating T cells after 35 days of tumor growth
(A) Total number per gram of tumor of $CD3^+$ T cells identified by flow cytometry in *Prkcd*$^{+/+}$ BM engrafted mice (blue), or *Prkcd*$^{-/-}$ BM engrafted mice (red) after 35 days of tumor growth. **(B)** Total number per gram of tumor of $CD8^+$ T cells identified by flow cytometry in *Prkcd*$^{+/+}$ BM engrafted mice (blue), or *Prkcd*$^{-/-}$ BM engrafted mice (red) after 35 days of tumor growth. **(C)** Total number per gram of tumor of conventional $CD4^+$ T cells identified by flow cytometry in *Prkcd*$^{+/+}$ BM engrafted mice (blue), or *Prkcd*$^{-/-}$ BM engrafted mice (red) after 35 days of tumor growth. **(D)** Total number per gram of tumor

of FoxP3$^+$ T regulatory cells identified by flow cytometry in *Prkcd*$^{+/+}$ BM engrafted mice (blue), or *Prkcd*$^{-/-}$ BM engrafted mice (red) after 35 days of tumor growth. **(E)** Percentages of splenic T cell populations per total CD3$^+$ T cell population measured by flow cytometry in *Prkcd*$^{+/+}$ BM engrafted mice (blue), or *Prkcd*$^{-/-}$ BM engrafted mice (red) after 35 days of tumor growth. **(F)** Total number of splenic T cell populations measured by flow cytometry in *Prkcd*$^{+/+}$ BM engrafted mice (blue), or *Prkcd*$^{-/-}$ BM engrafted mice (red) after 35 days of tumor growth.

3.9 PKCδ loss synergizes with anti-PD-L1-based therapy

With improved spontaneous immune-mediated tumor control and an increased accumulation of tumor-infiltrating CD8$^+$ T cells, we hypothesized PKCδ KO hosts may experience improved efficacy of PD-1/PD-L1 blockade. To this end, *Prkcd*$^{-/-}$ versus *Prkcd*$^{+/+}$ BM-engrafted mice were implanted with B16-SIY cells and treated with anti-PD-L1 antibody 3x per week beginning on day 26. Indeed, *Prkcd*$^{-/-}$ BM-engrafted mice showed improved anti-PD-L1 efficacy compared to *Prkcd*$^{+/+}$ BM-engrafted mice (Figure 3.18A), which was accompanied by significantly improved overall mouse survival including 2 complete responses (Figure 3.18B). Thus, loss of PKCδ in the hematopoietic compartment caused a CD8$^+$ T cell-dependent delay in tumor outgrowth, which could be further augmented with the addition of anti-PD-L1 antibody treatment.

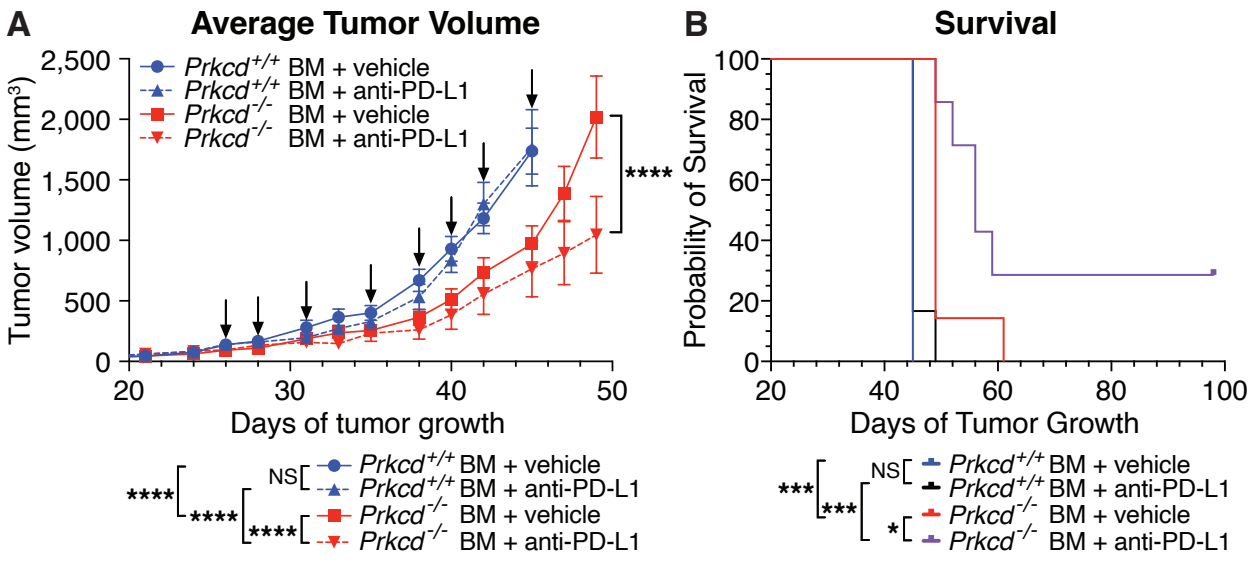

Figure 3.18: Anti-PD-L1 treatment synergizes with PKCδ loss resulting in delayed growth and improved survival
(A) B16-SIY tumor volume of animals engrafted with *Prkcd*$^{+/+}$ BM (blue) and treated with PBS vehicle (circle, solid line, N=7), or anti-PD-L1 (triangle, dotted line, N=6) or engrafted with *Prkcd*$^{-/-}$ BM (red) and treated with PBS vehicle (square, solid line, N=7), or anti-PD-L1 (upside down triangle, dotted line, N=7). Treatments are indicated with arrows and were administered 3x a week starting 26 days after tumor injection. **(B)** Survival curve of B16-SIY tumor bearing animals engrafted with *Prkcd*$^{+/+}$ BM and treated with PBS vehicle (blue, N=7), or anti-PD-L1 (black, N=6) or engrafted with *Prkcd*$^{-/-}$ BM and treated with PBS vehicle (red, N=7), or anti-PD-L1 (purple, N=7). Treatments were administered 3x a week starting 26 days after tumor injection.

3.10 Summary of findings

Our present results validate the approach of using germline susceptibility loci to identify novel targets involved in tumor immunity and add to recent literature describing associations between selected autoimmune-related SNPs and checkpoint blockade efficacy [116–118]. Our genome-wide approach identified *PRKCD* as a novel candidate, suggesting that decreased expression might lead to augmented anti-tumor immunity. This locus was previously associated with familial lupus, falling in line with the expectation that immune regulatory genes would be among the top hits in our GWA scan. Using BM chimeras, we showed that hematopoietic PKCδ loss improves anti-tumor immunity in a CD8^{+} T cell-dependent manner. Immunophenotyping of tumor-bearing animals revealed no differences in the initial priming steps or in early recruitment

of $CD8^+$ T cells into the TME, and we found that PKCδ loss did not intrinsically alter T cell functionality. In line with our GWA study results, we found that at the endpoint of tumor growth *Prkcd*$^{-/-}$ BM-engrafted animals had significantly more $CD8^+$ T cells compared to WT counterparts at later time points, arguing for a regulatory role for PKCδ within the established TME. We then took advantage of the improved $CD8^+$ T cells response by treating tumors with anti-PD-L1 therapy and found that hematopoietic PKCδ loss synergized with anti-PD-L1 providing greater therapeutic benefit than either alone. These data imply that PKCδ negatively influences T cell immunity in a way that is complementary to PD-1 blockade.

Chapter 4: Loss of PKCδ shifts tumor-associated macrophages towards an inflammatory phenotype, resulting improved anti-tumor immunity and response to checkpoint

4.1 Single cell RNA sequencing allows for an unbiased investigation of tumor resident CD45$^+$ cells in PKCδ WT and KO bone-marrow engrafted animals.

To investigate the mechanism underlying the improvement in anti-tumor immunity at the level of the tumor microenvironment, we took the approach of single cell RNA sequencing (scRNAseq). Tumor-infiltrating live dsRed$^-$ CD45$^+$ cells were isolated by flow cytometry after 26 days of tumor growth, which is the time frame in which the *Prkcd*$^{+/+}$ and *Prkcd*$^{-/-}$ BM-engrafted mouse tumor growth curves just began to separate. Excluding dsRed+ cells eliminated contaminating tumor cells. After sequencing, samples were demultiplexed and aligned using the Cell Ranger analysis pipeline. Low quality cells, suspected to be dead or dying cells, with high mitochondrial gene expression (5%) and/or low read counts (500) were removed from the dataset as part of standard quality control processing, while cells having between 50 and 3000 RNA features were kept. Utilizing the Seurat package sequencing data was analyzed, and the subsequent uniform manifold approximation and projection (UMAP) dimensional reduction revealed a total of 24 uniquely identifiable clusters (Figure 4.1). Populations clustered into major groups, with myeloid lineage populations and lymphoid lineage populations separated across UMAP dimension 1 as expected. The genes used for functional annotation of unknown clusters are listed below (Figure 4.2). Lymphoid lineage populations comprise B cells (cluster 4, 22, 23, expressing CD79), T cells (clusters 0, 8, 9,11, 12, 15, 16, expressing CD3) with multiple CD8 and CD4 populations, as well as NK cells (clusters 2, 14, expressing NK1.1). Myeloid clusters were identified by expression of CD11b and/or MHC-II, as certain DC subsets do not express

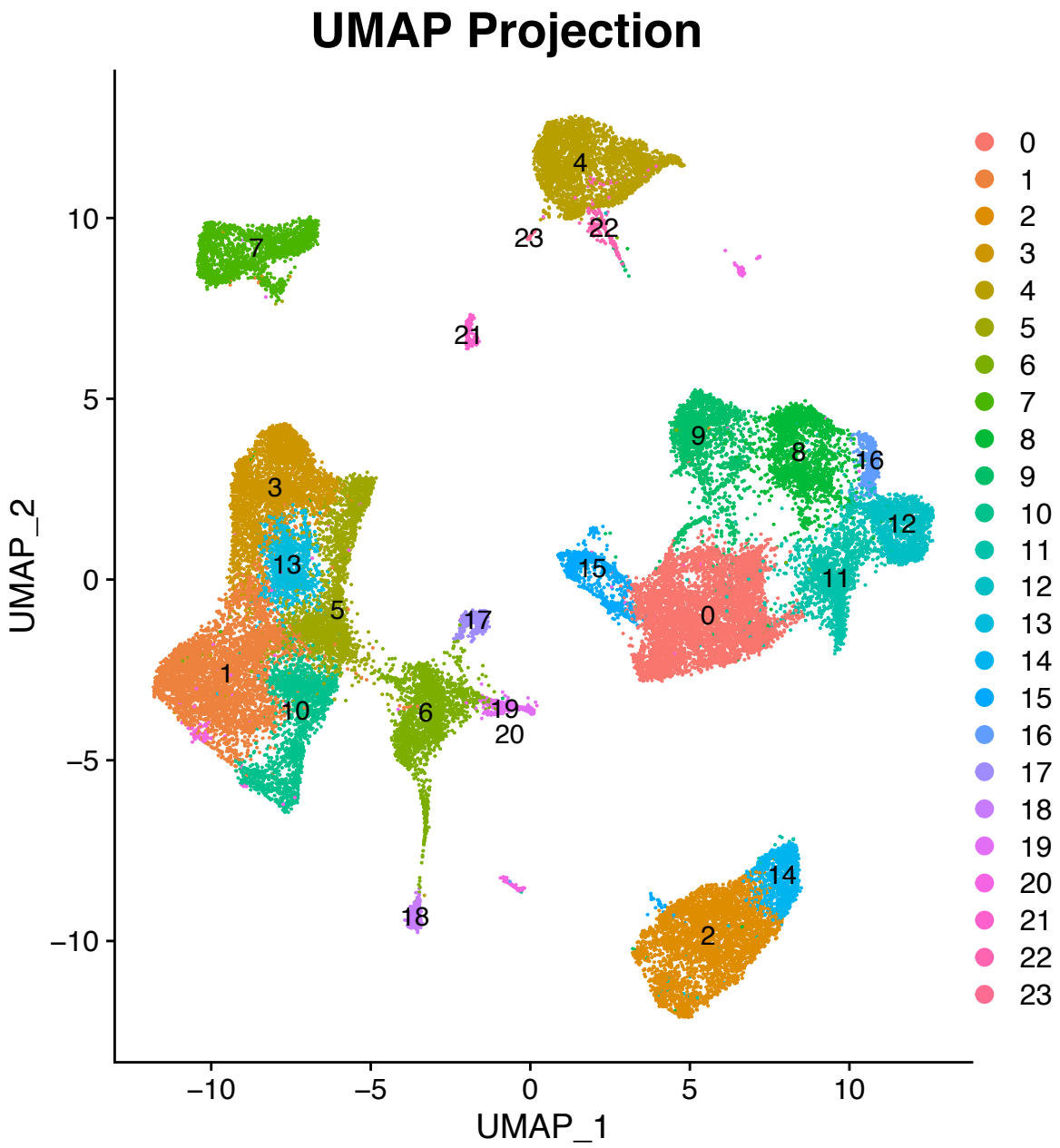

Figure 4.1: Unlabeled UMAP reduction of tumor infiltrating CD45^{+} cells
Based on unsupervised clustering of scRNAseq data and a resolution of 0.6.

CD11b but are still myeloid lineage cells. Of non-dendritic cell populations, we identified a cluster of cells likely representing the spectrum of monocyte to macrophage cells with strong expression of F4-80 (clusters 1, 3, 5, 10, 13). A neutrophil population was identified by expression of S100A9 (cluster 7), while a small population of cells highly expressing IL-4 were

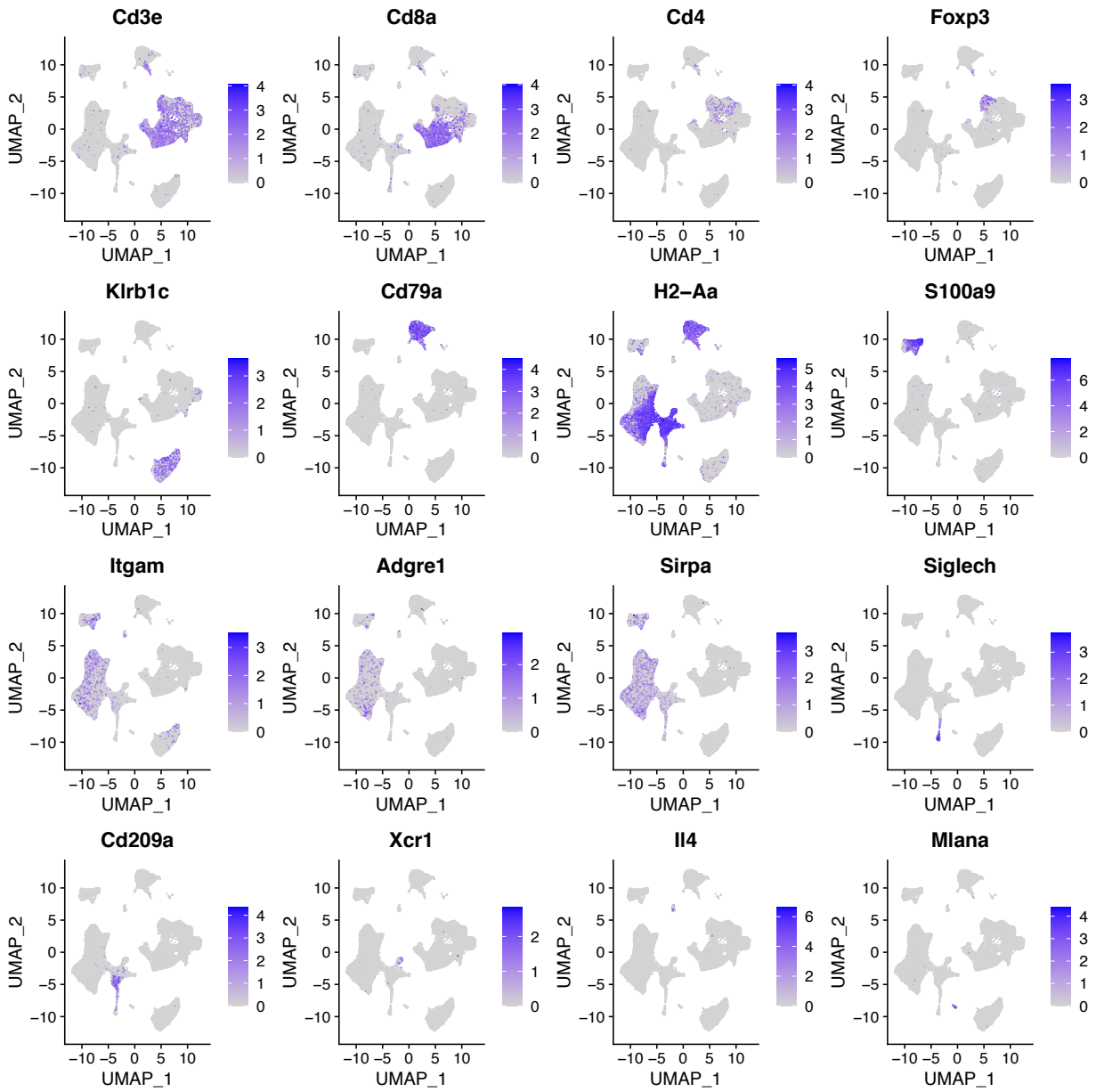

Figure 4.2: Genes used in functional annotation of unknown clusters
Log transformed, normalized gene expression of indicated transcripts expressed as dot plots and used for functionally annotating the clusters.

identified as mast cells (cluster 21). For the dendritic cell clusters, we identified plasmacytoid DCs (cluster 18, marker siglech), classical DC1s expressing XCR1 (cluster 17), classical DC2s expressing CD11b, Clec10a, and Cd209a (cluster 6), and a population of CCR7-expressing DCs which is required for DC trafficking to the lymph nodes. Each population labeled above was then

further characterized by determining a uniquely expressed "cluster-defining gene" (Table S1). For example, cluster 10 was classified as macrophages by CD11b and F4-80 expression and had uniquely high expression of C1qa (Figure 4.3). Samples were then split by genotype, but we detected no gross changes to the relative size of any labeled cell group indicating that at this time point there were likely no large population shifts in any immune compartment (Figure 4.4).

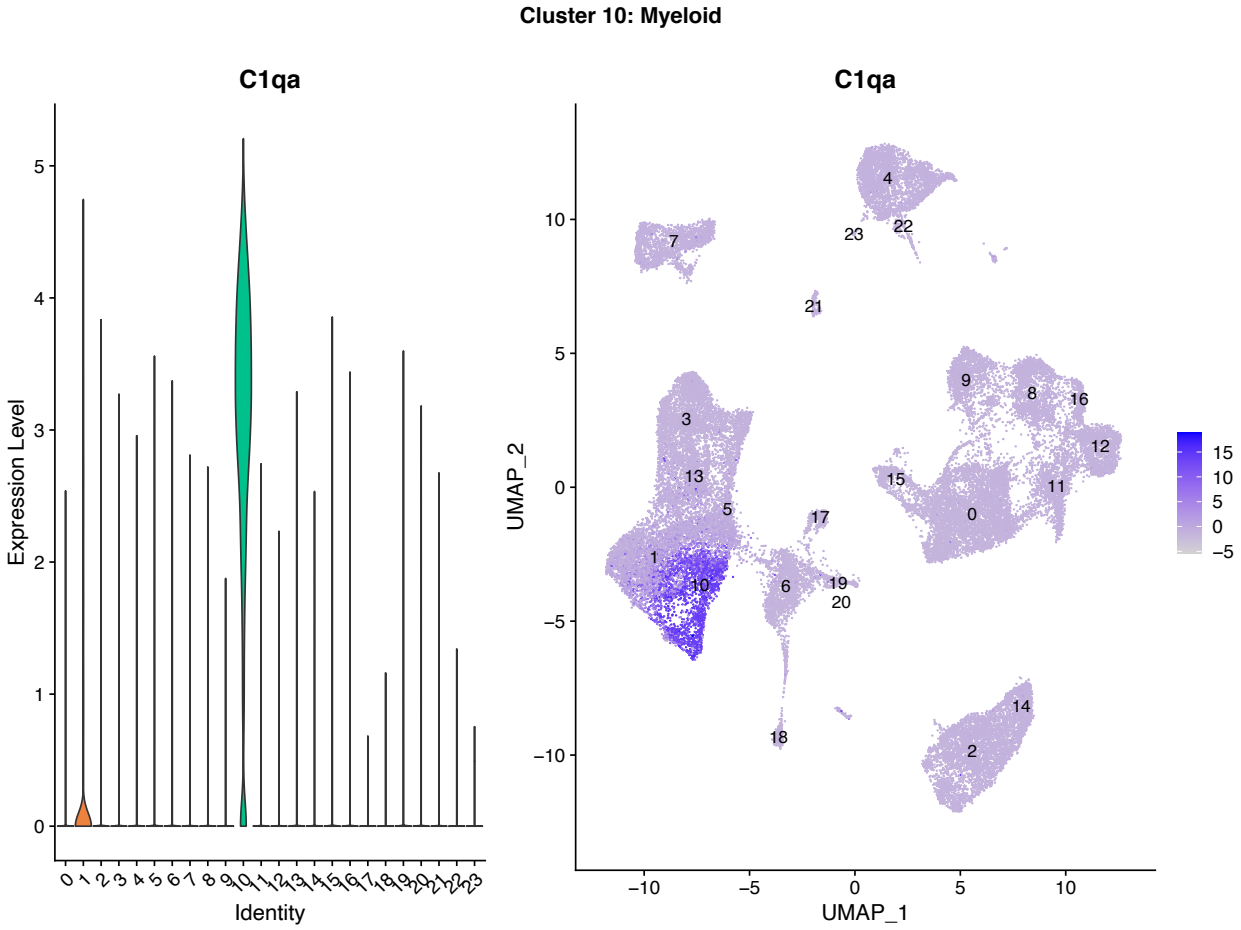

Figure 4.3: *C1qa* is the defining gene for cluster 10
Log transformed, normalized gene expression of C1qa transcript displayed as a violin plot (left) or dot plot overlay (right) across all populations.

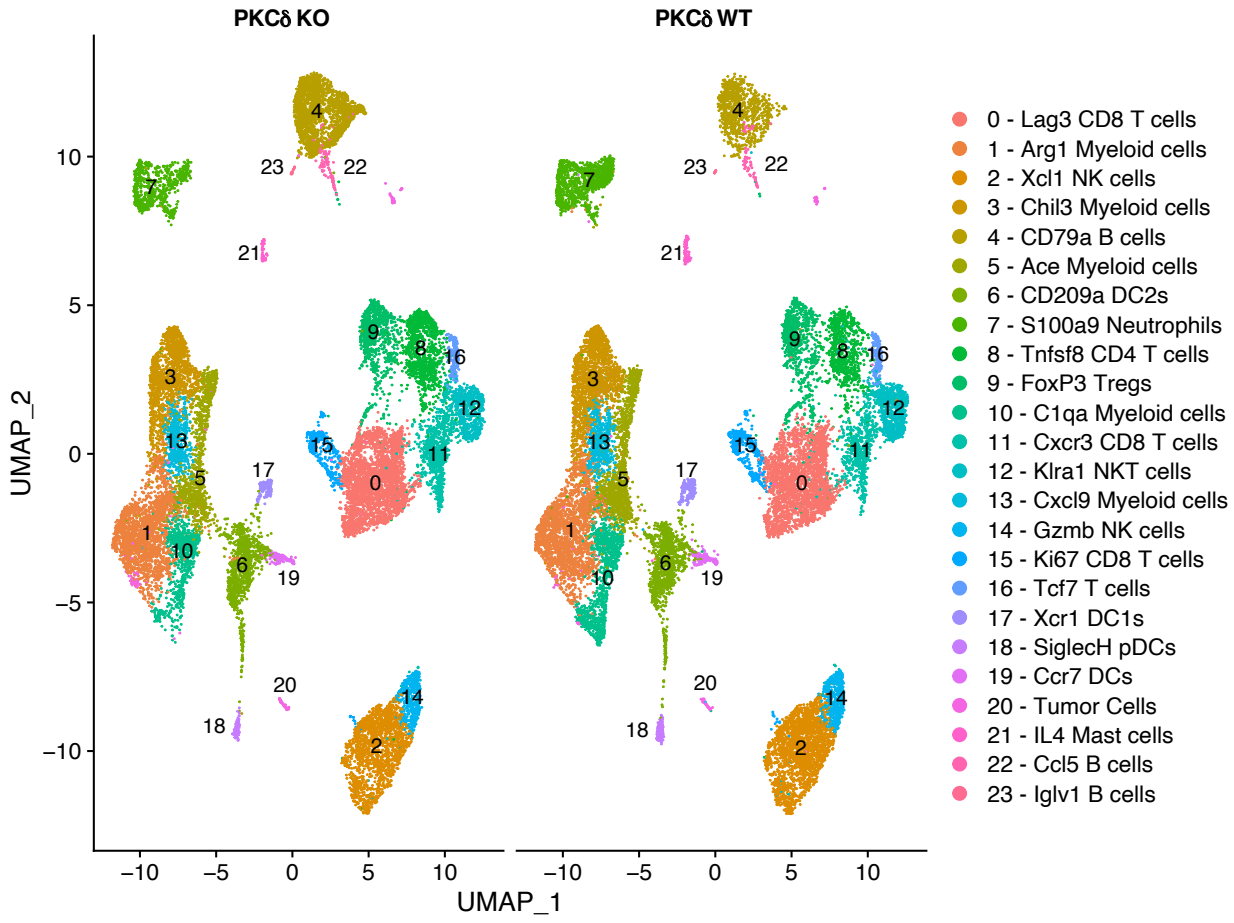

Figure 4.4: Labeled UMAP reduction split by genotype show no shifts in populations

4.2 Differentially expressed genes are primarily found in the myeloid compartments

To narrow down which cells may be directly affected by PKCδ deficiency, *Prkcd* expression itself was probed in the WT samples. High *Prkcd* expression was mainly identified in the various myeloid cell subsets, with the highest expression found in the subsets belonging to the monocyte/macrophage spectrum (Figure 4.5). There was also lower, but detectable expression found in the neutrophil compartment and the mast cell compartment, with very little expression detected in any of the lymphoid clusters. This expression pattern generally agrees with previously published datasets found in the Immunological Genome Project database [119].

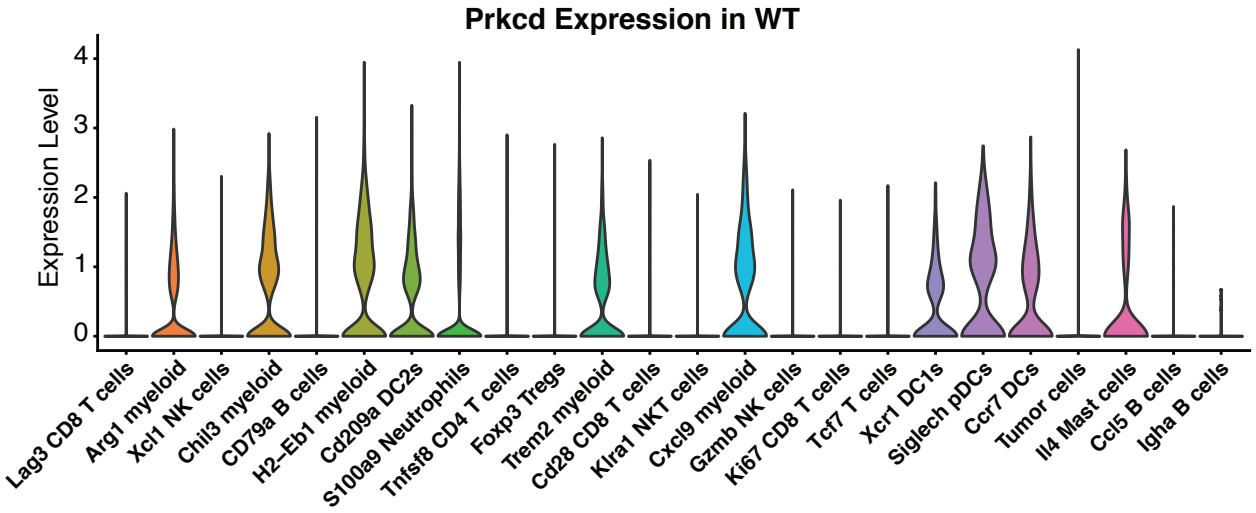

Figure 4.5: *Prkcd* expression is highest in myeloid populations
PKCδ expression data in *Prkcd*$^{+/+}$ BM engrafted samples across all uniquely identified cell populations.

Differentially expressed genes (DEGs) between WT and PKCδ KO samples with a false discovery rate (fdr) ≤ 0.05 and a log fold-change (fc) magnitude ≥ 0.25 were then identified across all populations. In total 1286 DEGs were detected across all cell populations with 2 clusters identified by macrophage and neutrophil lineage markers comprising of over 50% of all DEGs detected (Figure 4.6). No other cell population had more than 75 total DEGs (5.8%). Because *Prkcd* expression was expressed higher in macrophages at baseline compared to S100a9 neutrophils, and given their defined role in anti-tumor immunity, the macrophage subsets were focused upon for further analysis.

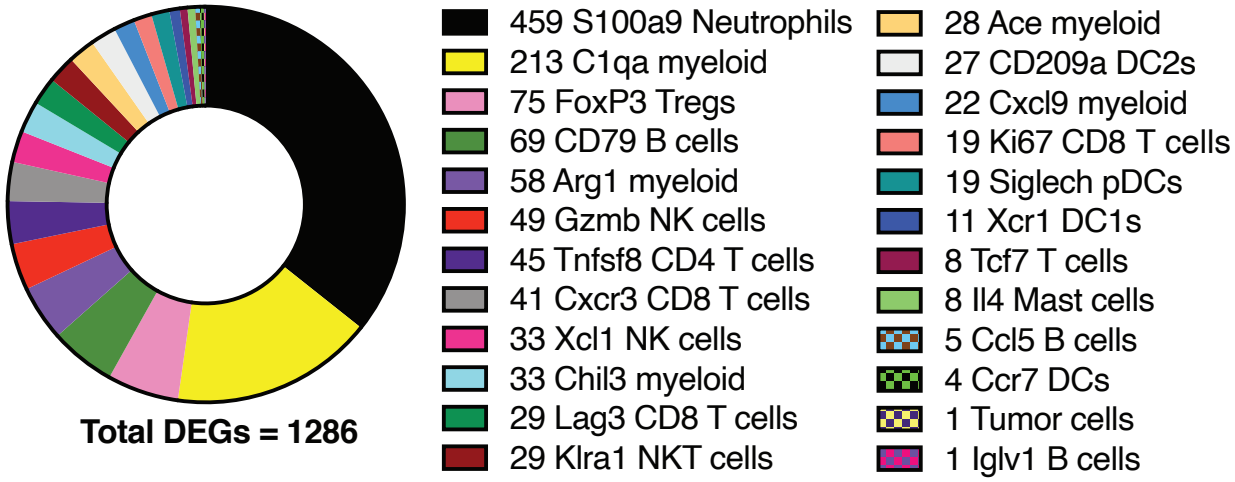

Figure 4.6: Donut plot reveals over 50% of all DEGs found in C1qa^{+} myeloid population and S100a9^{+} neutrophil population
Number of differentially expressed genes between *Prkcd*$^{+/+}$ BM engrafted and *Prkcd*$^{-/-}$ BM engrafted populations within each cell population shown in a donut plot. Exact number of differentially expressed genes for each population is in legend.

4.3 DEGs in the macrophage cluster correlate with M1-like and M2-like states

To interrogate the C1qa^{+} DEG list in an unbiased way, gene set enrichment analysis (GSEA) of the C1qa^{+} macrophage cluster was performed and revealed an enrichments of M1-type inflammatory pathways in the PKCδ KO context (Figure 4.7A) (Table S2, Table S3). One particular pathway (GSE35825) involving genes expressed after IFN-γ stimulation, was of particular interest as macrophages treated with IFN-γ are known to strongly polarize to an M1-like phenotype (Figure 4.7B) [120,121]. Further examination of the top immune-related differentially expressed genes revealed upregulation of CD14 (which is a coreceptor for multiple TLRs), and IL-1β (Figure 4.8) [122]. In contrast, multiple M2-related genes were expressed at higher levels in the WT context, including Trem2, C1qc, and CD72 (Figure 4.8) [123–125]. Taken together, these results suggest that genetic loss of PKCδ leads to a shift in the TAM expression profile from an immunosuppressive M2-like phenotype to a pro-inflammatory M1-like phenotype.

A

Pathway name	pAdj	ES	NES
GSE14769_UNSTIM_VS_60MIN_LPS_BMDM_DN	1.57E-08	-0.7376585	-2.4033763
GSE14769_UNSTIM_VS_80MIN_LPS_BMDM_DN	1.57E-08	-0.7289422	-2.3745565
GSE14769_UNSTIM_VS_40MIN_LPS_BMDM_DN	1.57E-08	-0.6964576	-2.2736835
GSE14769_UNSTIM_VS_120MIN_LPS_BMDM_DN	1.57E-08	-0.6570544	-2.1450464
GSE36891_UNSTIM_VS_POLYIC_TLR3_STIM_PERITONEAL_MACROPHAGE_UP	1.57E-08	-0.7541973	-2.2417286
GSE26343_UNSTIM_VS_LPS_STIM_NFAT5_KO_MACROPHAGE_DN	1.57E-08	-0.686618	-2.2393307
GSE26343_UNSTIM_VS_LPS_STIM_MACROPHAGE_UP	1.57E-08	-0.642289	-2.0984091
GSE35825_IFNA_VS_IFNG_STIM_MACROPHAGE_UP	1.55E-07	-0.6709844	-2.0981869
GSE35825_UNTREATED_VS_IFNG_STIM_MACROPHAGE_UP	1.20E-06	-0.611017	-1.990411
GSE9509_LPS_VS_LPS_AND_IL10_STIM_IL10_KO_MACROPHAGE_10MIN_UP	2.58E-06	-0.6174491	-1.9708081

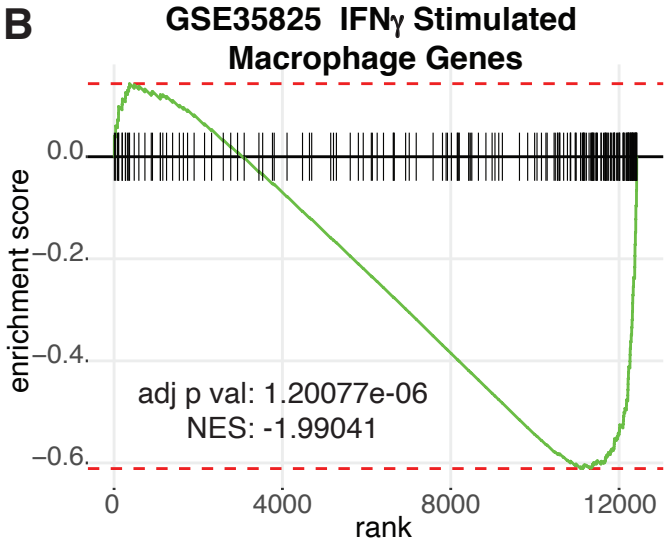

Figure 4.7: GSEA of the C1qa^{+} macrophage cluster revealed an enrichment of IFN-γ induced genes in PKCδ KO samples

(A) Table of GSEA results showing the top 10 macrophage related pathways along with the Benjamini-Hochberg adjusted p-value (padj), enrichment score (ES), and normalized enrichment score (NES). Red text highlights pathway of interest. **(B)** Gene set enrichment analysis of differentially expressed genes identified in the C1qa^{+} myeloid cluster via scRNAseq with genes ranked from highest expression in PKCδ WT samples (left) to highest expression in PKCδ KO samples (right). Adjusted p value calculated using the fgsea R package.

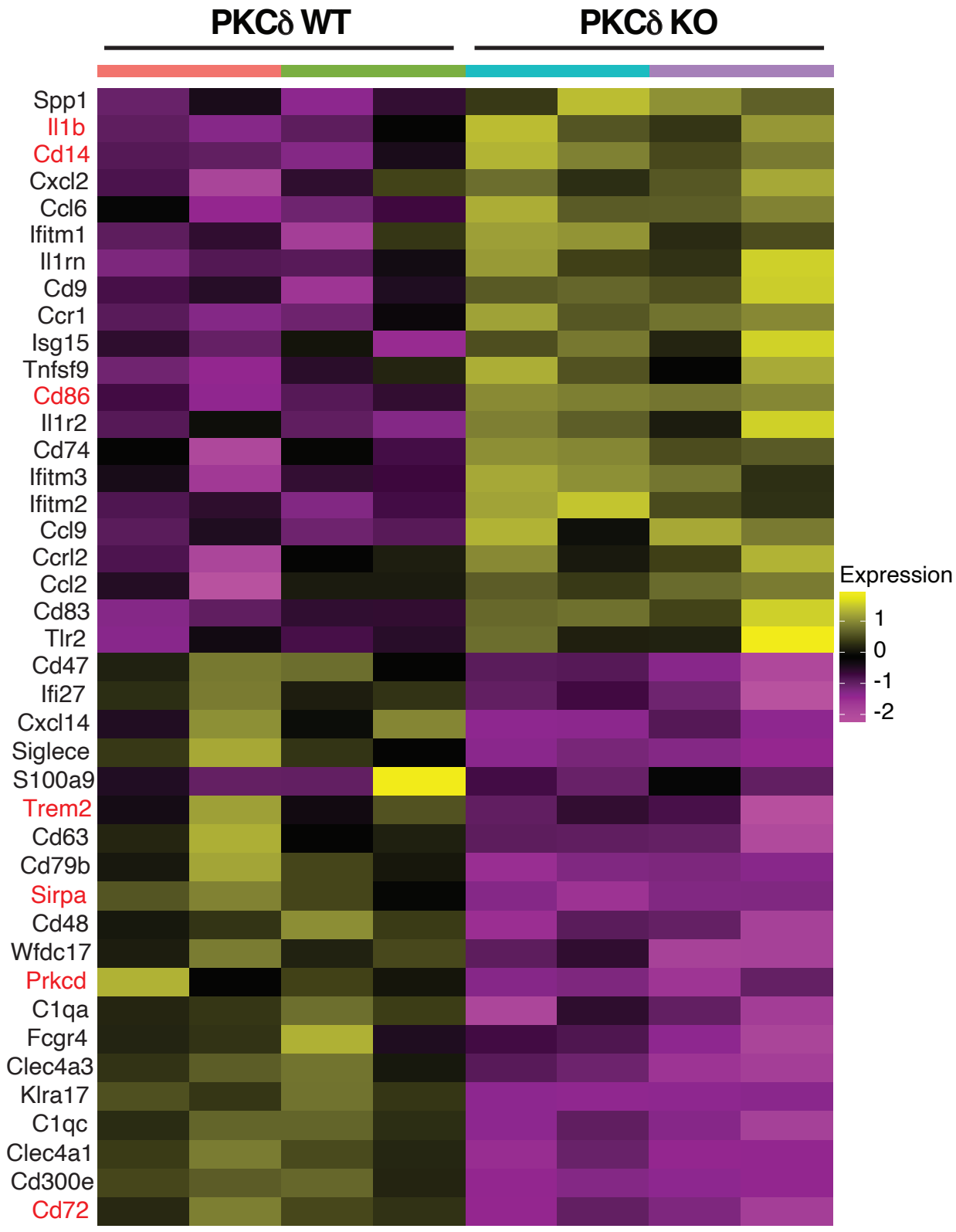

Figure 4.8: Heatmap of top DEGs in the C1qa+ myeloid population reveals enrichment of M1-type genes in KO samples and M2-type genes in WT samples

Heatmap of log normalized expression of the top immune related differentially expressed genes in the C1qa^{+} myeloid cluster. Red gene names highlight genes of particular interest. Each row represents a technical replicate.

4.4 Conditional KO mouse model with hematopoietic PKCδ loss confirms top scRNAseq hits

To further investigate the functional role of host PKCδ, and to identify cell lineages in which PKCd loss had functional impact, we generated a conditional KO (cKO) mouse model enabling targeted deletion of the PKCδ gene. Exons 7-9 were flanked by LoxP sites in C57BL/6 ES cells, which were used to generate genetically engineered mice (Figure 4.9). *Prkcd*$^{fl/fl}$ mice

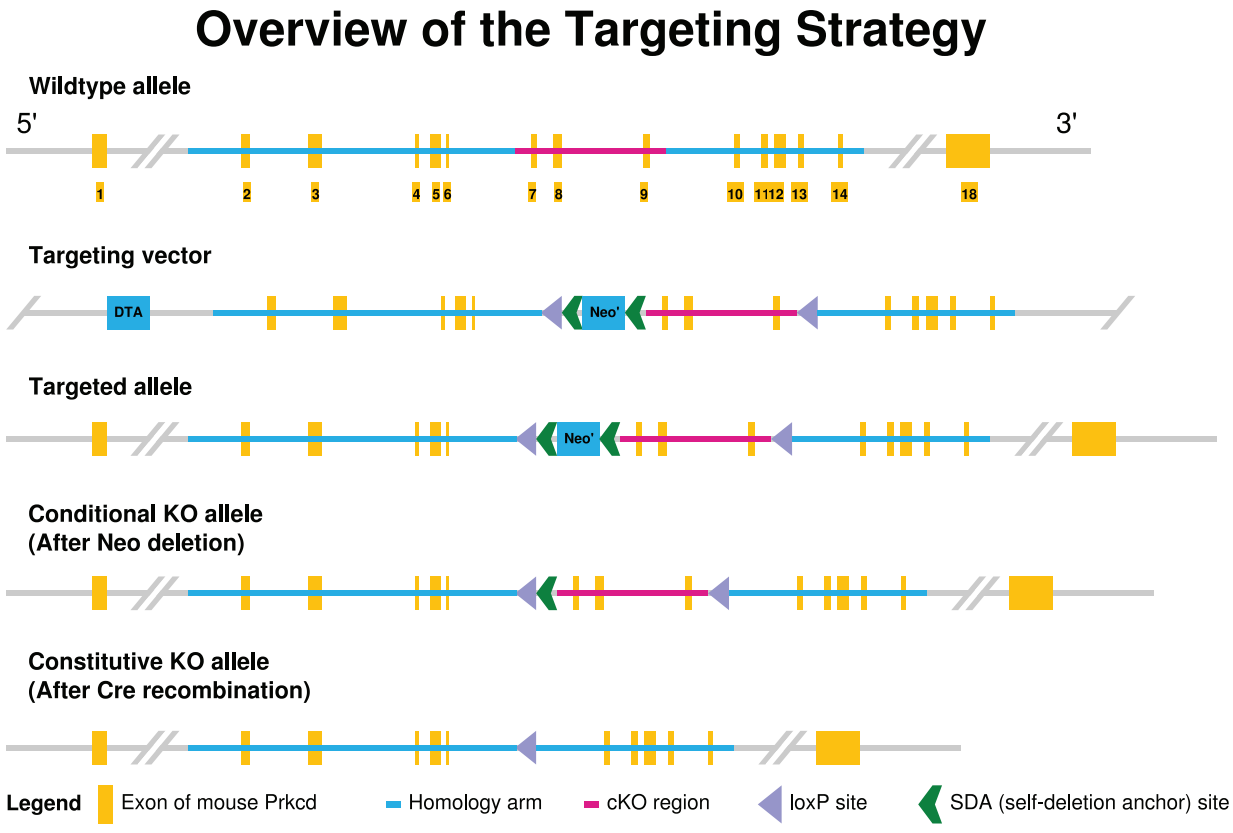

Figure 4.9: Overview of the targeting strategy employed for creation of the *Prkcd* conditional knockout mice

were first intercrossed with *Vav1*-iCre transgenic (tg) mice, to generate mice lacking *Prkcd* expression in all hematopoietic cells. When B16-SIY tumors were implanted, tumor growth was slower in *Prkcd*$^{fl/fl}$ / *Vav1*-iCre^{+} mice compared to Cre^{-} controls (Figure 4.10A, Figure 4.10B), confirming our previous results using the BM chimera model.

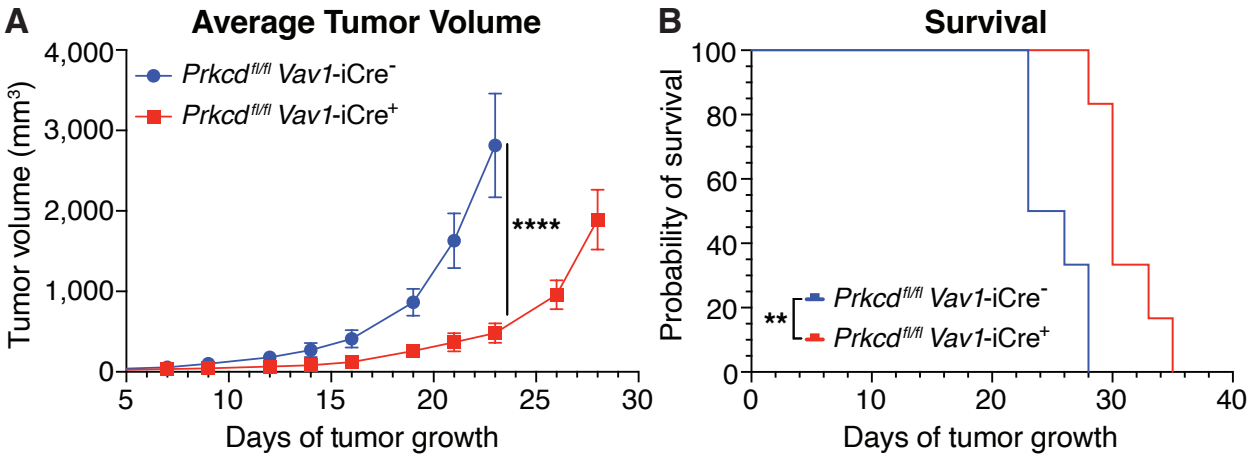

Figure 4.10: Prkcd cKO mice crossed to a hematopoietic Cre phenocopy tumor delay observed in PKCδ KO engrafted mice
(A) B16-SIY tumor volume in *Prkcd*$^{fl/fl}$ *Vav1*-iCre^{-} (blue, N=6) or *Prkcd*$^{fl/fl}$ *Vav1*-iCre^{+} animals (red, N=6). **(B)** Survival curve of B16-SIY tumor bearing *Prkcd*$^{fl/fl}$ *Vav1*-iCre^{-} animals (blue, N=6), or *Prkcd*$^{fl/fl}$ *Vav1*-iCre^{+} animals (red, N=6).

We then examined the inflammatory profile of tumor-infiltrating macrophages, first probing for representative M1 and M2 genes via RT-qPCR in TAMs isolated from *Prkcd*$^{fl/fl}$ / *Vav1*-iCre^{+} and *Prkcd*$^{fl/fl}$ / *Vav1*-iCre^{-} endpoint tumors. We found that the characteristic M2 gene *Trem2* was more highly expressed in macrophages isolated from tumors in Cre^{-} mice, and that the characteristic M1 genes *Il1b* and *Tnf* were more highly expressed in macrophages from tumors in Cre^{+} mice (Figure 4.11) [120]. As a parallel approach, we evaluated surface expression of CD14 and CD72, as these markers were top scRNAseq hits and have respectively been used to characterize M1 versus M2 differentiation states [123,126]. In agreement with the RT-qPCR data, we

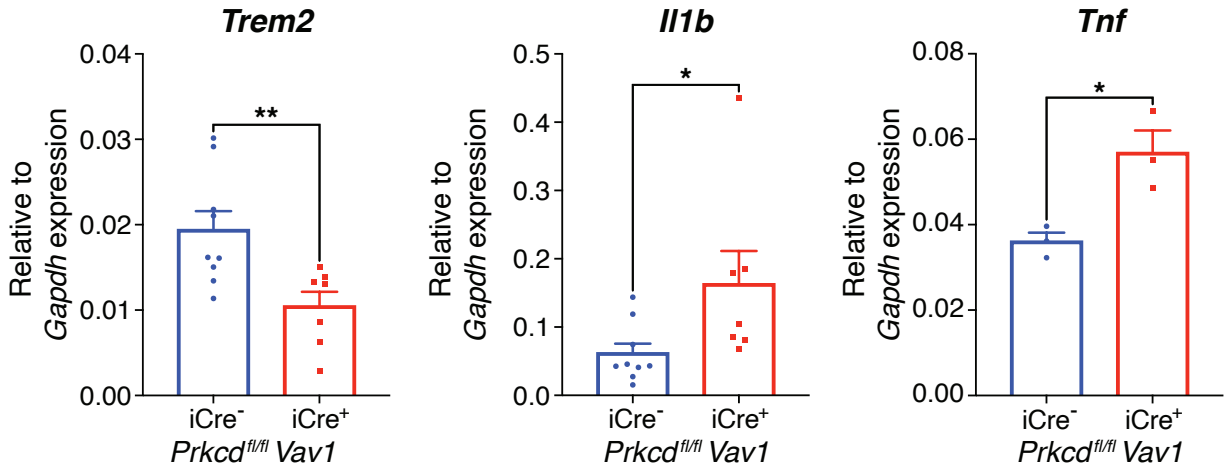

Figure 4.11: qPCR of sorted TAMs confirms shift in M1 and M2 associated genes
RT-qPCR measuring expression of *Trem2*, *Il1b*, and *Tnf* (left to right) relative to *Gapdh* in tumor associated macrophages (TAMs) sorted from *Prkcd*$^{fl/fl}$ *Vav1*-iCre^{-} tumors (blue) or *Prkcd*$^{fl/fl}$ *Vav1*-iCre^{+} tumors (red) at day 24 endpoint.

found that Cre^{+} animals had a higher percentage of TAMs expressing CD14, as well as the known activation markers CD69 and CD86, while Cre^{-} TAMs had a higher percentage of CD72-expressing TAMs, further validating our scRNAseq results (Figure 4.12) [61,127]. We confirmed these data by crossing *Vav1*-iCre mice to a second independently derived PKCδ cKO mouse line

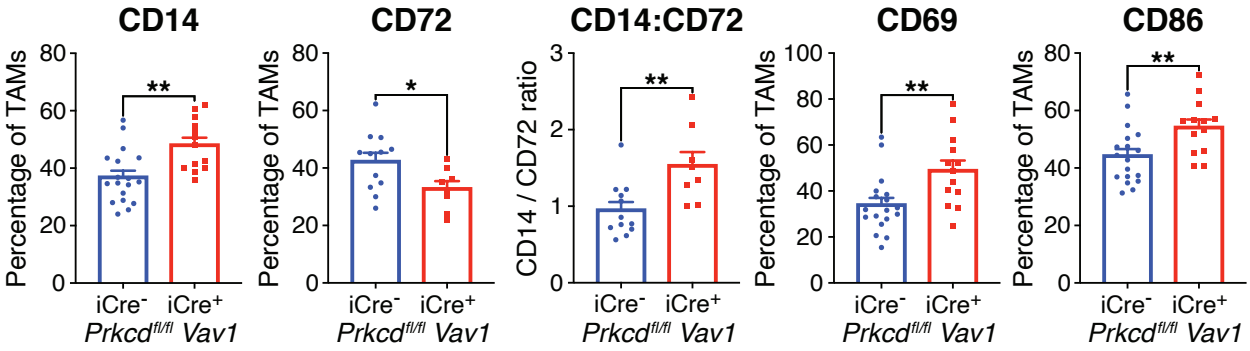

Figure 4.12: Surface expression of M1 and M2 related markers is shifted in PKCδ KO TAMs
Percentages of TAMs expressing CD14, CD72, CD69, and CD86 markers as measured by flow cytometry from *Prkcd*$^{fl/fl}$ *Vav1*-iCre^{-} mice (blue) or *Prkcd*$^{fl/fl}$ *Vav1*-iCre^{+} mice (red) at day 24 endpoint. CD14:CD72 ratio was determined by taking the % of CD14^{+} macrophages divided by the % of CD72^{+} macrophages.

and saw similar results, both in terms of the tumor growth phenotype and TAM marker expression (Figure 4.13A, Figure 4.13B). Together, these data confirm that the genetic loss of PKCδ in hematopoietic cells leads to improved immune-mediated tumor growth control and is associated with a shift in macrophages from an M2-like to an M1-like phenotype within the tumor microenvironment.

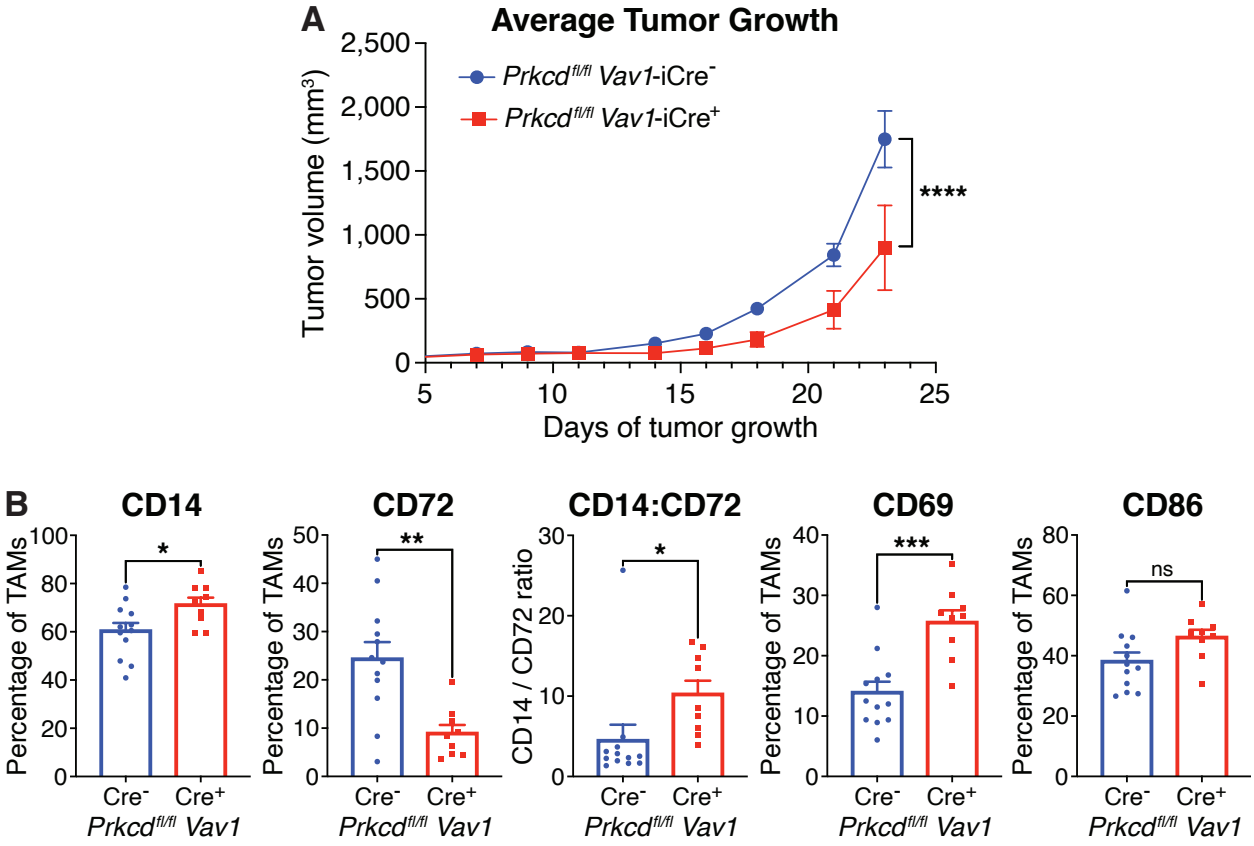

Figure 4.13: Alterative cKO strain "2C1" exhibits an identical phenotype to main "2B4" strain
(A) B16-SIY tumor volume in the alterative *Prkcd*$^{fl/fl}$ clone "2C1" expressing either *Vav1*-iCre^{-} (blue, N=8) or *Vav1*-iCre^{+} (red, N=6). **(B)** Percentages of TAMs expressing CD14, CD72, CD69, and CD86 markers as measured by flow cytometry in alterative *Prkcd*$^{fl/fl}$ clone "2C1" expressing either *Vav1*-iCre^{-} (blue) or *Vav1*-iCre^{+} mice (red) at day 24 endpoint. CD14:CD72 ratio was determined by taking the % of CD14^{+} macrophages divided by the % of CD72^{+} macrophages.

4.5 PKCδ loss in the LysM compartment is sufficient to confer tumor growth delay phenotype

To evaluate loss of PKCδ exclusively in the macrophage lineage, we crossed *Prkcd*$^{fl/fl}$ mice to LysM-Cre tg mice. We found that growth of B16-SIY tumors was significantly delayed in *Prkcd*$^{fl/fl}$ / LysM-Cre^{+} mice when compared to Cre^{-} littermate controls, phenocopying the results in the *Vav1*-Cre tg system (Figure 4.14). Similarly, we found that TAM surface marker

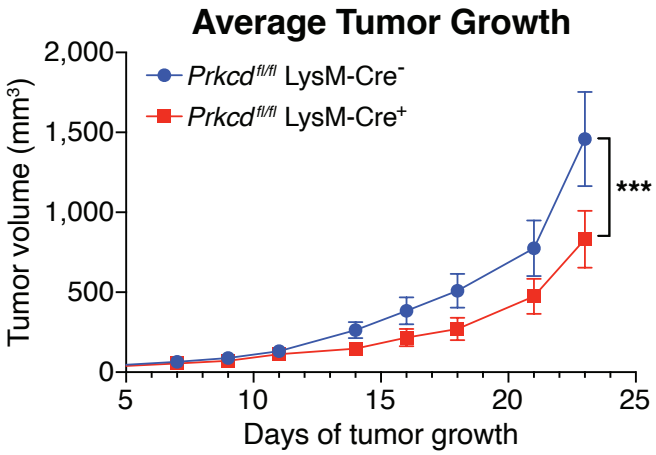

Figure 4.14: Loss of PKCδ in macrophage compartment is sufficient to confer tumor growth delay phenotype
B16-SIY tumor volume in *Prkcd*$^{fl/fl}$ LysM-Cre^{-} (blue, N=12) or *Prkcd*$^{fl/fl}$ LysM-Cre^{+} animals (red, N=11).

expression matched expression patterns observed in *Vav1*-Cre Tg system, with M1-associated genes CD14, CD69, and CD86 increased in Cre^{+} animals, while the M2-associated gene CD72 was increased in Cre- animals (Figure 4.15). We then investigated whether PKCδ loss selectively in myeloid cells could synergize with PD-1/PD-L1 blockade, similar to the results seen with complete hematopoetic loss of PKCδ. Indeed, we found a significant additional therapeutic benefit of anti-PD-L1 therapy when administered to *Prkcd*$^{fl/fl}$ / LysM-Cre^{+} mice compared to control mice (Figure 4.16A, Figure 4.16B). When LysM-Cre Tg mice were crossed to our second

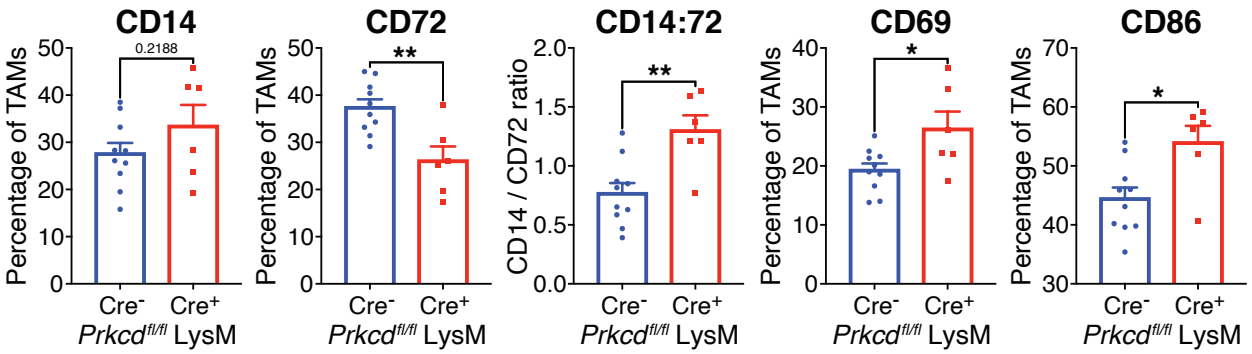

Figure 4.15: Loss of PKCδ in macrophage compartment is sufficient to confer shift in surface expression of M1 and M2 related genes
Percentages of TAMs expressing CD14, CD72, CD69, and CD86 markers as measured by flow cytometry from *Prkcd*$^{fl/fl}$ LysM-Cre^{-} mice (blue) or *Prkcd*$^{fl/fl}$ LysM-Cre^{+} mice (red) at day 24 endpoint. CD14:CD72 ratio was determined by taking the % of CD14^{+} macrophages divided by the % of CD72^{+} macrophages.

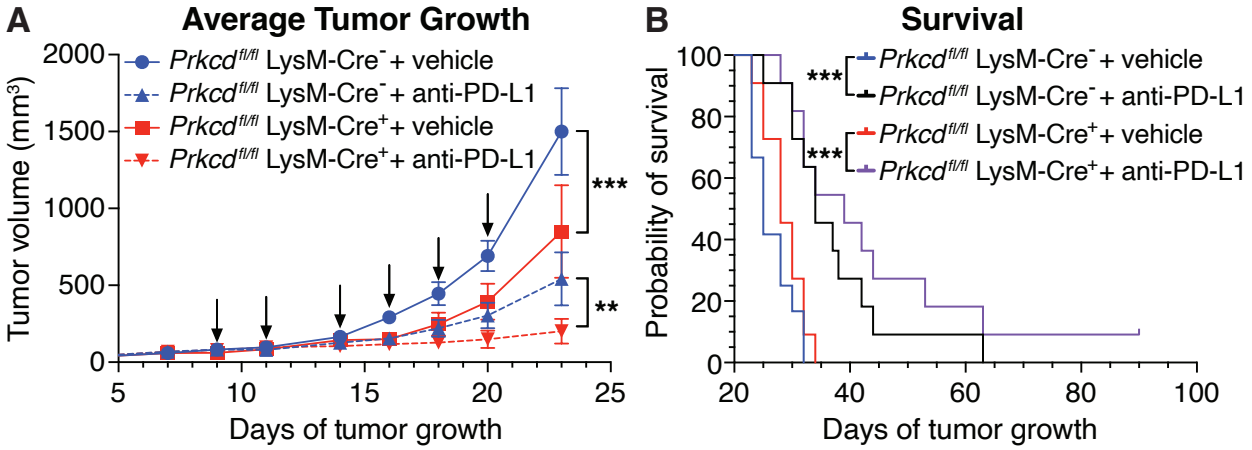

Figure 4.16: Loss of PKCδ exclusively in macrophages is sufficient to synergize with anti-PD-L1 therapy
(A) B16-SIY tumor volume in *Prkcd*$^{fl/fl}$ LysM-Cre^{-} (blue) animals treated with PBS (circle, solid line, N=10), or anti-PD-L1 (triangle dotted, dotted line, N=11), or *Prkcd*$^{fl/fl}$ LysM-Cre^{+} (red) animals treated with PBS (square, solid line, N=8), or anti-PD-L1 (upside down triangle, dotted line, N=9). Treatments are indicated with arrows and were administered 3x a week starting 7 days post tumor injection and ending after 5 doses. **(B)** Survival curve of B16-SIY tumor bearing *Prkcd*$^{fl/fl}$ LysM-Cre^{-} animals treated with PBS (blue, N=12), or anti-PD-L1 (black, N=11), or *Prkcd*$^{fl/fl}$ LysM-Cre^{+} animals treated with PBS (red, N=11), or anti-PD-L1 (purple, N=11). Treatments were administered 3x a week starting 7 days post tumor injection and ending after 5 doses.

cKO founder line, similar synergistic results with anti-PD-L1 therapy were observed (Figure 4.17). From these data we conclude that loss of PKCδ exclusively in the myeloid compartment is sufficient to delay tumor growth, shift TAM gene expression, and synergize with anti-PD-L1 therapy.

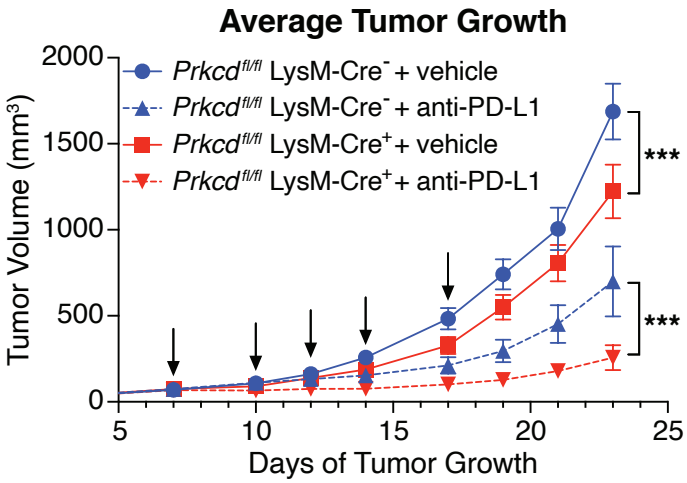

Figure 4.17: Alterative cKO strain "2C1" also exhibits anti-PD-L1 synergy with PKCδ loss in macrophages
B16-SIY tumor volume in alterative *Prkcd*$^{fl/fl}$ clone "2C1" expressing either LysM-Cre^{-} (blue) treated with PBS (solid line, N=13), or anti-PD-L1 (dotted line, N=14), or *Prkcd*$^{fl/fl}$ LysM-Cre^{+} (red) animals treated with PBS (solid line, N=11), or anti-PD-L1 (dotted line, N=11). Treatments are indicated with arrows and were administered 3x a week starting 7 days post tumor injection and ending after 5 doses.

4.6 eQTLs for *PRKCD* correlate with shifts in M1/M2 gene expression patterns

As our mouse model data indicated that loss of host PKCδ loss predominantly altered the M1/M2 phenotypic ratio in the TAM compartment, we hypothesized that eQTLs reducing *PRKCD* expression should have predictable effects on TAM gene expression in patients, similar to the effects these eQTLs have on T cell-associated genes. To this end, we utilized a previously validated list of M1 and M2 genes to create an M1 and an M2 signature score for each patient sample [108], then converted this into an M1/M2 ratio score (Table S4). Interestingly, we found that

all 3 germline eQTLs with minor alleles that correlated with decreased *PRKCD* expression, also correlated with a higher M1/M2 gene expression ratio score (Figure 4.18A, Figure 4.18B, Figure 4.18C). Thus, patients with the minor alleles of SNPs rs1483185, rs1483186, or rs750170 have diminished *PRKCD* expression which is associated with increased T cell-associated transcripts and an elevated M1/M2 ratio score in their tumors.

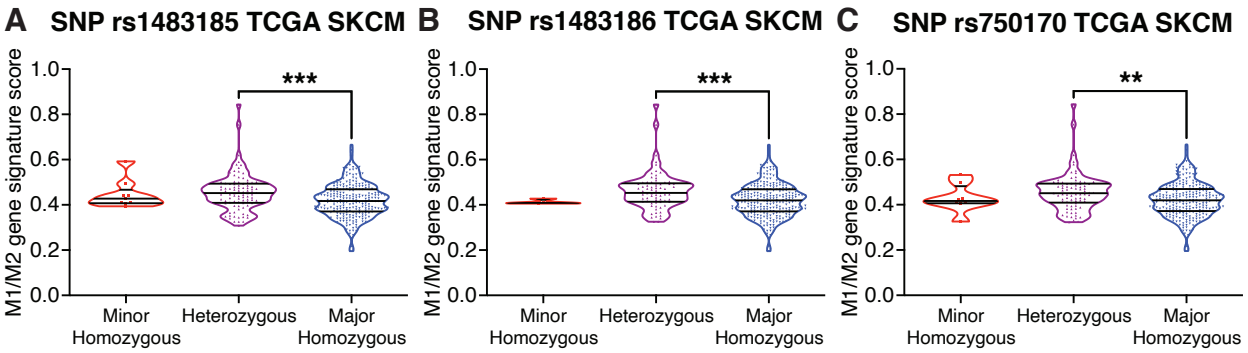

Figure 4.18: SNP alleles correlate with an M1/M2 gene signature score
(A) Violin plot of patient M1/M2 gene signature scores from a TCGA skin cutaneous melanoma (SKCM) dataset, separated by homozygous minor, heterozygous, or homozygous major alleles at the rs1483185 SNP. **(B)** Violin plot of patient M1/M2 gene signature scores from a TCGA skin cutaneous melanoma (SKCM) dataset separated by homozygous minor, heterozygous, or homozygous major alleles at the SNP rs1483186. **(C)** Violin plot of patient M1/M2 gene signature scores from a TCGA skin cutaneous melanoma (SKCM) dataset separated by homozygous minor, heterozygous, or homozygous major alleles at the SNP rs750170. Scores for (A-C) were compared between each group by ordinary one-way ANOVA and Tukey's multiple comparisons test.

4.7 A PKCδ KO-like gene signature correlates with patient response to immunotherapy

A lower M1/M2 ratio score has been reported to correspond with a "non-brisk" tumor with very little immune infiltrate [128]. As PKCδ loss appears to alter this ratio, and since immune infiltration in melanoma correlates strongly with patient response to anti-PD-1 therapy, we investigated whether a baseline PKCδ KO-related gene signature might similarly predict clinical outcome. To this end, we created a gene signature using the C1qa^{+} macrophage cluster DEGs

that were increased in PKCδ KO mouse samples and identified a human ortholog gene score (Table S5). This PKCδ KO-like gene score was then applied to a cohort of 60 metastatic melanoma patients treated with anti-PD-1-based immunotherapy, from whom baseline tumor bulk RNAseq data was available. When patients were analyzed with respect to clinical benefit, we found that the group exhibiting disease control had a significantly higher PKCδ KO-like gene signature score compared to patients with progressive disease (Figure 4.19). Together, these results suggest that patients with tumors exhibiting a gene expression profile comparable to that caused by PKCδ-deficiency in myeloid cells are predicted to have an improved response to anti-PD-1 based immunotherapy.

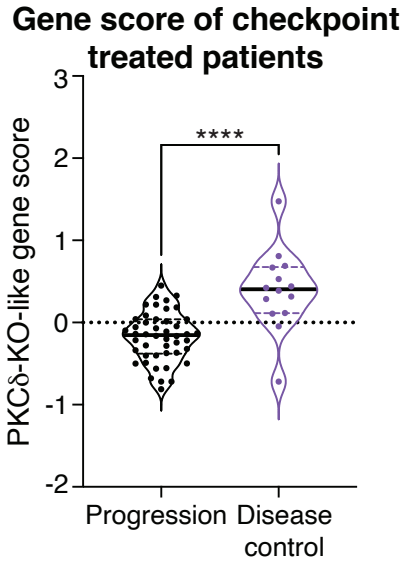

Figure 4.19: PKCδ KO-like gene signature predicts patient response to anti-PD-1 based immunotherapy
Violin plot of patient PKCδ KO-like gene signature scores calculated from bulk RNAseq samples collected before anti-PD-L1 based therapy. Patients were then split by progression (progressive disease) or disease control (stable disease, partial response, complete response) and significance calculated by Student's T-test.

4.8 Summary of findings

Our results identified an altered phenotype of tumor-associated macrophages as being a major driver of improved anti-tumor immunity in a PKCδ-deficient setting. Utilizing single cell RNA sequencing, we identified that *PRKCD* is most highly expressed in macrophages and monocytes, and over half of all differentially expressed genes between PKCδ WT and PKCδ KO samples came from neutrophils and macrophages. Investigation of these DEGs using GSEA revealed primarily a shift in expression from anti-inflammatory M2-like genes to pro-inflammatory M1-like genes. To investigate and validate the idea that PKCδ loss increases the M1:M2 phenotypic ratio, a PKCδ conditional KO mouse model crossed to a hematopoietic Cre was used. These results confirmed that TAMs isolated from PKCδ KO conditions consistently had higher expression of M1-associated genes, while WT TAMs had higher M2-associated gene expression. Expanding on this, crossing *Prkcd*$^{fl/fl}$ to LysM-Cre Tg mice revealed that loss of PKCδ in the macrophage compartment was sufficient to convey the tumor growth delay phenotype, the M2 to M1 shift in TAM surface markers, and improved response to anti-PD-L1 blockade. Translating back to human melanoma patients, the germline SNPs originally identified in chapter 3 that correlated with increased T cell gene expression and decreased *PRKCD*, also correlated with an increased M1/M2 gene expression signature. Encouragingly, we determined that patients with expression patterns mimicking the gene expression profile (GEP) observed in PKCδ KO macrophages preferentially respond to anti-PD-1-based therapies. These data highlight the clinical relevance for PKCδ status and raise the notion that development of pharmacologic inhibitors of PKCd might have therapeutic potential through shifting an M2-like TAM phenotype towards an M1-like phenotype.

Chapter 5: Discussion

5.1 Genome-wide association studies and the promise of novel target discovery

The degree of endogenous immune cell infiltration in solid tumors can be predictive of response to PD-1/PD-L1 blockade yet is dramatically variable between individual patients. The underlying mechanisms determining the degree of a T cell-inflamed versus non-T cell-inflamed tumor microenvironment are not fully understood, although investigations have shown significant contributions from tumor cell-intrinsic oncogenic events and from the composition of the gut microbiota. Similar to their influence on the severity of autoimmunity, we theorized that germline genetic determinants located in immune regulatory genes may influence tumor inflammation. Proof of concept studies have been done to partially validate this idea, with multiple groups correlating small numbers of SNPs that either have known associations with autoimmune disorders, or have a well characterized association with T cells, with patient outcome data. [116–118]. While successful, these types of candidate gene association studies have well documented issues with reproducibility, selection bias, and false positives [129]. A larger issue lies with the use of SNPs known to be immune regulatory eQTLs, as this methodology only serves to confirm previously known targets or explores potential biomarkers for the preselection of patient populations, but precludes any ability to identify novel targets. Overcoming these criticisms requires unbiased screening methods that examine the entire genome at once.

Constraints and limitations of genome-wide association studies

Most genome-wide association (GWA) studies typically have patient sample numbers in the low thousands, and it is well accepted that larger the patient pool, the more sensitive the scan will be [130]. Even in studies with large patient pools, oftentimes genuine susceptibility loci will

not rank highly in a singular study and rather are found to be moderately significant across multiple studies, leading to the observation that combining different datasets can substantially increase the power of a GWA study [131]. Indeed, we suspect that size is a major factor constraining our own GWA study as the original dataset only contained 258 patients and this lack of power likely explains why we only identified a single SNP above the genome level of significance. Despite this, our results validate the theory of identifying genetic loci responsible for anti-tumor immunity through unbiased genome-wide means, and a theoretical future study performed on a larger number of melanoma patients would likely yield many additional novel targets beyond what we have shown here.

Moving beyond melanoma and T cell-inflamed gene signatures

Additionally, we see no reason why this methodology should be isolated to SKCM datasets and postulate that the framework of our study is adaptable to address multiple questions facing tumor immunity. Specifically for questions addressed by the T cell-based gene signature score, cancers that have a large range of patient tumors spanning from T cell-inflamed to non-inflamed such as Lung, Bladder, and Kidney clear cell (among others), are excellent candidates for similar studies [9]. On the other hand, predominantly non-inflamed tumors such as Paraganglioma and Prostate are likely poor candidates for this approach. Furthermore, one could imagine complementary approaches involving alternatively developed gene signature scores. For example, if a tumor type is suspected be heavily reliant on the presence of Tregs for resistance to PD-1-based immunotherapies, a Treg gene signature score used as the quantitative phenotype in a GWA study could reveal novel control mechanisms. In fact, one could imagine creation of such scores based on T regs, myeloid cells, innate signaling, and more, as all have shown to strongly influence anti-tumor immunity.

5.2 Alternative single cell RNA sequencing hits

Many C1qa differentially expressed genes have known roles in altering cytotoxic lymphocyte function

In chapter 4.2 the C1qa^{+} macrophage population was chosen for further study as it had the second highest number of DEGs, very high expression of *PRKCD*, and because macrophages have well known positive and negative effects on tumor immunity. Indeed, the GSEA suggested that inflammatory M1-like genes were enriched in PKCδ KO DEGs, and a deeper examination of the PKCδ KO DEG list revealed many genes that are known to directly improve CTL function in the TME, providing a potential mechanistic basis for the tumor delay phenotype. For example, cytokines IL-1β and CCRL2 have been reported to directly improve CD8^{+} T cell anti-tumor immunity by increasing IFN-γ and Granzyme B production, leading to an overall improvement in cytolytic activity [132,133]. Meanwhile, CD86 and CD83 are costimulatory receptors which enhance CD8^{+} TCR signaling, preventing anergy and were both had increased expression in PKCδ KO samples. It is important to note that increased expression of Il-1β and CD86 were confirmed in TAM sorted from *Prkcd*$^{fl/fl}$/*Vav1*-iCre^{+} mice. Moving beyond our DEG list, if a shift towards a M1-like program is indeed occurring, we would expect other classical M1 genes to also be increased. Concordantly, other genes that normally accompany an M1-like inflammatory response like TNFα and CD80 were also confirmed to have increased expression in TAMs found in *Prkcd*$^{fl/fl}$/*Vav1*-iCre^{+} mice. The combination of confirmed DEG hits, along with classical inflammatory genes, strengthen the hypothesis that PKCδ KO TAMs undergo a shift towards a M1-like program and positively influence CD8^{+} T cell immunity.

Examining the other side of the DEG list, many genes increased in PKCδ WT samples (or down in PKCδ KO) are associated with promoting T cell dysfunction. One such hit was

Trem2, which has been shown to directly induce suppression and anergy on tumor-infiltrating CD8⁺ T cells. Impressively, treatment with anti-Trem2 blocking antibodies was sufficient to reverse these effects on CTL functionality and simultaneously promote response to anti-PD-L1 therapy [123,134]. Other hits increased in WT samples were CD47 and Sirpa, which are important receptors for "don't eat me signals" and loss of these receptors leads to increased phagocytosis of tumor cells, as well as improved CD8⁺ T cell functionality [135,136]. In all cited cases, these studies observed that loss of these markers leads to improved tumor immunity, and all markers are consistently lower in PKCδ KO samples. While our studies testing T cell functionality strongly imply that T cells themselves are not intrinsically altered with PKCδ loss, this does not rule out the possibility that while within the PKCδ KO TME, CD8⁺ T cells have improved functionality compared to counterpart CD8⁺ T cells in PKCδ WT TMEs. As such, further investigation into the functionality and phenotypes of tumor-infiltrating CD8⁺ T cells could be fruitful but must be done within the context of the tumor microenvironment.

Neutrophil PKCδ KO DEGs point towards a less suppressive phenotype

Despite the success with the C1qa⁺ macrophage population, the sheer number of DEGs found within the S100a9 neutrophil population warrants further investigation. It was reasoned that due to the relatively low *Prkcd* expression detected in neutrophils, it was less likely these DEGs were due to intrinsic differences caused by PKCδ loss. To investigate this, crossing PKCδ cKO to Mrp8-Cre mice would cause loss of PKCδ exclusively in the neutrophil compartment, thus determining any intrinsic contributions neutrophils may have to anti-tumor immunity. Even if no intrinsic effects are seen in these mice, this doesn't rule out a functional role for neutrophils in PKCδ KO tumors. Due to neutrophil plasticity, a shift in the cytokine milieu produced by

other cells within the TME could induce the large change in neutrophil gene expression, and these gene changes could have a functional effect contributing to improved $CD8^+$ T cell immunity.

Regardless of whether the effect is intrinsic, examining the neutrophil DEG list can shed light on the potential effects that the PKCδ KO TME has on the neutrophil compartment. Utilizing GSEA of the neutrophil DEG list revealed that PKCδ KO DEGs were enriched for genes associated with naïve-like phenotypes, while WT DEGs were enriched for genes associated with MDSC-like phenotypes (data not shown). Aligning with these data, the top overall DEG increased in PKCδ WT samples was Wfdc17, which was identified as the number one gene that differentiates MDSCs from naïve neutrophil counterparts in a recent study that used scRNAseq to a find a defining gene signature for MDSCs [137]. However, whether Wfdc17 has any functional role in neutrophils, or is simply marking a more suppressive population is completely unknown. Previous investigations of neutrophils in PKCδ KO mice have similarly shown a potential loss of suppressive activity. While activation of the NF-kB pathway, phagolysosomal maturation, autophagy, and intracellular killing of pathogens were all unaffected in PKCδ KO neutrophils, these cells were found to be deficient in reactive oxygen species (ROS) production [138]. Any potential defect in ROS production is interesting from a tumor immunity standpoint, as MDSCs completely lose their suppressive abilities *in vitro* after inhibition of ROS production [139]. There is also clear rational here for checkpoint blockade synergy, as loss of neutrophil recruitment via CXCR2 disruption enhances PD-1 efficacy. From this, a working model arises where PKCδ inhibition causes a loss of ROS-mediated suppression in neutrophils, leading to an improved $CD8^+$ CTL response [140]. Overall, these data encourage further investigation into the neutrophil compartment as a loss of suppressive ability in tumor-infiltrating

neutrophils could at least partially contribute to the mechanism of PKCδ KO improved anti-tumor immunity.

FoxP3⁺ Tregs express homeostatic maintenance genes

Interestingly the population with the third largest number of DEGs was FoxP3⁺ Tregs, despite no real detectable expression of *Prkcd* transcript. This was perhaps not completely surprising as we consistently detected increased systemic numbers of FoxP3⁺ Tregs, consistent with counter-regulation of heightened endogenous immunity. In concordance with this observation, one of the top DEGs in this population with increased expression in PKCδ KO samples was IL-7R, a gene required for Tregs to maintain homeostasis and proliferate outside of the thymus [141]. However as there were only 75 total FoxP3⁺ DEGs compared to 672 DEGs in macrophages and neutrophils, we hypothesize any functional impacts on the FoxP3⁺ Treg population within the TME are likely to be incidental and marginal in regards to anti-tumor immunity.

5.3 Potential molecular mechanisms for PKCδ in myeloid cells

PKCδ literature review reveals conflicting mechanistic roles

PKCδ is unique among other PKC isoforms in that there is a very wide range of publications describing distinct, and often contradictory, functional roles including but not limited to, apoptosis induction [142–144], proliferation and survival [145–147], immune tolerance [100], inflammation [148], transcriptional regulation [149], vasculature arteriosclerosis [104], and insulin sensitivity [102,103]. This is not meant to be an exhaustive list, but rather illustrate how wide ranging the literature is on PKCδ. Indeed, even for the most commonly cited functional role for PKCδ,

apoptosis, there are disagreements on the fundamental molecular mechanisms, such as whether caspase-3 cleavage of PKCδ controls and induces it's proapoptotic activity, or if PKCδ is upstream and regulates caspase signaling instead [142,150].

Several factors contribute to this lack of clarity in the field. First, all commercially available PKCδ inhibitors target multiple PKC isoforms and have many off-target effects. This includes Rottlerin which has been used for years as a "PKCδ specific" inhibitor [151,152]. The development of PKCδ genetic knockout models has provided effective alternatives, however groups continue to publish with these unreliable inhibitors. Second, the ligands and downstream targets for PKCδ are highly cell context specific across different cell types. Even within the same cell type, simply altering the location of PKCδ can lead to vastly different functions. For example, a study found that constitutive PKCδ targeted to the cytosol, mitochondria, or nucleus resulted in rapid apoptosis, whereas constitutive PKCδ targeted to the endoplasmic reticulum had a strong pro-survival effect in the very same cell type [153]. Finally, the phosphorylation of the unique tyrosine phosphorylation (Tyr-p) sites found throughout PKCδ cause distinct regulatory mechanisms on PKCδ's enzymology and function in ways not found with other PKCs [97,154]. This level of functional regulation could contribute to the wide variety of recorded functions. There is even evidence that PKCδ can even be activated by Tyr-p without the need of the DAG cofactor, normally required for all "novel" PKC isoforms [155]. Taken as a whole, conclusions regarding PKCδ cannot be made across cell types and stimulatory conditions, and any successful mechanistic study of PKCδ must take place within the exact cell type of interest and in the proper cellular context.

PKCδ in myeloid cells is tied to inhibition of inflammation

When examining the myeloid cell context, PKCδ is most often cited as having an anti-inflammatory function. For example, in a mouse model of tuberculosis, PKCδ KO macrophages are shown to produce large amounts of inflammatory cytokines which is predictably detrimental to the host in the context of tuberculosis infection [156]. While the mechanism of inflammatory repression remains unclear, there is evidence that PKCδ could be working through IFN signaling pathways to repress inflammatory cytokine production via direct STAT3 phosphorylation [157]. Supporting this, bone marrow derived macrophages (BMDMs) created from *Prkcd*$^{-/-}$ mice had active STAT1 signaling despite being treated with the anti-inflammatory cytokine IL-10, and these BMDMs experienced a consistent decrease in PKCδ protein after sustained treatment with IFN-α [158]. However, whether the increase in inflammatory markers observed in PKCδ KO TAMs is directly due to IFN signaling has not been examined. To initially investigate this hypothesis beyond the published *in vitro* work, we can cross our *Prkcd*$^{fl/fl}$ / LysM-Cre mice with Ifnar1$^{fl/fl}$ mice, allowing for the deletion of both PKCδ and the IFN receptor exclusively in the LysM compartment. If *Prkcd*$^{fl/fl}$ / Ifnar1$^{fl/fl}$ / LysM-Cre^{+} mice lose the phenotype of improved anti-tumor immunity and delayed growth when compared to Ifnar1$^{fl/fl}$ / LysM-Cre^{+} controls with normal PKCδ expression, then IFN signaling is likely required for transmission of inflammatory signaling caused by PKCδ loss and thus the IFN signaling pathways warrant further investigations.

Alternatively, PKCδ KO macrophages might not need IFN signaling to induce inflammatory markers. A recent CRISPR screen revealed that loss of PKCδ lead to increased expression of the inflammatory marker CD14 in THP-1 monocytic cells without any stimulatory factors, arguing that PKCδ is involved in a signaling pathway promoting an anti-inflammatory

state while actively restricting a pro-inflammatory state [159]. In fact, our data partially agrees with this as one of the top DEGs for macrophages was CD14, and significantly more PKCδ KO TAMs expressed CD14 on the surface. Clearly careful, in-depth mechanistic studies are needed to clarify the role of PKCδ in inflammation and whether IFN signaling is critically involved.

Potential non-inflammatory roles of PKCδ in myeloid cells

Although inflammatory signaling and cytokine production is the most commonly cited effect of PKCδ loss in myeloid cells, there are studies showing other possible mechanistic roles. As stated previously, PKCδ is commonly associated with apoptosis in other cells and this holds true in myeloid cells as well. Monocytes isolated from the PBMCs of human donors and treated with PKCδ siRNA revealed reduced apoptosis, although it is mechanistically unclear exactly how this occurs [160]. Similarly, patients with PKCδ null mutations had increased B cell proliferation and survival [99]. There is also evidence that PKCδ loss may improve immune function more directly, as shRNA inhibition of PKCδ in the RAW macrophage cell line significantly enhanced FCγR-mediated phagocytosis [161,162]. In totality, these data highlight the necessity to examine PKCδ not only in the appropriate cell type, but also in the relevant cellular context. Therefore, follow up studies examining PKCδ in myeloid cells should be done within the tumor context as much as possible, as *in vitro* studies may not be able to replicate the unique mix of inflammatory and suppressive characteristics that define the TME.

5.4 Therapeutic implications of PKCδ inhibition

Potential mechanisms for M1 influences on CD8⁺ T cell immunity

While shifting TAMs from an M2-state to an M1-state has been an intriguing idea for many years, there are no clinically available drugs capable of inducing such a change. Our data clearly show a shift in PKCδ KO TAMs towards M1-like gene expression, but it is less clear in our model how this phenotypic shift results in increased CD8⁺ T cells at endpoint and improved anti-tumor immunity. Recruitment of new CD8⁺ T cells to the TME could be augmented as there is evidence that M2-like TAMs can exclude CD8⁺ T cells via inhibition of CXCL9, CXCL10, and CCL2 cytokines [60,78], while M1-like TAMs may boost CD8⁺ T cell recruitment directly through increased CXCL9 production [163]. In addition to measuring cytokine expression in isolated TAMs, one could directly test for improved recruitment through an intravenous transfer of labeled tumor-antigen specific CD8⁺ T cells. By examining the tumor-infiltrating lymphocyte compartment before proliferation can occur in the transferred cells, you insure that all labeled CD8⁺ T cells identified within the tumor are newly recruited, allowing a direct comparison across groups.

Aside from improved recruitment, there are other mechanisms that can improve CD8⁺ T cell number in the TME. Previously our lab demonstrated that a subset of the CD8⁺ tumor-infiltrating lymphocytes (TILs) experience ongoing proliferation while suffering from a high rate of apoptosis, and the dynamic between these two processes strongly influences anti-tumor immunity [111,164]. In theory, if the local TME becomes more permissive for CD8⁺ T cell survival and/or proliferation, this could result in increased CD8⁺ T cell numbers by the tumor's endpoint. To this point, a recent study involving scRNAseq of non-small cell lung cancer biopsies revealed that a small subset of patients had a population of TAMs highly enriched for M1 genes. These

patients with M1-like TAM populations also had increased $CD8^+$ T resident memory cells, which they hypothesized was due to improved $CD8^+$ T cell survival [163]. Indeed, many inflammatory cytokines produced in M1-like TAMs such as IL-6 and IL-12 have well known effects on both survival and proliferation of $CD8^+$ T cells [63,165–167].

On the other hand, M2 TAMs can directly inhibit $CD8^+$ T cell survival and proliferation through metabolism of L-arginine and production of iNOS, and reductions in these factors can positively impact the $CD8^+$ T cell compartment [60,168]. Indeed, any direct effects of TAMs on $CD8^+$ T cells is likely a combined effect from both the loss of M2 suppressive factors and increased M1 inflammatory cytokines. Examination of these factors in TAMs could shed light on any connections between the macrophages and $CD8^+$ T cells in the TME. Similarly, careful examination of proliferative markers like Ki-67 and apoptotic markers like Caspase-3 in $CD8^+$ TIL may prove informative by indicating any shifts in proliferation or apoptosis respectively. Importantly, one must remember these mechanisms are not mutually exclusive and it is entirely possible improved $CD8^+$ T cell numbers are due to a combination of improved recruitment, survival, and proliferation. Regardless, a deeper mechanistic understanding can be informative in helping select future therapies to pair with a theoretical therapy based around PKCδ inhibition.

Characteristics of an ideal PKCδ inhibitor

PKCδ is a ser/ther kinase and thus can be targeted by allosteric inhibitors, although currently available inhibitors are not clinical grade and are not specific to PKCδ. Thus, we hypothesize that there is opportunity for the development of a hyper specific PKCδ inhibitor that does not impact other PKC isoforms. While chapter 5.3 showcased the wide variety of function roles that PKCδ is associated with *in vitro*, there is strong rationale that even global inhibition of

PKCδ could be relatively well tolerated on a short-term basis because it is reasonable to expect that even the best, hyper-specific PKCδ inhibitor could never reach the penetrance and complete inhibition observed in *PRKCD*^{null} humans. These well-studied patients experience moderate familial lupus symptoms, and all respond very well to immunomodulatory treatments. Even the fastest onset of lupus like symptoms in a *PRKCD*^{null} human was 15 months, with most other patients experiencing onset sometime later during early childhood [169]. While a PKCδ inhibitor will almost certainly have side effects, such as hyperproliferative B cells, there is strong reason to suspect that any side effects should be manageable and reversable based on available human data.

Of course, these conclusions are made off the assumption of a perfectly "clean" inhibitor with no unintended off target effects. Due to the structural similarities across isoforms, it might not be possible to develop an inhibitor without at least some partial overlap with the other PKCs. In both mouse and human cells, myeloid cells preferentially express PKCδ, while all other PKC isoforms range from significantly lower expression to no expression at all [119,156]. We were able to confirm these data with our own scRNAseq results and similarly found that all 9 other PKC isoforms had little to no detectable expression in myeloid cells (data not shown). These expression patterns are informative as opens the possibility of utilizing a PKCδ inhibitor that has a minor inhibitory overlap with other isoforms. If these isoforms have little to no expression in myeloid cells, the likelihood of off target effects within our intended cell type is much lower.

With the widespread expression across cell types of the other PKC isoforms, a "less-specific" PKCδ inhibitor should ideally employ a mechanism of direct targeting to the myeloid compartment to mitigate any effects it may have in other cell types and improve the therapeutic window. Due to the theoretical potential of myeloid focused therapeutics, there has been much

interest in developing methods of targeting drugs to macrophages and myeloid cells in the TME, typically using nanoparticle-based delivery methods [170]. Methods such as coating nanoparticles with mannose sugars or polyethylene glycol (PEG) allows for preferential uptake by cells expression the mannose receptor CD206, which is expressed highly on M2-like TAMs [171]. These studies, along with others targeting folate receptor B which is similarly expressed by M2-like TAMs, have allowed for very efficient targeting in preliminary mouse studies and could be utilized to specifically target a PKCδ inhibitor to the TAM compartment.

Questions remain regarding temporal mechanics surrounding inhibition of PKCδ

A critical point that remains unanswered by our study is whether temporal control matters for improved anti-tumor control and checkpoint synergy. Due to the static nature of the genetic KO models used, it remains unclear whether PKCδ inhibition must be continuous or if a short-term block is sufficient to permanently shift the TME towards inflammation. Indeed, one could imagine a scenario where once macrophage inflammation from PKCδ inhibition reaches a certain tipping point, the increase in IFN-γ produced by the introduction of additional $CD8^+$ T cells causes a sustained snowball effect resulting in TAMs remaining in an M1-like state despite the return of functional PKCδ. Alternatively, it is entirely possible that due to macrophage plasticity and the inherently suppressive effects of the TME, once PKCδ inhibition is halted there is an inevitable shift back towards M2 gene expression eventually causing T cell suppression and tumor escape. Discussed in the introduction, M2-like phenotypic TAMs have strong positive feedback loops and produce the very same cytokines that originally influence their development into the M2-like phenotype. As such, in the likely scenario where PKCδ does not cause complete conversion of the entire TAM population to an M1-like state, any remaining M2-like TAMs

could directly influence the others back towards M2-like phenotype after removal of PKCδ inhibition. These questions can be answered with the development of an efficient, effective inhibitor which can temporally control PKCδ expression. Alternatively, there is also the possibility of utilizing the Tet-Off doxycycline-inducible gene expression systems to temporally control PKCδ expression in vivo [172]. A mouse with the Tet-Off system would allow for PKCδ expression to be inhibited upon doxycycline administration. Utilizing these models during tumor development would help answer questions regarding temporal mechanics, ultimately helping determine how long patients should receive treatment.

Theoretical methods to identify patients most susceptible to PKCδ inhibition

Identifying patients that will benefit most from PKCδ inhibition can improve the likelihood of successful clinical trials and minimize any potential negative effects to patients. Based on our theoretical model, the patients most likely to respond to and benefit from PKCδ inhibition will have a T cell-inflamed TME that is dominantly suppressed by strong M2 signaling and unable to respond to checkpoint therapies. To identify these patients, development of an immunosuppressive gene signature that measures the extent anti-inflammatory M2 TAM activation, as well as possible MDSC activity, could be essential. By examining the gene expression profiles of patients with a heavy burden of M2 TAMs (as measured by IHC), and who fail to initially respond to checkpoint therapies, one could develop a core list of genes that strongly correlate to this phenotype before expanding the list in a manner similar to what was done with the T cell signature score. Pairing this theoretical suppressive gene score with a T cell-inflamed gene signature could expand the dimensionality of current patient classification from the current binary of T cell inflamed/non-inflamed to theoretically 4 different patient groups.

Group one consists of patients with a low suppressive score and a low T cell score. These patients are “immune deserts”, with strong cellular exclusion mechanisms and very little immune infiltration. As these effects are likely caused by tumor cell intrinsic pathways, these patients may benefit best from an examination of their oncogenic pathways. It is doubtful these patients would respond at all to PKCδ inhibition, as there are no TAMs present and it is unlikely PKCδ inhibition causes myeloid cells to overcome strong immune exclusion phenotypes or induce infiltration of cDC1s.

The second group are patients with a low suppressive score and a high T cell score. These patients already likely respond quite well to checkpoint blockade therapy, with strong T cell activity and weak T cell-extrinsic suppressive mechanisms. Any TAMs in these patients are likely to already be M1-like, and therefore this patient group is unlikely to further benefit from PKCδ inhibition. However, it would be very beneficial to further examine any patients in this group that fail to respond to checkpoint therapy for alterative suppression mechanisms or novel checkpoint markers. Additionally, patients who eventually relapse should be examined again using the immunosuppressive gene score, as secondary resistance to checkpoint could be occurring through an M2 TAM related immunosuppressive mechanism and thus could potentially benefit from subsequent PKCδ inhibition during a second round of therapy.

The third group and perhaps the most difficult to predict, are patients with a high suppressive score but a low T cell score. One likely scenario is that these patients suffer from a failure of cDC1s to enter the tumor, mature, pick-up antigen, and prime $CD8^+$ T cells in the TdLN. As our mouse models of PKCδ KO saw no improvements in priming, it is unlikely that PKCδ inhibition would kickstart cDC1-mediated priming and trigger a $CD8^+$ T cell response. However, there is another possible scenario where $CD8^+$ T cells have been primed but are unable

to efficiently enter the TME in great numbers. For example, this situation can occur when reactive nitrogen species cause posttranslational modifications of T cell recruitment cytokines like CCL2, resulting in antigen specific $CD8^+$ T cells failing to enter the TME [173]. As mentioned earlier in the chapter, it is unclear whether the increase in $CD8^+$ T cells observed in our model is due to improved proliferation, recruitment, or both. If PKCδ indeed improves $CD8^+$ T cell numbers through increased recruitment, then it is possible a select portion of patients in this unique scenario could see benefit from a PKCδ inhibitor.

The fourth and final population would be patients with a high immunosuppressive score and a high T cell score. These patients are theoretically less likely to respond checkpoint-based therapies than patients in group two, as the strong presence of immunosuppressive cells would presumably be the dominant form of CTL suppression in some patients. As stated earlier, we hypothesize these are the patients that would receive the most benefit from a PKCδ inhibitor, specifically in combination with checkpoint inhibitors. By alleviating this method of myeloid cell-based suppression, patients who previously would not have responded to checkpoint therapy likely would now be sensitized to it.

5.5 Summary of future directions

Looking forward, we postulate that this is just the first step in mining germline sequencing data for novel targets. The fact that a relatively small data set still yielded an actionable result that was mechanistically confirmed in mouse models bodes well for future GWA studies on larger scales. Our methodology of using a quantitative score to measure immunity could also be expanded outside of our T cell signature score, instead utilizing a theoretical immunosuppressive score or another custom gene score targeted to the immune

phenotype of interest. Inasmuch as therapeutic strategies aiming to decrease M2 phenotype macrophages from the tumor microenvironment and promote an M1-like state are highly desirable yet still lacking, our results suggest that PKCδ may be an attractive therapeutic target in this regard. While there is substantial work that needs to be done to uncover the molecular basis for PKCδ inflammation, we suspect that uncovering the upstream ligands and downstream phosphorylation substrates will ultimately be insightful. These unknowns notwithstanding, our data supports prioritizing the future development of allosteric inhibitors that preferentially inhibit PKCδ activity while sparing other important PKC isoforms.

References

1. Ayers, M. *et al.* IFN-γ–related mRNA profile predicts clinical response to PD-1 blockade. *J. Clin. Invest.* **127**, (2017).

2. Tumeh, P. C. *et al.* PD-1 blockade induces responses by inhibiting adaptive immune resistance. *Nature* **515**, 568–571 (2014).

3. Danaher, P. *et al.* Pan-cancer adaptive immune resistance as defined by the Tumor Inflammation Signature (TIS): Results from The Cancer Genome Atlas (TCGA). *J. Immunother. Cancer* **6**, (2018).

4. Gokuladhas, S., Schierding, W., Golovina, E., Fadason, T. & O'Sullivan, J. Unravelling the Shared Genetic Mechanisms Underlying 18 Autoimmune Diseases Using a Systems Approach. *Front. Immunol.* **12**, 3262 (2021).

5. Kandoth, C. *et al.* Mutational landscape and significance across 12 major cancer types. *Nat. 2013 5027471* **502**, 333–339 (2013).

6. van der Kooij, M. K., Speetjens, F. M., van der Burg, S. H. & Kapiteijn, E. Uveal Versus Cutaneous Melanoma; Same Origin, Very Distinct Tumor Types. *Cancers 2019, Vol. 11, Page 845* **11**, 845 (2019).

7. Dagogo-Jack, I. & Shaw, A. T. Tumour heterogeneity and resistance to cancer therapies. *Nat. Rev. Clin. Oncol. 2017 152* **15**, 81–94 (2017).

8. Sweis, R. F. *et al.* Molecular Drivers of the Non-T-cell-Inflamed Tumor Microenvironment in Urothelial Bladder Cancer. *Cancer Immunol. Res.* **4**, 563–568 (2016).

9. Spranger, S. *et al.* Density of immunogenic antigens does not explain the presence or absence of the T-cell–inflamed tumor microenvironment in melanoma. *Proc. Natl. Acad. Sci.* **113**, E7759–E7768 (2016).

10. Chowell, D. *et al.* Improved prediction of immune checkpoint blockade efficacy across multiple cancer types. *Nat. Biotechnol. 2021 404* **40**, 499–506 (2021).

11. Spranger, S. & Gajewski, T. Rational combinations of immunotherapeutics that target discrete pathways. *J. Immunother. Cancer* **1**, 1 (2013).

12. Melaiu, O., Lucarini, V., Cifaldi, L. & Fruci, D. Influence of the Tumor Microenvironment on NK Cell Function in Solid Tumors. *Front. Immunol.* **10**, 3038 (2020).

13. Hildner, K. *et al.* Batf3 Deficiency Reveals a Critical Role for CD8a+ Dendritic Cells in Cytotoxic T Cell Immunity. *Science (80-.).* **322**, 1097–1100 (2008).

14. Fuertes, M. B. *et al.* Host type I IFN signals are required for antitumor CD8+ T cell responses through CD8α+ dendritic cells. *J. Exp. Med.* **208**, 2005–2016 (2011).

15. Böttcher, J. P. *et al.* NK Cells Stimulate Recruitment of cDC1 into the Tumor Microenvironment Promoting Cancer Immune Control. *Cell* **172**, 1022-1037.e14 (2018).

16. Spranger, S., Bao, R. & Gajewski, T. F. Melanoma-intrinsic β-catenin signalling prevents anti-tumour immunity. *Nature* **523**, 231–235 (2015).

17. Fuertes, M. B., Woo, S. R., Burnett, B., Fu, Y. X. & Gajewski, T. F. Type I interferon response and innate immune sensing of cancer. *Trends Immunol.* **34**, 67–73 (2013).

18. Sistigu, A. *et al.* Cancer cell-autonomous contribution of type I interferon signaling to the efficacy of chemotherapy. *Nat. Med.* **20**, 1301–1309 (2014).

19. Diamond, M. S. *et al.* Type I interferon is selectively required by dendritic cells for immune rejection of tumors. *J. Exp. Med.* **208**, 1989–2003 (2011).

20. Lim, J. Y. H., Gerber, S. A., Murphy, S. P. & Lord, E. M. Type i interferons induced by radiation therapy mediate recruitment and effector function of CD8+ T cells. *Cancer Immunol. Immunother.* **63**, 259–271 (2014).

21. Woo, S. R. *et al.* STING-dependent cytosolic DNA sensing mediates innate immune recognition of immunogenic tumors. *Immunity* **41**, 830–842 (2014).

22. Ishikawa, H., Ma, Z. & Barber, G. N. STING regulates intracellular DNA-mediated, type i interferon-dependent innate immunity. *Nature* **461**, 788–792 (2009).

23. Woo, S. R., Corrales, L. & Gajewski, T. F. The STING pathway and the T cell-inflamed tumor microenvironment. *Trends Immunol.* **36**, 250–256 (2015).

24. Spranger, S. *et al.* Up-regulation of PD-L1, IDO, and T(regs) in the melanoma tumor microenvironment is driven by CD8(+) T cells. *Sci. Transl. Med.* **5**, 200ra116 LP-200ra116 (2013).

25. Salmon, H. *et al.* Expansion and Activation of CD103+ Dendritic Cell Progenitors at the Tumor Site Enhances Tumor Responses to Therapeutic PD-L1 and BRAF Inhibition. *Immunity* **44**, 924–938 (2016).

26. Cummings, R. J. *et al.* Exposure to Ionizing Radiation Induces the Migration of Cutaneous Dendritic Cells by a CCR7-Dependent Mechanism. *J. Immunol.* **189**, 4247–4257 (2012).

27. Roberts, E. W. *et al.* Critical Role for CD103(+)/CD141(+) Dendritic Cells Bearing CCR7 for Tumor Antigen Trafficking and Priming of T Cell Immunity in Melanoma. *Cancer Cell* **30**, 324–336 (2016).

28. Broz, M. L. *et al.* Dissecting the Tumor Myeloid Compartment Reveals Rare Activating Antigen-Presenting Cells Critical for T Cell Immunity. *Cancer Cell* **26**, 638–652 (2014).

29. Broz, M. L. & Krummel, M. F. The Emerging Understanding of Myeloid Cells as Partners and Targets in Tumor Rejection. *Cancer Immunol. Res.* **3**, 313–319 (2015).

30. Merad, M., Sathe, P., Helft, J., Miller, J. & Mortha, A. The Dendritic Cell Lineage: Ontogeny and Function of Dendritic Cells and Their Subsets in the Steady State and the Inflamed Setting. *Annu. Rev. Immunol.* **31**, 563–604 (2013).

31. Gutiérrez-Martínez, E. *et al.* Cross-Presentation of Cell-Associated Antigens by MHC Class I in Dendritic Cell Subsets. *Front. Immunol.* **6**, 363 (2015).

32. Durai, V. & Murphy, K. M. Functions of Murine Dendritic Cells. *Immunity* **45**, 719–736 (2016).

33. Nowacki, T. M. *et al.* Granzyme B production distinguishes recently activated CD8+ memory cells from resting memory cells. *Cell. Immunol.* **247**, 36–48 (2007).

34. Spranger, S., Dai, D., Horton, B. & Gajewski, T. F. Tumor-Residing Batf3 Dendritic Cells Are Required for Effector T Cell Trafficking and Adoptive T Cell Therapy. *Cancer Cell* **31**, 711-723.e4 (2017).

35. Harlin, H. *et al.* Chemokine expression in melanoma metastases associated with CD8 + T-CeII recruitment. *Cancer Res.* **69**, 3077–3085 (2009).

36. Gajewski, T. F., Schreiber, H. & Fu, Y.-X. Innate and adaptive immune cells in the tumor microenvironment. *Nat. Immunol.* **14**, 1014–1022 (2013).

37. Ziblat, A., Horton, B., Higgs, E., Hatogai, K. & Gajewski, T. 328 Batf3 dendritic cells and 4–1BB/4–1BB ligand axis are required at the effector phase within the tumor microenvironment for anti-PD-L1 efficacy. *J. Immunother. Cancer* **9**, A354–A354 (2021).

38. Kim, J. *et al.* Cutting Edge: Depletion of Foxp3+ Cells Leads to Induction of Autoimmunity by Specific Ablation of Regulatory T Cells in Genetically Targeted Mice. *J. Immunol.* **183**, 7631–7634 (2009).

39. Shang, B., Liu, Y., Jiang, S. J. & Liu, Y. Prognostic value of tumor-infiltrating FoxP3+ regulatory T cells in cancers: a systematic review and meta-analysis. *Sci. Reports 2015 51* **5**, 1–9 (2015).

40. Speiser, D. E., Ho, P. C. & Verdeil, G. Regulatory circuits of T cell function in cancer. *Nat. Rev. Immunol. 2016 1610* **16**, 599–611 (2016).

41. Munn, D. H. & Bronte, V. Immune suppressive mechanisms in the tumor microenvironment. *Curr. Opin. Immunol.* **39**, 1–6 (2016).

42. Yang, S. H. *et al.* The molecular basis of immune regulation in autoimmunity. *Clin. Sci.* **132**, 43–67 (2018).

43. Singh, S., Ross, S. R., Acena, M., Rowley, D. A. & Schreiber, H. Stroma Is Critical for Preventing or Permitting Immunological Destruction of Antigenic Cancer Cells.

44. Schito, L. Bridging angiogenesis and immune evasion in the hypoxic tumor microenvironment. *Am. J. Physiol. - Regul. Integr. Comp. Physiol.* **315**, R1072–R1084 (2018).

45. Semenza, G. L. Intratumoral hypoxia and mechanisms of immune evasion mediated by hypoxia- inducible factors. *Physiology* **36**, 73–83 (2021).

46. OTA, Y. *et al.* Effect of nutrient starvation on proliferation and cytokine secretion of peripheral blood lymphocytes. *Mol. Clin. Oncol.* **4**, 607 (2016).

47. Batlle, E. & Massagué, J. Transforming Growth Factor-β Signaling in Immunity and Cancer. *Immunity* **50**, 924–940 (2019).

48. Meireson, A., Devos, M. & Brochez, L. IDO Expression in Cancer: Different Compartment, Different Functionality? *Front. Immunol.* **11**, 2340 (2020).

49. Spranger, S. & Gajewski, T. F. Impact of oncogenic pathways on evasion of antitumour immune responses. *Nat. Rev. Cancer 2018 183* **18**, 139–147 (2018).

50. Li, J. *et al.* Tumor Cell-Intrinsic Factors Underlie Heterogeneity of Immune Cell Infiltration and Response to Immunotherapy. *Immunity* **49**, 178-193.e7 (2018).

51. Bassler, K., Schulte-Schrepping, J., Warnat-Herresthal, S., Aschenbrenner, A. C. & Schultze, J. L. The Myeloid Cell Compartment—Cell by Cell. *https://doi.org/10.1146/annurev-immunol-042718-041728* **37**, 269–293 (2019).

52. Gabrilovich, D. I. Myeloid-derived suppressor cells. *Cancer Immunol. Res.* **5**, 3 (2017).

53. Veglia, F., Sanseviero, E. & Gabrilovich, D. I. Myeloid-derived suppressor cells in the era of increasing myeloid cell diversity. *Nat. Rev. Immunol. 2021 218* **21**, 485–498 (2021).

54. Grzywa, T. M. *et al.* Myeloid Cell-Derived Arginase in Cancer Immune Response. *Front. Immunol.* **11**, 938 (2020).

55. Ostrand-Rosenberg, S. & Fenselau, C. Myeloid-Derived Suppressor Cells: Immune-Suppressive Cells That Impair Antitumor Immunity and Are Sculpted by Their Environment. *J. Immunol.* **200**, 422–431 (2018).

56. Groth, C. *et al.* Immunosuppression mediated by myeloid-derived suppressor cells (MDSCs) during tumour progression. *Br. J. Cancer 2018 1201* **120**, 16–25 (2018).

57. Orecchioni, M., Ghosheh, Y., Pramod, A. B. & Ley, K. Macrophage polarization: Different gene signatures in M1(Lps+) vs. Classically and M2(LPS-) vs. Alternatively activated macrophages. *Front. Immunol.* **10**, 1084 (2019).

58. Chen, Y. *et al.* Tumor-associated macrophages: An accomplice in solid tumor progression. *J. Biomed. Sci.* **26**, 1–13 (2019).

59. Zhang, B. *et al.* M2-Polarized tumor-associated macrophages are associated with poor prognoses resulting from accelerated lymphangiogenesis in lung adenocarcinoma. *Clinics* **66**, 1879 (2011).

60. Pan, Y., Yu, Y., Wang, X. & Zhang, T. Tumor-Associated Macrophages in Tumor Immunity. *Front. Immunol.* **11**, 3151 (2020).

61. Li, C. *et al.* Tumor-associated macrophages: potential therapeutic strategies and future prospects in cancer. *J. Immunother. Cancer* **9**, e001341 (2021).

62. Fujimura, T., Kambayashi, Y., Fujisawa, Y., Hidaka, T. & Aiba, S. Tumor-associated macrophages: Therapeutic targets for skin cancer. *Front. Oncol.* **8**, 3 (2018).

63. Lu, D. *et al.* Beyond T Cells: Understanding the Role of PD-1/PD-L1 in Tumor-Associated Macrophages. *J. Immunol. Res.* **2019**, (2019).

64. Zhou, J. *et al.* Tumor-Associated Macrophages: Recent Insights and Therapies. *Front. Oncol.* **10**, 1–13 (2020).

65. Jayasingam, S. D. *et al.* Evaluating the Polarization of Tumor-Associated Macrophages Into M1 and M2 Phenotypes in Human Cancer Tissue: Technicalities and Challenges in Routine Clinical Practice. *Front. Oncol.* **9**, 1512 (2020).

66. Liu, J., Geng, X., Hou, J. & Wu, G. New insights into M1/M2 macrophages: key modulators in cancer progression. *Cancer Cell Int.* **21**, 1–7 (2021).

67. Pantano, F. *et al.* The role of macrophages polarization in predicting prognosis of radically resected gastric cancer patients. *J. Cell. Mol. Med.* **17**, 1415–1421 (2013).

68. Murray, P. J. *et al.* Macrophage Activation and Polarization: Nomenclature and Experimental Guidelines. *Immunity* **41**, 14–20 (2014).

69. Murray, P. J. Macrophage Polarization. *http://dx.doi.org/10.1146/annurev-physiol-022516-034339* **79**, 541–566 (2017).

70. Kakizaki, A. *et al.* Immunomodulatory effect of peritumorally administered interferon-beta on melanoma through tumor-associated macrophages. *Oncoimmunology* **4**, (2015).

71. He, X. & Xu, C. Immune checkpoint signaling and cancer immunotherapy. *Cell Res. 2020 308* **30**, 660–669 (2020).

72. Alsaab, H. O. *et al.* PD-1 and PD-L1 checkpoint signaling inhibition for cancer immunotherapy: mechanism, combinations, and clinical outcome. *Front. Pharmacol.* **8**, 561 (2017).

73. Spranger, S. *et al.* Mechanism of tumor rejection with doublets of CTLA-4, PD-1/PD-L1, or IDO blockade involves restored IL-2 production and proliferation of CD8+T cells directly within the tumor microenvironment. *J. Immunother. Cancer* **2**, 1–14 (2014).

74. Hodi, F. S. *et al.* Improved Survival with Ipilimumab in Patients with Metastatic Melanoma. *N. Engl. J. Med.* **363**, 711–723 (2010).

75. Vafaei, S. *et al.* Combination therapy with immune checkpoint inhibitors (ICIs); a new frontier. *Cancer Cell Int.* **22**, 1–27 (2022).

76. Larkin, J. *et al.* Five-Year Survival with Combined Nivolumab and Ipilimumab in Advanced Melanoma. *N. Engl. J. Med.* **381**, 1535–1546 (2019).

77. Varayathu, H., Sarathy, V., Thomas, B. E., Mufti, S. S. & Naik, R. Combination Strategies to Augment Immune Check Point Inhibitors Efficacy - Implications for Translational Research. *Front. Oncol.* **11**, 1844 (2021).

78. Peranzoni, E. *et al.* Macrophages impede CD8 T cells from reaching tumor cells and limit the efficacy of anti–PD-1 treatment. *Proc. Natl. Acad. Sci. U. S. A.* **115**, E4041–E4050 (2018).

79. Chen, J. *et al.* Predictive immune biomarker signatures in the tumor microenvironment of melanoma metastases associated with tumor-infiltrating lymphocyte (TIL) therapy. *J. Immunother. Cancer* **2**, P243 (2014).

80. Gerber, S. A. S. A. *et al.* IFN-γ mediates the antitumor effects of radiation therapy in a murine colon tumor. *Am. J. Pathol.* **182**, 2345–2354 (2013).

81. Spranger, S. Mechanisms of tumor escape in the context of the T-cell-inflamed and the non-T-cell-inflamed tumor microenvironment. *Int. Immunol.* **28**, 383–391 (2016).

82. Peng, W. *et al.* Loss of PTEN promotes resistance to T cell–mediated immunotherapy. *Cancer Discov.* **6**, 202–216 (2016).

83. Fessler, J., Matson, V. & Gajewski, T. F. Exploring the emerging role of the microbiome in cancer immunotherapy. *J. Immunother. Cancer* **7**, 108 (2019).

84. Sivan, A. *et al.* Commensal Bifidobacterium promotes antitumor immunity and facilitates anti-PD-L1 efficacy. *Science* **350**, 1084–9 (2015).

85. Matson, V. *et al.* The commensal microbiome is associated with anti-PD-1 efficacy in metastatic melanoma patients. *Science (80-.).* **359**, 104–108 (2018).

86. Davar, D. *et al.* Fecal microbiota transplant overcomes resistance to anti-PD-1 therapy in melanoma patients. *Science (80-.).* **371**, 595–602 (2021).

87. Surolia, I. *et al.* Functionally defective germline variants of sialic acid acetylesterase in autoimmunity. *Nat. 2010 4667303* **466**, 243–247 (2010).

88. Ni, J. *et al.* Integration of GWAS and eQTL Analysis to Identify Risk Loci and Susceptibility Genes for Gastric Cancer. *Front. Genet.* **11**, 679 (2020).

89. Ricaño-Ponce, I. & Wijmenga, C. Mapping of Immune-Mediated Disease Genes. *http://dx.doi.org/10.1146/annurev-genom-091212-153450* **14**, 325–353 (2013).

90. Auton, A. *et al.* A global reference for human genetic variation. *Nat. 2015 5267571* **526**, 68–74 (2015).

91. Nica, A. C. & Dermitzakis, E. T. Expression quantitative trait loci: present and future. *Philos. Trans. R. Soc. B Biol. Sci.* **368**, (2013).

92. Bush, W. S. & Moore, J. H. Chapter 11: Genome-Wide Association Studies. *PLOS Comput. Biol.* **8**, e1002822 (2012).

93. Mellor, H. & Parker, P. J. The extended protein kinase C superfamily. *Biochem. J.* **332**, 281 (1998).

94. Spitaler, M. & Cantrell, D. A. Protein kinase C and beyond. *Nat. Immunol.* **5**, 785–790 (2004).

95. Kikkawa, U., Matsuzaki, H. & Yamamoto, T. Protein Kinase C (PKC): Activation Mechanisms and Functions. *J. Biochem.* **132**, 831–839 (2002).

96. Pappa, H., Murray-Rust, J., Dekker, L. V., Parker, P. J. & McDonald, N. Q. Crystal structure of the C2 domain from protein kinase C-δ. *Structure* **6**, 885–894 (1998).

97. Steinberg, S. F. Distinctive activation mechanisms and functions for protein kinase Cdelta. *Biochem. J.* **384**, 449–59 (2004).

98. Belot, A. *et al.* Protein kinase Cδ deficiency causes mendelian systemic lupus erythematosus with B cell-defective apoptosis and hyperproliferation. *Arthritis Rheum.* **65**, 2161–2171 (2013).

99. Kuehn, H. S. *et al.* Loss-of-function of the protein kinase C d (PKCd) causes a B-cell lymphoproliferative syndrome in humans. *Blood* **121**, 3117–3126 (2013).

100. Mecklenbräuker, I., Saijo, K., Zheng, N.-Y., Leitges, M. & Tarakhovsky, A. Protein kinase Cδ controls self-antigen-induced B-cell tolerance. *Nature* **416**, 860–865 (2002).

101. Miyamoto, A. *et al.* Increased proliferation of B cells and auto-immunity in mice lacking protein kinase Cδ. *Nature* **416**, 865–869 (2002).

102. Li, M., Vienberg, S. G., Bezy, O., O'Neill, B. T. & Kahn, C. R. Role of PKCδ in Insulin Sensitivity and Skeletal Muscle Metabolism. *Diabetes* **64**, 4023–32 (2015).

103. Bezy, O. *et al.* PKCδ regulates hepatic insulin sensitivity and hepatosteatosis in mice and humans. *J. Clin. Invest.* **121**, 2504–2517 (2011).

104. Leitges, M. *et al.* Exacerbated vein graft arteriosclerosis in protein kinase C δ – null mice. *J. Clin. Invest.* **108**, 1505–1512 (2001).

105. Shabalin, A. A. Matrix eQTL: ultra fast eQTL analysis via large matrix operations. *Bioinformatics* **28**, 1353–1358 (2012).

106. Lappalainen, T. *et al.* Transcriptome and genome sequencing uncovers functional variation in humans. *Nature* **501**, 506–511 (2013).

107. Luke, J. J., Bao, R., Sweis, R. F., Spranger, S. & Gajewski, T. F. WNT/b-catenin pathway activation correlates with immune exclusion across human cancers. *Clin. Cancer Res.* **25**, 3074–3083 (2019).

108. Newman, A. M. *et al.* Robust enumeration of cell subsets from tissue expression profiles. *Nat. Methods* **12**, 453–457 (2015).

109. Hoadley, K. A. *et al.* Cell-of-Origin Patterns Dominate the Molecular Classification of 10,000 Tumors from 33 Types of Cancer. *Cell* **173**, 291-304.e6 (2018).

110. Gao, J. *et al.* Integrative analysis of complex cancer genomics and clinical profiles using the cBioPortal. *Sci. Signal.* **6**, 1–2 (2013).

111. Williams, J. B. *et al.* The EGR2 targets LAG-3 and 4-1BB describe and regulate dysfunctional antigen-specific CD8+ T cells in the tumor microenvironment. *J. Exp. Med.* **214**, 381–400 (2017).

112. Zappia, L. & Oshlack, A. Clustering trees: a visualization for evaluating clusterings at multiple resolutions. *Gigascience* **7**, 1–9 (2018).

113. Stranger, B. E. *et al.* Population genomics of human gene expression. *Nat. Genet.* **39**, 1217–1224 (2007).

114. Ma, W., Baumann, C. & Viveiros, M. M. Lack of protein kinase C-delta (PKCδ) disrupts fertilization and embryonic development. *Mol. Reprod. Dev.* **82**, 797–808 (2015).

115. Theisen, D. J. *et al.* WDFY4 is required for cross-presentation in response to viral and tumor antigens. *Science (80-.).* **362**, 694–699 (2018).

116. Chat, V. *et al.* Autoimmune genetic risk variants as germline biomarkers of response to melanoma immune-checkpoint inhibition. *Cancer Immunol. Immunother.* **68**, 897–905 (2019).

117. Breunis, W. B. *et al.* Influence of cytotoxic T lymphocyte-associated antigen 4 (CTLA4) common polymorphisms on outcome in treatment of melanoma patients with CTLA-4 blockade. *J. Immunother.* **31**, 586–590 (2008).

118. Wang, Q. *et al.* Genetic associations of T cell cancer immune response-related genes with T cell phenotypes and clinical outcomes of early-stage lung cancer. *J. Immunother. Cancer* **8**, e000336 (2020).

119. Heng, T. S. P. *et al.* The Immunological Genome Project: networks of gene expression in immune cells. *Nat. Immunol. 2008 910* **9**, 1091–1094 (2008).

120. Stout, R. D. *et al.* Macrophages Sequentially Change Their Functional Phenotype in Response to Changes in Microenvironmental Influences. *J. Immunol.* **175**, 342–349 (2005).

121. Castro, F., Cardoso, A. P., Gonçalves, R. M., Serre, K. & Oliveira, M. J. Interferon-gamma at the crossroads of tumor immune surveillance or evasion. *Front. Immunol.* **9**, 847 (2018).

122. Zanoni, I. & Granucci, F. Role of CD14 in host protection against infections and in metabolism regulation. *Front. Cell. Infect. Microbiol.* **4**, 32 (2013).

123. Molgora, M. *et al.* TREM2 Modulation Remodels the Tumor Myeloid Landscape Enhancing Anti-PD-1 Immunotherapy. *Cell* **182**, 886-900.e17 (2020).

124. Arlauckas, S. P. *et al.* Arg1 expression defines immunosuppressive subsets of tumor-associated macrophages. *Theranostics* **8**, 5842 (2018).

125. Xiong, D., Wang, Y. & You, M. A gene expression signature of TREM2hi macrophages and γδ T cells predicts immunotherapy response. *Nat. Commun. 2020 111* **11**, 1–12 (2020).

126. Dobrovolskaia, M. A. & Vogel, S. N. Toll receptors, CD14, and macrophage activation and deactivation by LPS. *Microbes Infect.* **4**, 903–914 (2002).

127. Marzio, R., Jirillo, E., Ransijn, A., Mauël, J. & Corradin, S. B. Expression and function of the early activation antigen CD69 in murine macrophages. *J. Leukoc. Biol.* **62**, 349–355 (1997).

128. Scali, E. *et al.* Inflammation and macrophage polarization in cutaneous melanoma: Histopathological and immunohistochemical study. *Int. J. Immunopathol. Pharmacol.* **29**, 715 (2016).

129. Menon, D. K. & Rosand, J. Finding a Place for Candidate Gene Studies in a Genome-Wide Association Study World. *JAMA Netw. Open* **4**, e2118594–e2118594 (2021).

130. Uffelmann, E. *et al.* Genome-wide association studies. *Nat. Rev. Methods Prim. 2021 11* **1**, 1–21 (2021).

131. Wang, K. *et al.* Diverse Genome-wide Association Studies Associate the IL12/IL23 Pathway with Crohn Disease. *Am. J. Hum. Genet.* **84**, 399–405 (2009).

132. Van Den Eeckhout, B., Tavernier, J. & Gerlo, S. Interleukin-1 as Innate Mediator of T Cell Immunity. *Front. Immunol.* **11**, 621931 (2020).

133. Yin, W. *et al.* CCRL2 promotes antitumor T-cell immunity via amplifying TLR4-mediated immunostimulatory macrophage activation. *Proc. Natl. Acad. Sci. U. S. A.* **118**, (2021).

134. Binnewies, M. *et al.* Targeting TREM2 on tumor-associated macrophages enhances immunotherapy. *Cell Rep.* **37**, 109844 (2021).

135. Liu, X. *et al.* CD47 blockade triggers T cell–mediated destruction of immunogenic tumors. *Nat. Med. 2015 2110* **21**, 1209–1215 (2015).

136. Gauttier, V. *et al.* Selective SIRPα blockade reverses tumor T cell exclusion and overcomes cancer immunotherapy resistance. *J. Clin. Invest.* **130**, 6109–6123 (2020).

137. Alshetaiwi, H. *et al. Defining the emergence of myeloid-derived suppressor cells in breast cancer using single-cell transcriptomics*. *Science Immunology* **5**, (Science Immunology, 2020).

138. Li, X. *et al.* PKC- activation in neutrophils promotes fungal clearance. *J. Leukoc. Biol.* **100**, 581–588 (2016).

139. Gabrilovich, D. I. & Nagaraj, S. Myeloid-derived suppressor cells as regulators of the immune system. *Nat. Rev. Immunol. 2009 93* **9**, 162–174 (2009).

140. Highfill, S. L. *et al.* Disruption of CXCR2-mediated MDSC tumor trafficking enhances anti-PD1 efficacy. *Sci. Transl. Med.* **6**, (2014).

141. Simonetta, F. *et al.* Interleukin-7 Influences FOXP3+CD4+ Regulatory T Cells Peripheral Homeostasis. *PLoS One* **7**, e36596 (2012).

142. Holmgren, C., Cornmark, L., Lønne, G. K., Masoumi, K. C. & Larsson, C. Molecular characterization of protein kinase C delta (PKCδ)-Smac interactions. *BMC Biochem.* **17**, 11 (2016).

143. Zhang, X. M., Chen, J., Xia, Y. G. & Xu, Q. Apoptosis of murine melanoma B16-BL6 cells induced by quercetin targeting mitochondria, inhibiting expression of PKC-α and translocating PKC-δ. *Cancer Chemother. Pharmacol.* **55**, 251–262 (2005).

144. Ghayur, T. *et al.* Proteolytic Activation of Protein Kinase C δ by an ICE/CED 3-like Protease Induces Characteristics of Apoptosis. *J. Exp. Med.* **184**, 2399–2404 (1996).

145. Chen, Z., Forman, L. W., Williams, R. M. & Faller, D. V. Protein kinase C-delta inactivation inhibits the proliferation and survival of cancer stem cells in culture and in vivo. *BMC Cancer* **14**, 1–15 (2014).

146. Grossoni, V. C., Falbo, K. B., Kazanietz, M. G., Bal De Kier Joffé, E. D. & Urtreger, A. J. Protein kinase C δ enhances proliferation and survival of murine mammary cells. *Mol. Carcinog.* **46**, 381–390 (2007).

147. Keshamouni, V. G., Mattingly, R. R. & Reddy, K. B. Mechanism of 17-β-Estradiol-induced Erk1/2 Activation in Breast Cancer Cells: A ROLE FOR HER2 AND PKC-δ. *J. Biol. Chem.* **277**, 22558–22565 (2002).

148. Schwegmann, A. *et al.* Protein kinase C δ is essential for optimal macrophage-mediated phagosomal containment of Listeria monocytogenes. *Proc. Natl. Acad. Sci. U. S. A.* **104**, 16251–16256 (2007).

149. Abbas, T. *et al.* Inhibition of Human p53 Basal Transcription by Down-regulation of Protein Kinase Cδ *. *J. Biol. Chem.* **279**, 9970–9977 (2004).

150. Sitailo, L. A., Tibudan, S. S. & Denning, M. F. The protein kinase Cδ catalytic fragment targets Mcl-1 for degradation to trigger apoptosis. *J. Biol. Chem.* **281**, 29703–29710 (2006).

151. Soltoff, S. P. Rottlerin Is a Mitochondrial Uncoupler That Decreases Cellular ATP Levels and Indirectly Blocks Protein Kinase Cδ Tyrosine Phosphorylation. *J. Biol. Chem.* **276**, 37986–37992 (2001).

152. Leitges, M., Elis, W., Gimborn, K. & Huber, M. Rottlerin-Independent Attenuation of Pervanadate-Induced Tyrosine Phosphorylation Events by Protein Kinase C-δ in Hemopoietic Cells. *Lab. Investig. 2001 818* **81**, 1087–1095 (2001).

153. Gomel, R. *et al.* The Localization of Protein Kinase CD in Different Subcellular Sites Affects Its Proapoptotic and Antiapoptotic Functions and the Activation of Distinct Downstream Signaling Pathways. *Mol. Cancer Res.* (2007). doi:10.1158/1541-7786.MCR-06-0255

154. Li, W. *et al.* Tyrosine phosphorylation of protein kinase C-delta in response to its activation. *J. Biol. Chem.* **269**, 2349–2352 (1994).

155. Konishi, H. *et al.* Activation of protein kinase C by tyrosine phosphorylation in response to H2O2. *Proc. Natl. Acad. Sci. U. S. A.* **94**, 11233–11237 (1997).

156. Parihar, S. P. *et al.* Protein kinase C-delta (PKCδ), a marker of inflammation and tuberculosis disease progression in humans, is important for optimal macrophage killing effector functions and survival in mice. *Mucosal Immunol.* **11**, 496–511 (2018).

157. Jain, N., Zhang, T., Kee, W. H., Li, W. & Cao, X. Protein Kinase C δ Associates with and Phosphorylates Stat3 in an Interleukin-6-dependent Manner *. *J. Biol. Chem.* **274**, 24392–24400 (1999).

158. Sharif, M. N. *et al.* IFN-α Priming Results in a Gain of Proinflammatory Function by IL-10: Implications for Systemic Lupus Erythematosus Pathogenesis. *J. Immunol.* **172**, 6476–6481 (2004).

159. Jimenez-Duran, G. *et al.* Pharmacological validation of targets regulating CD14 during macrophage differentiation. *EBioMedicine* **61**, (2020).

160. Malavez, Y., Voss, O. H., Gonzalez-Mejia, M. E., Parihar, A. & Doseff, A. I. Distinct contribution of protein kinase C *δ* and protein kinase C *ε* in the lifespan and immune response of human blood monocyte subpopulations. *Immunology* **144**, 611–620 (2015).

161. Hazeki, K., Inoue, K., Nigorikawa, K. & Hazeki, O. Negative Regulation of Class IA Phosphoinositide 3-kinase by Protein Kinase Cδ Limits Fcγ Receptor-Mediated Phagocytosis in Macrophages. *J. Biochem.* **145**, 87–94 (2009).

162. Joshi, S., Singh, A. R., Zulcic, M. & Durden, D. L. A PKC-SHP1 signaling axis desensitizes Fcγ receptor signaling by reducing the tyrosine phosphorylation of CBL and regulates FcγR mediated phagocytosis. *BMC Immunol.* **15**, 1–11 (2014).

163. Garrido-Martin, E. M. *et al.* Open access M1 hot tumor-associated macrophages boost tissue-resident memory T cells infiltration and survival in human lung cancer. *J Immunother Cancer* **8**, 778 (2020).

164. Horton, B. L., Williams, J. B., Cabanov, A., Spranger, S. & Gajewski, T. F. Intratumoral CD8+ T-cell apoptosis is a major component of T-cell dysfunction and impedes antitumor immunity. *Cancer Immunol. Res.* **6**, 14–24 (2018).

165. Beyranvand Nejad, E. *et al.* IL-6 signaling in macrophages is required for immunotherapy-driven regression of tumors. *J. Immunother. Cancer* **9**, e002460 (2021).

166. Li, B., Jones, L. L. & Geiger, T. L. IL-6 Promotes T Cell Proliferation and Expansion under Inflammatory Conditions in Association with Low-Level RORγt Expression. *J. Immunol.* **201**, 2934–2946 (2018).

167. Del Vecchio, M. *et al.* Interleukin-12: Biological Properties and Clinical Application. *Clin. Cancer Res.* **13**, 4677–4685 (2007).

168. Pathria, P., Louis, T. L. & Varner, J. A. Targeting Tumor-Associated Macrophages in Cancer. *Trends in Immunology* **40**, 310–327 (2019).

169. Salzer, E. *et al.* B-cell deficiency and severe autoimmunity caused by deficiency of protein kinase C δ. *Blood* **121**, 3112–3116 (2013).

170. Amoozgar, Z. & Goldberg, M. S. Targeting myeloid cells using nanoparticles to improve cancer immunotherapy. *Adv. Drug Deliv. Rev.* **91**, 38–51 (2015).

171. Chaib, M., Chauhan, S. C. & Makowski, L. Friend or Foe? Recent Strategies to Target Myeloid Cells in Cancer. *Front. Cell Dev. Biol.* **8**, 351 (2020).

172. Das, A. T., Tenenbaum, L. & Berkhout, B. Tet-On Systems For Doxycycline-inducible Gene Expression. *Curr. Gene Ther.* **16**, 156 (2016).

173. Molon, B. *et al.* Ar ticle Chemokine nitration prevents intratumoral infiltration of antigen-specific T cells The Journal of Experimental Medicine. *J. Exp. Med* **208**, 1949–1962 (2011).